Experimental Characterization and Finite Element Modelling of Cervical Facet Joint Mechanics

by

Gwennyth Alexandra Carroll

A thesis

presented to the University of Waterloo

in fulfilment of the

thesis requirement for the degree of

Master of Applied Science

in

Mechanical and Mechatronics Engineering

Waterloo, Ontario, Canada, 2023

Author's Declaration

I hereby declare that I am the sole author of this thesis. This is a true copy of the thesis, including any required final revisions, as accepted by my examiners.

I understand that my thesis may be made electronically available to the public.

Abstract

Cervical facet joints are involved in the complex movements and associated disorders of the head and neck. The capsular ligament of the cervical facet joint plays an important role in guiding and restraining joint motions under different loading modes. However, biomechanical studies on the capsular ligament to date have primarily focused on loading the ligament in tension to failure, with little understanding of the ligament response in other loading modes. Current computational human body models (HBMs) use simplified representations of the facet joint and capsular ligament. Experimental data for the multi-directional capsular ligament response could improve HBM capabilities. Therefore, the overall goal of this thesis was to investigate a hybrid experimental-computational approach to evaluate cervical facet joint mechanics under multi-directional loading and assess potential improvements to the cervical facet joint implementation in a motion segment from the GHMBC M50 neck model.

In the experimental study, ten human cervical facet joints were isolated and loaded cyclically to sub-failure displacements at 0.1 mm/s and 10 mm/s in three loading directions: (1) tension, (2) AP shear, and (3) LT shear. Displacement limits were determined independently for each specimen up to a maximum of 3.5 mm. Force and displacement data were recorded using a spinal loading simulator (AMTI VIVO). Additionally, a camera was used to record the displacement of a grid of markers on the capsular ligament surface. Force-displacement data for each test was separated into loading and unloading phases in the positive and negative loading directions. Two loading cycles from each specimen were extracted to calculate the average force-displacement curves using ARCGen, an arc-length re-parameterization and signal registration method. Ligament surface Green strain was estimated by digitizing the marker displacements and running them through a Matlab script. The average force-displacement curves showed the highest magnitude of force in tension, while AP shear and LT shear had similar magnitudes of force at the same displacement.

In the parallel computational study, the C4-C5 facet joint was extracted from the GHBMC M50 model. The first extraction, the FJ_{E1} model, was used to replicate the boundary conditions used in a previous tension to failure test (Mattucci et al). The FJ_{E1} model was also loaded in positive

and negative shear. A second facet joint extraction, the FJ_{E2} model, was setup for the multi-direction experimental study described above and replicated the boundary conditions for cyclic, sub-failure tension, AP shear and LT shear at the 10 mm/s rate. The FJ_{E2} model was then modified to examine potential enhancements to the force-displacement response. The first modification added 1D tension-only elements to the capsular ligament in a diagonal formation. The input curves for the original and diagonal elements were calculated to simultaneously fit the response in tension, positive AP and positive LT shear directions. The second modification used shell elements to represent the capsular ligament, characterized using the experimental tension data. R^2 values were calculated between the model output and the experimental data to monitor the improvements compared to the FJ_{E2} model. The FJ_{E1} model performed well in tension; however, the FJ_{E2} model overestimated the force response in positive AP shear and underestimated the force response in negative AP shear and LT shear. Additionally, the 1D tension-only elements representing the capsular ligament did not interact with the hard-tissue geometry, resulting in non-physiological load paths, and the elements changed orientation before carrying load. The addition of diagonal elements improved the response in positive AP shear while maintaining good agreement in tension; however, the implementation was unable to improve the response in LT shear or negative AP shear. Using shell elements to represent the capsular ligament resulted in similar improvements without requiring an iterative fitting procedure and overcame some of the limitations of 1D tension-only elements.

The hybrid experimental-modelling approach facilitated the translation of new experimental data to the computational GHBMC model. The VIVO simulator allowed loading of cervical facet joints in multiple modes of loading, providing new data to evaluate the GHMBC model in AP and LT shear, which has not previously been performed. However, several key limitations should be addressed in future experimental and modelling work to further improve understanding of facet joint mechanics. These include testing the facet joint in more complex loading scenarios, investigating the effect of specimen alignment, removing the geometric bias of the 1D tension-only elements, and improving the shell representation of the capsular ligament.

Acknowledgements

I am grateful to have had the support of many people during my thesis. First and foremost, I would like to thank my supervisors, Dr. Duane Cronin and Dr. Stewart McLachlin, for their unwavering support and guidance.

I had two wonderful mentors, Martine McGregor and Miguel Corrales. Martine (and baby Louise) spent long testing days with me in the lab, and Miguel was longsuffering with my many modelling questions.

In the lab, I was fortunate to have the technical expertise of Tom Gawel and the surgical expertise of Dr. Renan Fernandes. Special thanks to Tamara Maciel and her team at the Anatomy Lab for providing the space for specimen preparation. I would also like to acknowledge the specimen donors and ScienceCare. I hope I have honoured their contribution.

I would like to acknowledge the Global Human Body Models Consortium (GHBMC) for use of the M50 human body model and Digital Research Alliance of Canada for computational resources and support.

I would like to thank the Natural Sciences and Engineering Research Council of Canada, Ontario Graduate Scholarship Program and the Canada Research Chairs Program for funding, giving me the opportunity to do this research.

Finally, thanks to the IMMC and Orthotron Lab members, for being a great group of people to work with and learn from.

Dedication

To my parents.

Table of Contents

List of Figures

List of Tables

List of Nomenclature

CL	Capsular ligament
F	Deformation gradient
FJ_{E1}	First extraction of the isolated C4 - C5 facet joint from the GHBMC M50 model
FJ_{E2}	Second extraction of the isolated C4 - C5 facet joint from the GHBMC M50 model with additional bony structures, reoriented and potted
FJ_{E2_Di}	Modification of the FJ_{E2} model by adding additional 1D tension-only elements to the capsular ligament
FJ_{E2_Sh}	Modification of the FJ_{E2} model by using shell elements to represent the capsular ligament
GHBMC	Global human body models consortium
GHBMC M50	50^{th} percental male computation human body model developed by GHBMC
HBM	Computational human body model
I	Identity matrix
ILC	Iterative learning control
SSE	sum of squared residuals between the experiment and model curves
SST	total sum of squares for the experiment curve
R^2	R-squared value
THUMS	Commercial computational human body model
VIVA	Commercial computational human body model
VIVO	AMTI six degrees-of-freedom joint motion simulator
WAD	Whiplash associated disorder
2^{nd} PK stress	Second Piola-Kirchhoff stress

Chapter 1 Introduction

1.1 Motivation for Research

Cervical facet joint injuries are commonly the result of sport trauma and motor vehicle accidents [1]. Whiplash associated disorder (WAD) is of particular interest as a low severity but high frequency event accounting for between 27% to 56% of vehicle collision injuries seen in hospitals or emergency rooms [2] [3]. Although low severity, WAD can have a chronic impact on patient health and a high economic cost [4]. Numerical human body models (HBMs) are valuable tools to predict injury. However, with limited understanding of facet joint mechanics [5], there is a need for additional data to inform continued development of HBMs.

Cervical facet joints are key structures in the cervical spine that guide and restrict neck motions (Figure 1.1A) [1]. They are comprised of several tissues: bony articular pillars, cartilage, synovial fluid, and capsular ligaments. During normal physiological motions of the spine, facet joints undergo complex loading [1] [6], with the capsular ligament resisting tensile and shear loads [1] [7] [8].

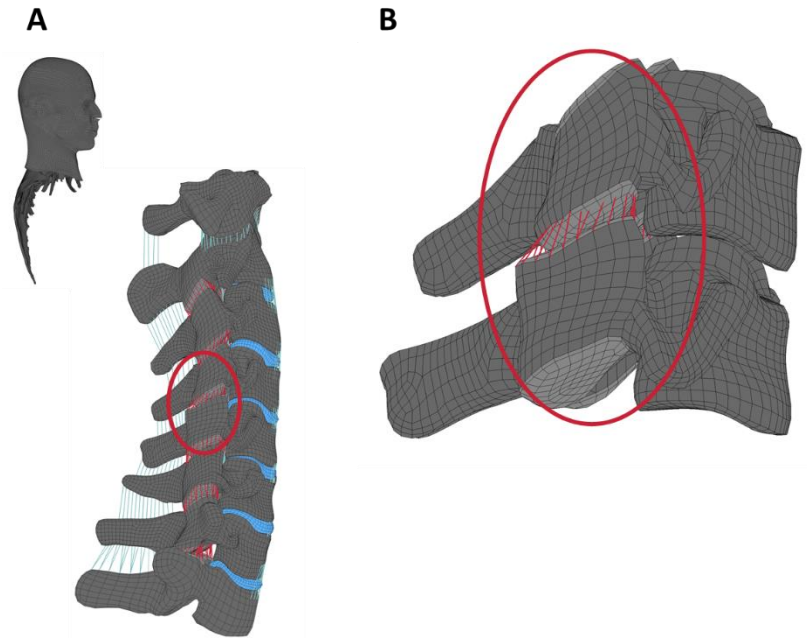

Figure 1.1: (A) GHBMC M50 ligamentous cervical spine with the C4 - C5 facet joint circled in red. Bone in dark grey, cartilage in light grey, spinal ligaments in turquoise, intervertebral disc in blue and capsular ligament of the facet joints in red. (B) Tissue of the C4 - C5 facet joint as implemented in the GHBMC M50 model.

Researchers have proposed several theories on the origin of pain in the facet joint including excessive stretch of the facet joint capsular ligament and pinching of the synovial folds or meniscoids [4] [9]. The most well-established theory, both clinically and biomechanically, is excessive strain in the facet joint capsular ligament. *In vivo* animal models have demonstrated that tensile forces across the facet joint lead to significant changes in behavioural measures of pain or nociceptive neuron discharge [4]. The reported peak strains in simulated vehicle impact studies falls within the range of sub-catastrophic strain identified in an isolated motion segment (35% +/- 21%)) [10] and the range of strain activating potential nociceptors in animal models. With implications for spinal injury and pain, it is important to develop deeper understanding of the biomechanics of facet joints at the tissue level.

Numerical computational HBMs predict tissue response under different load conditions. These models can provide estimations of local response that are difficult to measure experimentally [11] [12], predicting internal stress and strain in hard and soft tissues [13] [14]. Accurate geometric and material model inputs, appropriate boundary conditions and joint level validation data are required for developing HBMs that can then be used to develop injury prevention technologies [11] [13].

With experimental data of the facet joint largely restricted to tension loading to failure [15] [16] [17], there is a need for experimental data in shear and complex modes of loading to fully characterize capsular ligaments [18]. Current HBMs use simplified representations of facet joint tissues in terms of both geometry and material inputs, including a simplified representation of the capsular ligament [13]. For instance, the Global Human Body Models Consortium (GHBMC) average stature male (M50) and small stature female (F05) models use 1D tension-only elements characterized in facet joint tension to represent the capsular ligament (Figure 1.1B). The capsular ligament is an anisotropic, nonlinear, viscoelastic structure that responds to various loads, making material characterization challenging. While there are extensive studies on motion segment kinematics under various modes of loading and isolated facet joint response in tension, there is limited experimental data in non-tension modes of loading of isolated facet joints.

1.2 Objectives and Approach

A unique hybrid experimental-computational approach was employed to evaluate the cervical facet joint response and improve the capsular ligament implementation in a motion segment from the GHBMC M50 neck model. The three main objectives of this thesis were as follows:

Objective 1: Experimentally measure isolated cervical facet joint response (force-displacement data and ligament strain) under tension and shear modes of cyclic sub-catastrophic loading.

Ten human facet joints from three cadaveric cervical spines (C2 to C7) were isolated by a spine surgeon and loaded using a six-degrees-of-freedom dynamic force and motion simulator (AMTI VIVO). Each specimen was loaded at two rates (0.1 mm/s and 10 mm/s) in three directions (tension, AP shear and LT shear). Force and displacement data were recorded by the simulator and optical techniques were used to approximate capsular ligament surface strain. Average force-displacement curves for each mode of loading were found using ARCGen (R2023a) [19], an arc-length re-parameterization and signal registration method, to determine a characteristic average curve and statistical corridors.

Objective 2: Evaluate the capsular ligament implementation in a contemporary human body model (GHBMC M50) in sub-failure tension and shear modes of loading using data from Objective 1 and existing experimental data.

The current numerical implementation of the facet joint, which used 1D tension-only elements to represent the capsular ligament, was evaluated in tension by comparing the model force-displacement output with data reported by Mattucci [15]. The experimental data from Objective 1 was used to evaluate current implementation in AP and LT shear by comparing the model force-displacement output with the experimental average curves.

Objective 3: Develop an approach to enhance the response of the GHBMC facet joint model to improve agreement with the experimental data from Objective 1.

The capsular ligament implementation used 1D tension-only elements connected node-to-node between the inferior and superior pillars of the facet joint. The addition of 1D tension-only elements in a diagonal configuration was investigated to improve the response of the facet joint in shear modes of loading. Changes in the model force-displacement response were evaluated using the R^2 values comparing the model output to the Objective 1 experimental data.

1.3 Thesis Outline

This thesis document is structured in five chapters. Chapter 1 introduced the objectives and the motivation for the work. Chapter 2 introduces key background concepts and current literature regarding facet joint mechanics and modelling. The main contributions of this thesis are then separated into two chapters: Chapter 3 covers the experimental study (Objective 1) and Chapter 4 covers the modelling work (Objectives 2 and 3). Finally, Chapter 5 provides overall conclusions and recommendations for next steps.

Chapter 2 Background

2.1 Epidemiology

Whiplash associated disorder (WAD) accounts for 27% to 56% of vehicle collision injuries seen in hospitals or emergency rooms [2] [3]. Although low severity, WAD can have a long-term impact on patient health [4]. Radanov et. al. (1995) reported that 24% of patients presented symptoms one year after their accident, dropping to 18% after two years [20]. After 20 years, the prevalence of shoulder stiffness, headache, and arm pain were significantly greater in WAD patients than a control group, with subjects at both timepoints taken from the same cohort [21]. This results in significant economic burden, with annual societal costs estimated at 4.5 - 8 billion dollars in the United States [4] and 1.2 billion pounds in the United Kingdom [22].

The facet joints have been identified as a possible source of pain; clinical double-blind anesthetic block studies reported 54% to 77% whiplash patients experienced facet joint pain [23] [24] [25]. A study in healthy volunteers was able to induce pain in the facet joint by injecting contrast medium [26]. Additionally, capsular ligament strains in rear impact have been investigated and related to nociceptive strains. Simulated vehicle impact studies using post-mortem human subjects reported peak ligament strains between 30% to 60% [27] [28] [29] [30] [31].

Researchers have proposed several theories on the origin of pain in the facet joint including excessive stretch of the facet joint capsular ligament and pinching of the synovial folds or meniscoids [9] [4]. The most well-established theory, both clinically and biomechanically, is strain in the facet joint capsular ligament. Mechanoreceptors and nociceptive neurons have been identified in the facet joint capsular ligament [9] [32]. *In vivo* animal models demonstrated tensile distraction across the facet joint led to significant changes in behavioural measures of pain or nociceptive neuron discharge [4]. In a goat model, neural activity identified potential pain receptors that were activated above 47% strain of the capsular ligament [33], while in a rat model, facet strains of 11% to 42% were sufficient to generate pain [34]. The reported strains in HBM capsular ligaments for simulated vehicle impact studies fell within the range of sub-catastrophic strain identified in an isolated motion segment (35% +/- 21%)) [10] and the range of strain activating potential nociceptors in animal models.

2.2 Spine and Facet Joint Anatomy

The spine is sectioned into four regions: cervical, thoracic, lumbar, and sacral (Figure 2.1A) [35]. The cervical spine provides stability for the head; it is comprised of seven vertebrae (Figure 2.1B) [18] and is sub-divided into the upper cervical spine (occiput (base of the skull) to C2) and the lower cervical spine (C3 to C7) [36]. While C1 and C2 have unique anatomies, C2 to C7 have similar geometries [35].

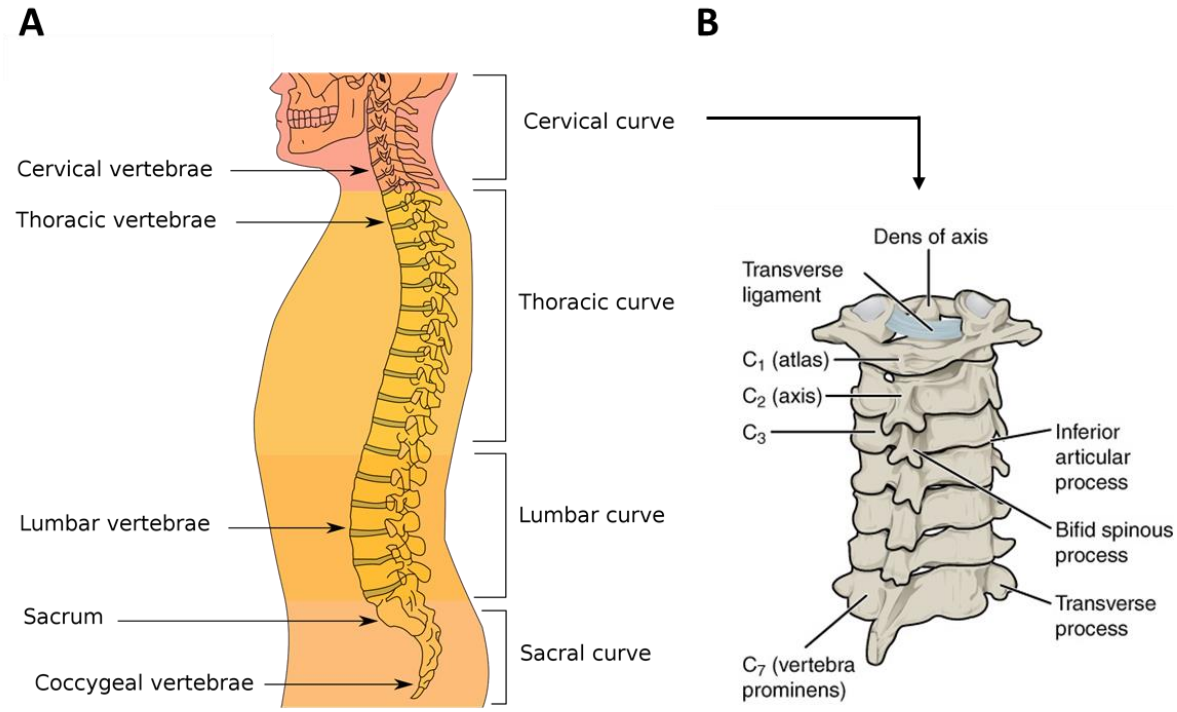

Figure 2.1: (A) Spinal column showing cervical, thoracic, lumbar, and sacral regions. (B) The cervical spine from C1 to C7. From Wikimedia Commons [37] and [38].

Vertebrae in the lower cervical spine are formed from the vertebral body and posterior elements including the pedicles, lamina, spinous and transverse processes, and facet articular pillars, otherwise known as the articular process (Figure 2.2) [35].

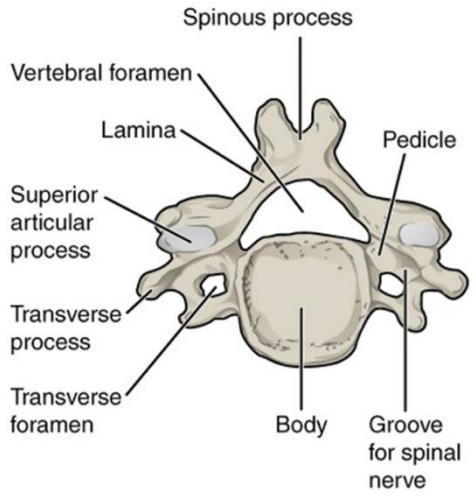

Figure 2.2: Structure of a typical lower cervical vertebra. From Wikimedia Commons [38].

Facet joints are positioned on the postero-lateral aspect of each motion segment (Figure 2.3A). Their role is to transmit load and guide and constrain the motion of adjacent vertebrae to prevent damage to the surrounding tissues, including the nerve roots and spinal cord [1] [7] [7]. More specifically, the facet joints lend torsional stiffness (axial rotation) and resistance to lateral and anterior-posterior vertebral translation and joint distraction (tension) [1].

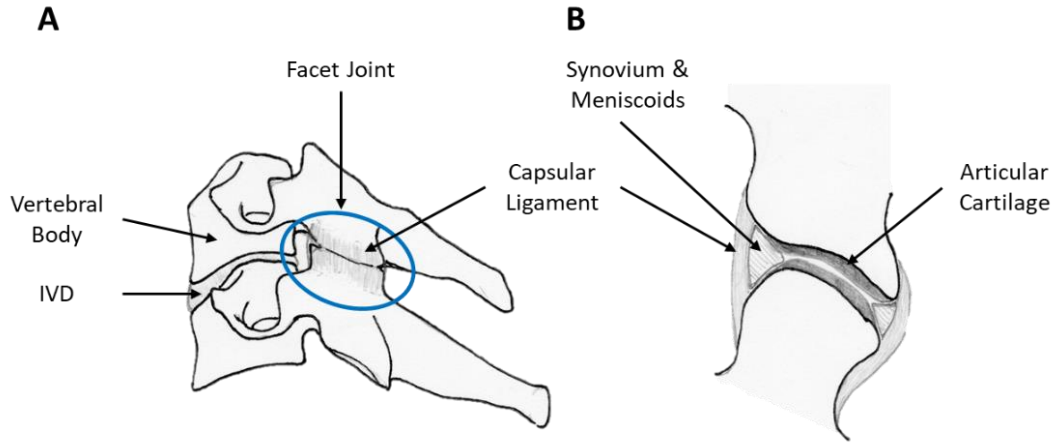

Figure 2.3: The cervical facet joint. (A) shows the location of the facet joint in a motion segment. (B) shows a schematic of the facet joint tissues. Adapted from [1] and [39].

Facet joints are comprised of several tissues: bony articular pillars, cartilage, synovial fluid, and capsular ligaments (Figure 2.3B). The articular pillars form the opposing surfaces of the facet joint and are elliptical in shape. While the superior facet in the joint is relatively flat in the cervical region, the opposing inferior facet is concave [1].

Spinal motion biomechanics are regionally dependent and influenced by the facet joint orientation and shape of the articular surface, which vary within the cervical spine and between regions [7]. At C3, the superior articular pillar faces posteromedial. This transitions to posterolateral orientation between the C3 to C4 joint and the C7 to T1 joint, with the C5 to C6 the most frequent [40]. The inclination angle of the articular pillar changes throughout the spinal regions; in the cervical spine the articular surfaces in the sagittal plane are at a 20° - 86° angle, compared to 55° - 80° in the thoracic and 82° - 86° in the lumbar spine (Figure 2.4). The lower angles in the cervical spine allow for a greater range in axial rotation and lateral bending [7]. In the axial plane, the orientation angle increases moving inferiorly. In the cervical spine, the facet joints are 45° - 96° off the midline [1] [40] [41].

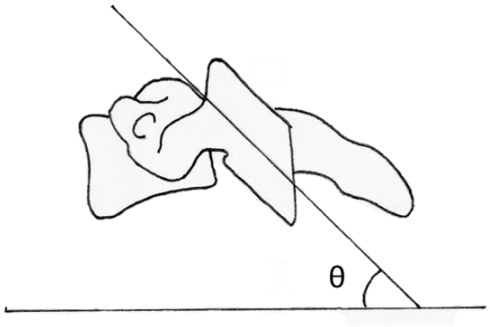

Figure 2.4: Cervical facet joint angle in sagittal plane.

The articulating surfaces of facet joints are covered by hyaline cartilage [1] [7]. Cartilage, in conjunction with synovial fluid, provides a low-friction environment for the joint while withstanding compressive, tensile and shear loads [1] [7]. It is formed by collagen fibers, glycosaminoglycans, proteoglycans, and chondrocytes. The proteoglycans trap water and increase stiffness [1]. The cartilage is structured in three zones. The superficial zone, nearest the joint, have collagen fibers that are oriented tangentially to the surface to resist tensile and shear loads. This is followed by the transition zone and then the deep zone which has collagen fibers perpendicular to the subchondral bone surface [1] [7]. The cartilage forms a layer of non-uniform thickness on the opposing surfaces, being thinner at the edges and increasing to about 1 mm in the center of the articular pillar [1] [42]. The shape has been defined as ovoid or half-sinusoidal [1]. The cartilage is reported not to extend across the entire articular pillar in every specimen,

leaving subchondral bone along the edges exposed. Yoganandan et. al. (2003) reported this gap to be 16.4% in the lower cervical spine [43].

The capsular ligament fully encloses the facet joint and resists tensile and shear loads, which is important to maintain stability of the joint [8] [44]. Ligaments are composed of protein and non-protein constituents. The dry mass of ligaments is primarily Type 1 collagen (70% to 80% of dry weight), with remaining components being elastin fibers, proteoglycans, and fibroblasts [1] [44]. The protein components, including collagen, are the primary determinant of ligament biomechanics while the non-protein components regulate development, growth, and repair [45]. The specific composition varies between ligaments; [46] however, compared to tendons, ligaments have lower collagen content with less alignment in the loading direction. This is appropriate for its role in constraining and guiding joint movement, including off-axis loading [46].

Notably, the organization of the collagen fibers in the cervical spine is heterogenous and anisotropic. A study that used spatial correlation analysis of optically obtained fiber orientation fields found high spatial heterogeneity and curvy substructures in the cervical capsular ligament with a lack of spatial correlation. The cervical capsular ligaments were also shown to have intra-specimen heterogeneity. In comparison, the lumbar capsular ligament is more homogeneous, with fibers tending to be aligned across the joint in the anterior-posterior direction [8]. Capsular ligaments are innervated by mechanoreceptors, including unencapsulated nociceptive nerve endings [32], with 77% of receptors identified in the capsular ligament respond to stretch. High-threshold mechanoreceptors were identified as potential nociceptors as these receptors did not increase their rate of discharge until greater levels of stretch were achieved [47]. This suggests the capsular ligament is monitored by the central nervous system and may play a role in proprioception and pain [32].

The geometry of the capsular ligament is important when investigating facet joint biomechanics. Length measurements of the capsular ligament in literature depend on the definition on length and the spinal level. One study defined the length as distance between insertion points, determined using tongued forceps to identify where the ligament no longer moved. Based on

this definition, the lengths for the capsular ligament from C3 to L5 ranged from 10.2 mm to 18.4 mm [41]. In contrast, Yoganandan et. al. (2001) defined the length to be the vertical distance between articular pillars, resulting in an average length of 6.92 mm for C2 to C5 [17]. Similarly, the reported cross-sectional area is different depending on definition and methods, with the study by Panjabi et. al. (1993) reporting 72.3 mm^2 to 211.9 mm^2 for C3 to L5 [41] and Yoganandan et. al. (2003) 42.2 mm^2 for C2 to C5 [17]. The thickness of the capsular ligament is non-uniform; it is thinnest at the posterior region (2 mm) and reaches up to 3.2 mm in the anterior region. At the superior and inferior regions, it is about 2.4 mm thick [1]. Muscle insertions have been found to cover 22.4% of the capsular ligament area of the C4 to C5 and C5 to C6 joints, which can locally alter the stress-strain response [8] [48].

2.3 Ligament Biomechanics

Mechanical properties of ligaments vary considerably depending on their composition, organization, and the test methodology [18] [46]. Ligaments function primarily in tension in the direction of the collagen fibers; however, the collagen fiber orientation can be non-uniform, allowing ligaments to resist multiaxial loading [44] [49]. Non-longitudinal orientation of collagen fibers has been documented by transmission electron microscopy and scanning electron microscopy [50].

Like many biological tissues, ligaments exhibit nonlinear, anisotropic, viscoelastic behaviour [18] [44]. Ligaments display the expected viscoelastic behaviours of stress relaxation and creep, in addition to hysteresis when subjected to cyclic loading (Figure 2.5A) [46]. This behaviour may be attributed to inherent viscoelasticity of individual components, the interaction between hierarchical levels, and the biphasic nature of ligaments — water movement through the solid phase [46] [45]. Additionally, ligaments are load and rate dependent; failure force and stiffness are reported to increase with rate of loading (Figure 2.5B) [49]. In cyclic loading, peak stress to reach the same strain decreases with each cycle until the ligament is conditioned [44].

Ligament force-displacement curves, and stress-strain curves, in uniaxial tension longitudinal to the primary fiber orientation have three distinct regions: the toe region, the linear region, and the traumatic (or yield) region (Figure 2.5C).

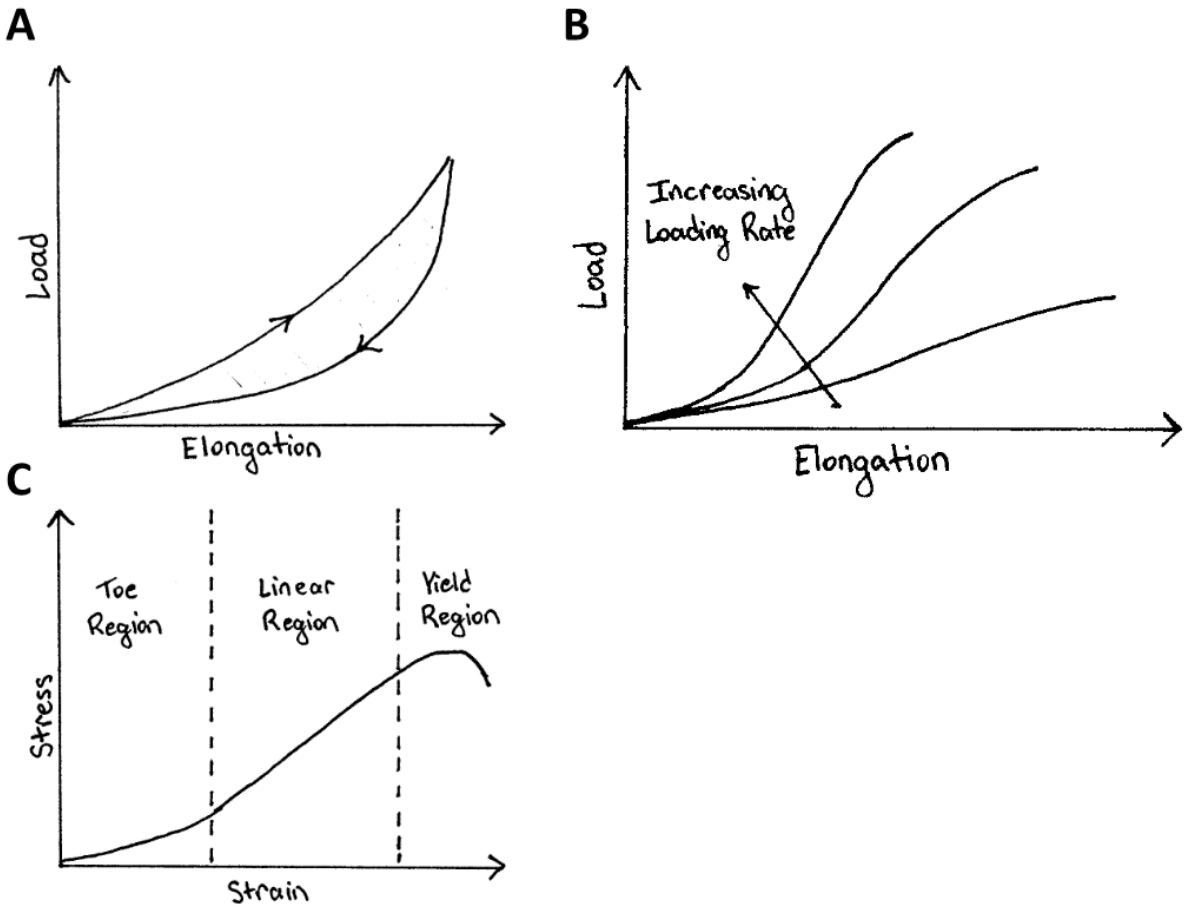

Figure 2.5: (A) Generic hysteresis curve for loading-unloading cycle of a ligament. (B) Rate-dependent mechanical response of soft tissue structures such as ligaments showing stiffness increases with increasing rate of loading. (C) Schematic of a stress-strain curve for a ligament displaying the typical toe, linear and yield regions. Adapted from [49] [51] [52].

In the toe region, ligament stiffness is low and increases nonlinearly as the collagen fibers uncrimp and align in the loading direction. Elastin was found to be the primary load-bearer in the toe region [53]. In the linear region, collagen fibers are generally aligned in the loading direction with extension resulting from extension of individual collagen fibers and relative movement between collagen fibers, mediated by proteoglycans and water content. Elastin also contributes to load support in the linear region for quasi-static loading [53]. Finally, in the traumatic region, ligament stiffness drops as collagen fibers and fiber bundles tear [18] [46].

Loading transverse to the main fiber orientation typically results in a linear force-displacement behaviour with a modulus an order of magnitude less than in the longitudinal direction [45]. Transverse loading tests measure contributions from the ground substance matrix and possible inter-fibril and fiber-matrix interactions [54]. While elastin contributes to tensile strength and shear, it is thought to be the primary determinant of transverse ligament behaviour [45]. One study of porcine medial collateral ligament found a 60% to 70% reduction in peak stress and 2 to 3 times reduction in modulus after elastin degradation [55].

Ligament shear response is typically an order of magnitude lower than longitudinal loading and is nonlinear, viscoelastic, and rate-independent [45] [56]. One study on the medial collateral ligament (MCL) proposed this nonlinearity to be a result of gradual loading of transversely oriented microstructures including collagen crosslinks or collagen-proteoglycan crosslinks [56] while a later study found elastin to govern the mechanical response [55].

In additional to variation between ligaments, the response of ligaments differs regionally within a ligament. This is due to variations in fiber organization and composition across a ligament, muscle insertion points that affect local strain distribution, and ligament-bone insertion points [44] [57].

Other factors that influence the mechanical properties of ligaments include age, sex, temperature, and hydration. Aging affects not only cellular function and healing, but also collagen fibers and the number and quality of bonds [58] [50]. As ligaments age, collagen fibril diameters tend to decrease and concentration of fibrils increase, resulting in an overall decrease in collagen content [58]. Younger specimens generally exhibit lower stiffness and ultimate load [44]. One study on the human anterior cruciate ligament demonstrated the linear region stiffness decreased 34 from 242 N/mm in the 20 to 35 age group to 180 N/mm in the 60 to 97 age group [59]. Another tensile test on human femur-ACL-tibia indicated a decrease in linear stiffness and ultimate load decreased with specimen age [60].

Ligaments display temperature dependence; as temperature decreases, peak force increases for similar peak strains. One study on uniaxial tension of the porcine anterior longitudinal ligament to 20% strain demonstrated strong temperature dependence between peak force and peak

strain, although relaxation showed that viscoelastic properties were less temperature dependent [61]. In contrast, an earlier study on canine MCL reported temperature dependent viscoelastic properties, with the area of hysteresis decreasing with increasing temperature. The same study reported that the tensile load at given strain increased as temperature decreased [62]. A separate study on sheep interspinous ligaments demonstrated no difference in mechanical characteristics at different temperatures to half of failure load [63].

Hydration is another factor affecting the mechanical properties of ligaments and tendons. Stiffness is increased and the toe region reduced by dehydration. The effect is rate dependent; for human patellar tendon specimens, at a strain rate of 50 s^{-1} the structure stiffness is higher in dehydrated specimens whereas at 0.5 s^{-1} there was no significant difference. Viscoelastic properties are also affected, with greater load relaxation and reduced creep rate of tendons immersed in water compared to saline or phosphate buffered saline (PBS). However, the changes were found to be reversed upon rehydration [64] [65].

2.4 Prior Work: Experimental Studies

This section will primarily introduce a subset of the experimental literature of the capsular ligament with a brief section on tissue prestrain and the enclosed volume effect of synovial fluid. Experimental studies on other facet joint tissues have also been performed including investigating morphology of meniscoids and strain or pressure on facet articular pillars.

2.4.1 Freeze-Thaw Effect on Ligament Mechanical Properties

Studies on human tissue tend to use specimens that have been fresh-frozen and thawed at least once because of access and time constraints. Due to the high-water content in ligaments, as water freezes and expands the formation of ice crystals may alter the collagen fiber arrangement and cause defects in the matrix [66]. Tendons have a similar composition to ligaments so were included in the search.

Recent studies reported a decrease in material properties after several freeze-thaw cycles. One such study on fascicle bundles of bovine superficial digital flexor tendon found the tensile modulus to significantly reduce after the third or fourth freeze-thaw cycle with reduced stress drop during relaxation after the eighth freeze-thaw cycle and reduced mechanical hysteresis after the tenth cycle. The specimens were frozen at -80 °C and thawed using a two-step procedure with 2 hours in the fridge at 4 °C then 2 hours at room temperature [66]. A decrease in material properties is supported by a study on human flexor digitorum superficialis and flexor pollicis longus tendons, which found stress-relaxation, creep, and load to failure of specimens with less than three freeze-thaw cycles to -80 °C to be similar to fresh specimens. At greater than five freeze-thaw cycles, the ultimate load, stiffness, ultimate stress, and Young's modulus significantly decreased [67].

Other studies reported no change in material properties following a certain number of freeze-thaw cycles. A study on rat bone-patellar tendon-bone specimens frozen at -80 °C and thawed in PBS for 3 hours found no effect on ultimate stress, Young's modulus, or strain at failure after five freeze-thaw cycles [68]. These finding are supported by a study on rat tail tendon fascicles, which also found no difference in tensile stress-relaxation after two freeze-thaw cycles to -20 °C [69], and a study on rabbit medial collateral ligament-bone complex which found no difference after

a single freeze-thaw cycle to -20 °C on cyclic stress relaxation, tensile strength, or ultimate strain; although the hysteresis area was reported to be reduced in the first few loading cycles [70].

These results are not necessarily contradictory; studies reporting no change in material properties do not tend to go above five freeze-thaw cycles, which is close to the thresholds reported for material property degradation. However, one study on porcine lumbar spine found the transitional zone size to decrease and the transitional zone slope to increase during flexion-extension and lateral bending after the initial freeze-thaw cycle, with no further changes up to three freeze-thaw cycles. No significant change in elastic zone or width of hysteresis loop were reported [71].

2.4.2 Prestrain and Enclosed Volume Effect on Capsular Ligament Response

Ligaments experience strain in the neutral position of a joint, as demonstrated by tissue retraction when excised. *In situ* strains for ligaments in diarthrodial joints, like the facet joint, are ~3% to 10% and contribute to the mechanical response of the joint. As such, prestrain can be important to include in computational models [72]. However, there are limited studies on capsular ligament prestrain and enclosed volume effect of synovial fluid related to the facet joint.

A recent study has addressed this gap in the lumbar facet joint. Gacek et. al. (2022) investigated capsular ligament strain due to enclosed synovial fluid and from residual strain. Verhoeff-Van Geison stain was used to pattern the capsular ligament for optical measurements, then PBS was injected at 1 mL/min to 0.55 mL. The PBS was removed, and the facet capsular ligament was cut into a rectangular specimen, with optical tracking used to track shrinkage. The paper reported a pressure-volume curve for the inflation test, with a nearly linear pressure-volume relationship but heterogeneous capsular ligament strain. The rectangular specimen shrank when excised with no clear primary direction of contraction. Even in the neutral position, the paper concluded the facet capsular ligament is under constant tensile strain due to attachment to bone and joint pressure [73].

2.4.3 Capsular Ligament Characterization

Facet joint kinematics and/or capsular ligament strain has been investigated at multiple scales: motion segment, isolated facet joint, and excised capsular ligament. At these different scales,

there are requisite differences in the specimen preparation, loading, and measurements performed. Capsular ligament strains have also been investigated when loading full head and neck specimens but will not be covered in this section.

Experimental Methods for Capsular Ligament Characterization

One key aspect in experimental study design is the tissue specimens. Most included studies used frozen unembalmed human cadaveric tissues that were thawed before testing. While most of the included studies included used cervical facet joints [15] [74], other studies used lumbar facet joints [75]. One group used porcine cervical spines as a surrogate for human lumbar spines, which has been shown to be an appropriate model given their anatomical, functional, and mechanical similarities [76]. However, transferability and applicability of results from these tests may be limited.

General specimen preparation was quite consistent across studies. Before being included in the test group, joint quality was typically evaluated using imaging modalities such as CT [77] and MRI [78] or visually [76]. The specimens that passed were prepared by removing non-ligamentous tissues to expose the capsular ligament. Further specimen preparation then depended on the scale of testing.

At the motion segment level, all ligaments and the intervertebral disc are typically kept intact [76] [77]. At the isolated facet joint level, the facet joint is excised by cutting through the pedicle and the lamina or transverse process [15] [74]. All ligaments except for the capsular ligament were then removed. In a series of studies using quantitative polarized light imaging to detect collagen fiber alignment, the isolated facet joint was further dissected to various degrees to allow light transmission [16] [74] [79]. In one of these studies, the lateral aspects of the capsular ligament were isolated and the articular processes of the joint removed [16]. In another study, the entire capsular ligament was kept, but very fine dissection was performed to remove all musculature and tendon insertions. The synovium and articular bone were also removed to allow light transmission [74] [79], which suggests some degree of capsular ligament disruption. Excised capsular ligament preparation was slightly more variable. Typically, bone was kept at two edges

to aid in fixation. The capsular ligament was then trimmed down, keeping tissue 'tabs' for fixation [78] [80].

While there were common techniques for specimen fixation across studies, different experimentalists had slightly different approaches. At the motion segment and isolated facet joint levels, the vertebral bodies were cast in a quick-hardening material, whether resin [15], dental cement, or FlowStone [16]. Screws, wires, and metal strips were commonly used to aid fixation [76]; however, there was less bony material for additional fixation methods for isolated facet joints. Wire has also been wrapped around the facet pillars to improve fixation [74].

Testing excised capsular ligaments exhibits the greatest variability. Two general methods appear to be gluing the capsular ligament to an acrylic mounting plate then fixing the plate or using clamps to fix the ligament directly [80]. Typically, bone was kept on two sides of the specimen to aid in fixation, either by drilling holes to pin or to clamp to the fixtures.

There have been multiple approaches developed to determine the zero or neutral posture of the specimen. At the motion segment level, there were two general approaches: using position or motion. Quarrington et. al. (2019) used spacing of pots and distance from bottom pot to center of rotation of motion segment to determine placement, which was effective for loading around the center of rotation [77]. Siegmund et. al. (2001) cast the vertebral bodies with the mid-discal plane horizontal [10]. Winkelstein et. al. (2000) cast the vertebral bodies based on neutral anatomic orientation or lordotic cervical spine [81]. In contrast, Fewster et. al. (2022) used the position of minimal stiffness about flexion/extension axis to find the neutral posture of the functional spinal unit [76].

At the isolated facet joint level, one approach used by several groups was to digitize landmarks or markers before excising the facet joint to obtain the facet joint orientation, then use this information to align the isolated facet joint [74] [79]. However, the process of positioning the motion segment itself was not always described [74]. Alternatively, alignment was performed manually along the primary axis of the ligament [15]. Excised ligaments were aligned in a similar manner. In one study, lumbar capsular ligaments were loaded with pins that would rotate for self-alignment [80]. For isolated facet joint and excised ligaments in tension, a preload ranging

from 0.01 N to 5 N [78] [80] [82] or a press of 5 kPa [16] was typically applied as the zero position. Researchers often made use of custom jigs to aid in alignment, highlighting the difficulty in aligning specimens and the inconsistencies across studies.

Before loading, all studies preconditioned specimens (except the study by Ivancic et. al. (2007) [82]), although each group tended to have their own protocol. The series of studies by Winkelstein's group used 30 cycles to 0.4 mm - 0.5 mm [16] [79] or 1 mm [74]. Fewster et. al. (2022) applied 4 cycles of test loads, with the final cycle used for analysis [76]. Mattucci (2011) used 20 cycles to 10% strain at 1 Hz to precondition their specimens [15]. Little et. al. (2005) [80] applied 6 cycles of preconditioning to 50% measured length at a rate of 15 s^{-1}. Claeson et. al. (2017) [78] applied 10 cycles of preconditioning to 12% grip strain at a rate of 2.4 s^{-1}. When using motion segments with an intact intervertebral disc, a static compressive preload was typically applied to address post-mortem swelling of the intervertebral disc [76].

So far, the methods discussed were, with some variation, similar across studies. The loading protocol, however, is one of the main variables and depends on the goal of the study. Most studies used displacement-controlled loading [16] [74] [79]. Where studies applied displacement-controlled loading, a rate of displacement was typically prescribed. However, in some cases, a strain rate was applied [15] [80], which depended on knowledge of the ligament length. Force or moment-controlled loading has also been applied [10] [76] [81].

The loading protocol, direction, and rate of loading was study specific. Studies on motion segments tended to have more complex loading than those on isolated facet joints. A study by Fewster et. al. (2022) [76] applied flexion-extension rotation (0.5 deg/s to +/- 8 Nm) and anterior-posterior translation (0.2 mm/s to +/- 400 N) overlaid with a constant 300 N of compression. In the same study, a simulated rear impact was performed with a shear force of 705.3 N. A study by Siegmund et. al. (2001) [10] applied posterior shear loads through the origin of the superior vertebra in 11 increments, resulting in compression, shear, and extension bending moments. Winkelstein et. al. (2001) [81] applied pure moments up to 2.5 Nm of flexion and extension with three pre-torque configurations: no pre-torque, contralateral axial pre-torque, and ipsilateral pre-torque.

Isolated facet joints were primarily loaded in tension. A selection of studies using human cadaver facet joints are summarized here. Quinn et. al. (2009) loaded facet joints at 0.5 mm/s until rupture [16]. Winkelstein et. al. (2000) removed isolated facet joints *en bloc* from motion segments used for flexion-extension testing and recast to load in tension at 0.5 mm/min until failure [81]. Two studies loaded at higher rates. Mattucci (2011) [15] loaded isolated facet joints at strain rates of 0.5 s^{-1}, 20 s^{-1} and 250 s^{-1} until failure. Ivancic et. al. (2007) [82] loaded isolated facet joints at 723 mm/s until failure.

A series of studies by Winkelstein's group loaded isolated facet joints in retraction. The study by Quinn et. al. (2011) loaded the superior articular pillar 2.5 mm in the posterior direction at 0.4 mm/s in between 30 cycles of tensile loading to 1 mm at 0.4 mm/s [79]. A related study by Lee et. al. (2012) loaded the superior facet at 0.5 mm/s until failure [74]. Finally, a study by Siegmund et. al. (2001) loaded isolated facet joints to failure at 0.01 mm/s in posterior shear in the orientation of the motion segment [10].

Briefly, excised capsular ligaments were tested under ramp loading and dynamic protocols. Little et. al. (2005) [80] performed a ramp loading protocol to lumbar capsular ligaments to strains between 10% and 50% at a loading rate of 15 s^{-1}. In the same study, a dynamic loading protocol tested specimens using 20 cycles to haversine strains between 10% to 50% at 0.2, 1, and 2 Hz. A separate study investigated biaxial tension of the lumbar facet capsular ligament, loading the ligament to 12% grip strain at 2.4 s^{-1} [78].

Figure 2.6 illustrates the experimental setup of select studies.

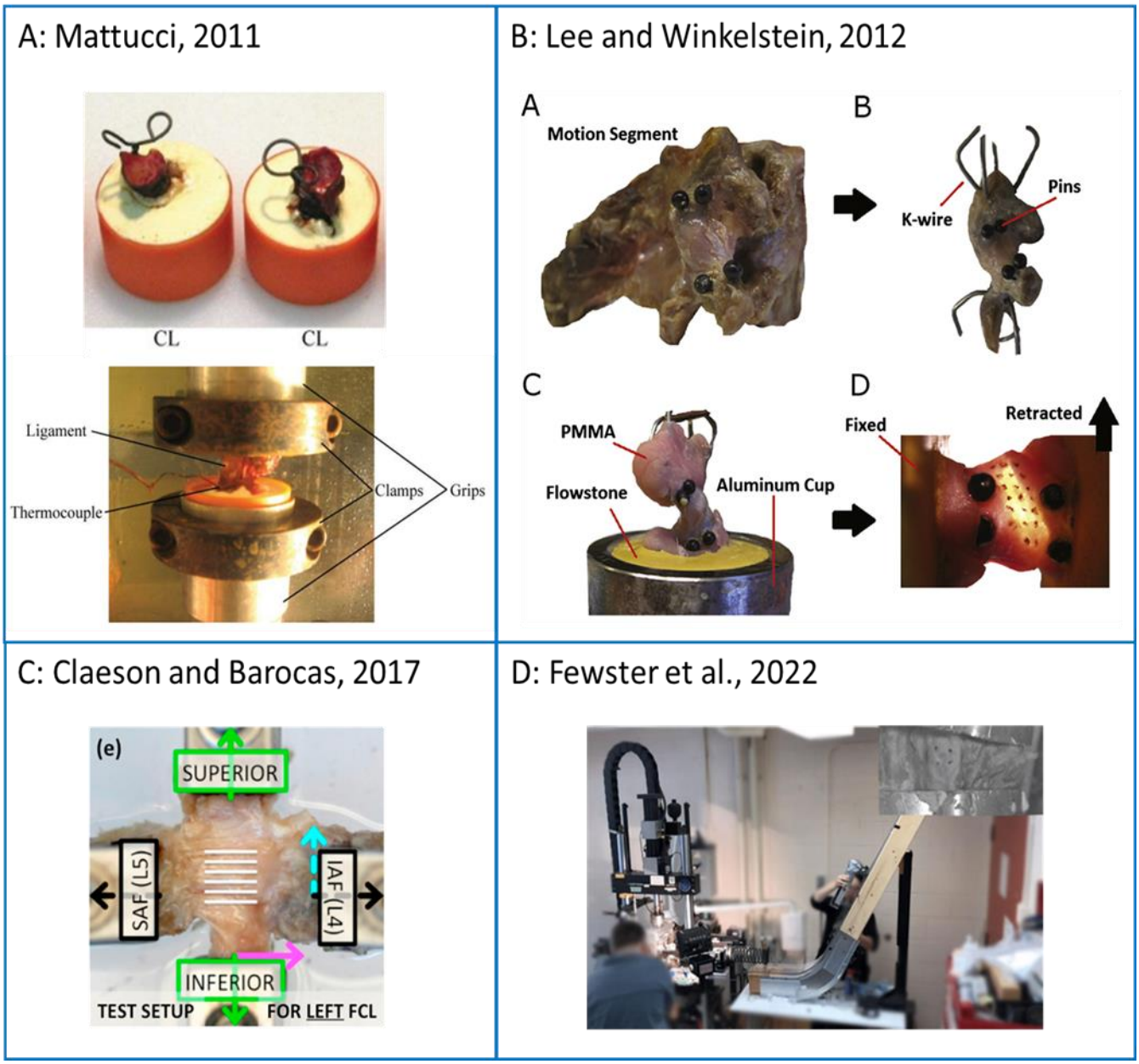

Figure 2.6: Experimental setup of select studies: (A) shows isolated human facet joints in tension (reprinted with permission from [15]); (B) shows isolated human facet joints in shear (reprinted with permission from Elsevier from [74]); (C) shows isolated human capsular ligament in biaxial extension (reprinted with permission from Elsevier from [78]); and (D) shows the setup for simulated rear impact of a porcine cervical functional spinal unit (reprinted with permission from ASME from [76]).

Experimental Measures from Capsular Ligament Characterization

Characterization of the capsular ligament most commonly measures forces and displacements of the loading actuators. Data acquisition varied from 4 Hz - 6300 Hz depending on rate of loading. In some studies, this data was used to estimate capsular stress and strain, either continuously or at key points. Initial geometric measurements were used to convert force-displacement to engineering stress-strain which necessitates several assumptions. One such assumption is uniform cross-sectional area and uniform application of force across the ligament, which is a simplification of the complex geometry of the facet joint capsular ligament. The measurement of ligament geometry itself is also challenging because of the non-uniform insertion points and tool limitations.

Optical measurement techniques were also commonly used to estimate surface ligament strain. A single camera perpendicular to the specimen was typically usually used, although some studies used multiple cameras for stereo imaging [10]. Optical resolution and rate of acquisition varied between studies, varying between 24 fps - 500 fps [16] [76] [78]. One study acquired stereo images at 0.067 Hz [10]. Several approaches were taken to mark the ligament for optical tracking: fiduciary markers glued to the ligament, [10] [81] ink to create a grid of dots, [16] [76] and speckled with a substance for digital image correlation (DIC) [78]. Commercial DIC software, custom Matlab scripts, and finite element analysis (FEA) approaches were used to convert digitized markers to ligament strain [16]. Optical data was synced to force-displacement data by time-synchronizing with voltage data [76] or by triggering to start at the same time [81]. One series of studies applied qualitative light polarization to detect mean collagen fiber direction and strength of alignment. Vector correlation was then used for pixel-wise detection of collagen fiber realignment during tension loading [16].

Reported force-displacement values at the motion segment level are not easily translatable to isolated facet joints due to load sharing in the motion segment. However, capsular ligament shear is applicable. Fewster et. al. (2022) [76] reported force-displacement and moment-angle graphs that were used to determine neutral zone limits, with the average midpoint used as the neutral position. Optical data was used to calculate ligament strain, with no difference in capsular

ligament shear reported pre- and post-simulated impact. Siegmund et. al. (2001) [10] reported that capsular ligament maximum principal strain increased with applied shear to the motion segment, but axial compression had no significant effect. Winkelstein et. al. (2000) [81] reported highly non-uniform capsular ligament strain distribution with principal strain distributions along the joint line during motion segment flexion-extension.

At the isolated facet joint level, force-displacement curves for many studies were reported, [15] [82] as well as several parameters derived from this data (Table 2.1). Mattucci (2011) concluded that loading rate is the most significant effect in tension, and both stiffness and modulus increased with rate [15]. This is supported by the conclusion by Ivancic et. al. (2007) that high speed elongation in tension may cause ligaments to fail at higher peak loads and smaller peak elongations, resulting in higher stiffness [82]. Quinn et. al. (2009) [16] reported anomalous fiber realignment during quasi-static tension to failure in 15 of the 16 specimens tested, with visible rupture occurring in the same region. Anomalous fiber realignment first occurred at 2.66 mm and 15.16 N on average, with visible rupture occurring at 3.47 mm. Winkelstein et. al. (2000) reported capsular ligament strains of 64.6% at sub-catastrophic failure.

Table 2.1: Summary of data derived from various studies

Study	*Spine Region*	*Rate*	*Stiffness*	*Elongation at Failure*	*Strain at Failure*	*Force at Failure*	*Stress at Failure*
[15]	Cervical	0.2, 20, 250 s^{-1}	85, 122, 142 N/mm	4.37, 4.18, 4.33 mm	0.97, 1.12, 1.11		3.5, 6.0, 6.1 MPa
[82]	Cervical	723 mm/s	69.4 N/mm	4.9 mm		220 N	
[16]	Cervical	0.5 mm/s		3.62 mm	1.02	21.53 N	
[81]	Cervical (C34/C56)	0.5 mm/min		5.1/6.4 mm	1.04	94.3/ 82.5 N	

In facet joint tension, Mattucci reported higher values of failure force and stiffness and lower failure elongation compared to previous studies at comparable rates [82]. The forces at failure reported by Quinn et. al. were much lower than the higher rate tests of Mattucci and Ivancic. Differences in reported values could be primarily attributed to the age of specimens and the rate of loading. Specimen preparation, potting, and alignment, as well as individual variability, may also play a role. For instance, the partial removal of the capsular ligament for light transmission in the study by Quinn et. al. [16] may have contributed to the lower force at failure.

A series of studies by Winkelstein's group investigated facet joint retraction (posterior shear). Quinn et. al. (2011) reported average peak force of 16.08 N and average strain of 0.42 and average shear strain of 0.28 at 2.5 mm of shear (at 0.4 mm/s) with substantial spatial variability [79]. The related study by Lee et. al. (2012) [74] reported an average peak (failure) force of 61.81 N and a displacement of 5.40 mm and ligament yield at 30.65 N and 2.77 mm. Fibre realignment was reported at 2.95 mm (32.86 N), similar to ligament yield but lower than ligament failure. Maximum principal strain was 0.66 at anomalous fiber realignment and 1.39 at ligament failure. Using the average force-displacement curve reported by Lee et. al., the force at 2.5 mm is approximately 25 N, which is higher than, but similar to, the value reported by Quinn et. al. Siegmund et. al. (2001) reported peak (failure) loads in posterior shear of 52 N to 146 N at displacements between 5.6 mm and 10.2 mm [10], which is much higher than reported by Lee et. al. [34]. Lee et. al. [34] attributed this to extensive dissection and removal of musculature and synovial tissue inside the capsule and bone; but inter-specimen variability may also play a role, particularly because of the relatively small specimen sizes (13 and 8).

At the excised ligament level, Little et. al. (2005) [80] reported a lumbar capsular ligament stiffness of 17.95 N/mm parallel to collagen fiber alignment and 2.29 N/mm perpendicular. This study reported no rate dependency of the lumbar capsular ligament moduli over the range of loading rates; however, the range was quite small (0.2 Hz, 1Hz, and 2 Hz). Claeson et. al. (2017) [78] reported peak normal forces of 16.11 N at 12% grip strain along the primary axis and 4.67 N in the perpendicular axis; the lumbar capsular ligament is stiffer in the primary axis.

Summary of Capsular Ligament Characterization

Ligaments are rate-dependent structures; however, most studies on isolated facet joints or excised ligaments were performed at a single rate, usually quasi-static. Mattucci (2011) [15] was one of the few to test ligaments at three strain rates (0.2 s^{-1}, 20 s^{-1}, 250 s^{-1}). Ligament response also depends on hydration and temperature. Most studies were performed at room temperature; however, Mattucci [15] used an environmental chamber to test specimens at body temperature. Some studies described specimen hydration methods, either by spraying or wrapping in saline or phosphate buffered saline (PBS) or by submerging in a PBS bath; [80] however, several studies did not explicitly report specimen hydration or temperature.

Studies that applied loading in several directions tended to require complex setups, often supplementing commercial testing devices like an Instron. [76] In some cases, the specimen was repositioned or repotted [79]. This introduced complexity to the study, increasing time and potential for error in alignment or fixation. Interestingly, several studies applied non-destructive testing followed by a destructive test.

Studies tended to report strain at key points, such as catastrophic or sub-catastrophic failure, or at discrete loads, [74] often lacking continuous strain data. While force and displacement data has been reported at the motion segment level, it is difficult to extract facet joint kinetics as load is transmitted through multiple spinal structures which limits its application in modelling. Complex loading has been applied at the head and neck level and the motion segment level, primarily simulating rear impact or investigating range of motion. However, at the isolated facet joint scale, studies tended to focus on joint distraction (tension).

Age of specimens is a major limitation of most cadaveric studies. Mattucci [15] is a notable exception where younger specimens (average age 44) were investigated.

2.5 Computational Models of the Facet Joint

There are several computational HBMs used in the automotive industry for evaluating passenger safety, including the THUMS [83], VIVA [84] [85], and the GHBMC [86] models. Each of these models used different representation of the cervical facet joint in predicting the response of the neck under different loading conditions.

The THUMS model is a series of computational models representing different sexes and ages. The 50th percentile male model included major bones and joints as well as the skin, musculature, brain and internal organs [87]. The facet joint bony pillars were represented by cortical and cancellous bone modelled as an isotropic elasto-plastic material. The facet joint itself was modelled as bony pillars and the capsular ligament. The capsular ligament was represented by triangular shell elements with a thickness of 1 mm using an isotropic elastic material model. The articular cartilage was not represented. The model was validated for frontal, lateral and rear impacts [88].

The VIVA model is a 50th percentile female human body model. Details on the development of the ligamentous cervical spine and a head-neck model can by found in papers by Osth et. al. [84] [85]. The model included representations of the vertebrae, intervertebral discs, cervical spine ligaments and musculature. The facet joint was comprised of the articular pillars, cartilage, and the capsular ligament. Cortical bone was modeled as triangular shell elements and trabecular as tetrahedral elements, both with isotropic elastic-plastic material models. The facet joint itself was modeled with frictionless contacts between the articular cartilage. The articular cartilage was modeled with a linear elastic material; however, the geometry was not specified. The capsular ligament was represented as quadrilateral shell elements with a 1.1 mm thickness using a nonlinear elastic orthotropic material model characterized using data by Mattucci et. al. [89] in quasi-static tension and supplemented with strain-rate effects to 250/s strain rate. The VIVA ligamentous cervical spine model was validated for physiological loads, with the best match for flexion-extension loads and less for axial rotation, and the head-neck model for physiological flexion-extension and rear impact, where the kinematic response at the segment level was comparable to human subjects.

The GHBMC models are a series of models representing different sexes and ages [86]. The GHBMC male 50th percentile neck model included all structural tissues of the cervical spine and neck, including vertebrae, intervertebral discs, ligaments, and musculature. The facet joint itself was comprised of the articular pillars, cartilage, and the capsular ligament (Table 2.2).

The articular pillars were modelled as cancellous and cortical bone. The cortical bone was represented using quadrilateral shell elements with an isotropic elastic plastic material model and cancellous bone was represented using hexahedral solid elements with an isotropic elastic plastic material model. The cartilage was modelled as linear viscoelastic hexahedral solid elements with sliding contacts. The geometry of the cartilage was recently enhanced based on literature data, resulting in increased validation ratings at the segment level and altered facet joint kinematics and intervertebral disk strain [5]. Finally, each capsular ligament was modelled using 28 tension-only one-dimensional elements that were non-linear, rate-dependent and incorporated progressive failure of the ligament using the tension mechanical properties from Mattucci [13]. One-dimensional elements are computationally efficient and numerically stable representations of the capsular ligament. The model was validated at the segment and full neck levels in papers by Barker et. al. [90] [91], DeWit and Cronin [92] and Corrales et. al. [5].

Table 2.2: Material models and properties of tissues in the GHBMC M50 facet joint. [90]

Tissue	**Constitutive Model**	**Mesh**	**Material Properties**		
Cortical bone	Isotropic elastic plastic	Shell elements	E_1 = 18.4 GPa ν = 0.28	E_2 = 1.25 GPa σ_y = 190 MPa	ε_{fail} = 1.78%
Cancellous bone	Isotropic elastic plastic	Solid elements	E_1 = 442 MPa ν = 0.30	E_2 = 30 MPa σ_y = 2.83 MPa	ε_{fail} = 9.5%
Facet cartilage	General viscoelastic	Solid elements	K = 2.0 GPa	G_1 = 0.2100 MPa G_2 = 0.0243 MPa G_3 = 1.0824 MPa G_4 = 1.9984 MPa	β_1 = 0 1/s β_2 = 0.000303 1/s β_3 = 0.80807 1/s β_4 = 0.012927 1/s
Capsular ligament	Elastic Spring	Beams			

2.6 Summary of Opportunities for Research Advances

Experimental studies on isolated facet joints have tended to focus on tension loading, providing valuable information on the force-displacement response [15], strain data [10], and collagen fiber organization [16]. While one series of studies applied non-tension loading to isolated facet joints, only a single direction was tested to failure at a single quasi-static rate [79] [74]. Additionally, these specimens were removed *en bloc*, repotted and realigned after being loaded at the motion segment level. Even fewer studies have reported the effect of capsular ligament prestrain [73], with no studies found on the cervical capsular ligament.

With the limited non-tension data available in literature, there is an opportunity to support existing data by loading isolated facet joints in non-tension loading at different rates and relate the experimental data directly to the GHBMC facet joint for model validation. Validation in tension and non-tension modes of loading is an important step towards improving tissue level injury prediction in computational HBMs.

Chapter 3 An *In Vitro* Experimental Investigation of Facet Joint Mechanics and Capsular Ligament Strain Under Three Modes of Loading

Understanding the biomechanics of the cervical facet joints at the tissue level is an important step towards assessing injury risk and developing prevention solutions. It is recognized that the facet joint undergoes complex motions associated with different loading modes; however, experimental studies on isolated facet joints have primarily focused on investigating tension directed loading [15] [82] [16] [81]. Studies that have applied non-tension loading to isolated facet joints have been limited to examining the facet joint failure response in a single direction at a single rate [79] [74] [10]. Therefore, the objective of this experimental investigation was to investigate the cervical facet joint capsular ligament mechanics (force-displacement response and ligament strain) during sub-catastrophic displacements of isolated facet joints in tension and non-tension modes of loading.

3.1 Methods

3.1.1 Test Specimens and Preparation

Three un-embalmed fresh frozen human cervical spines, from occiput to T1 were acquired from ScienceCare (Arizona, USA) (Table 3.1). 3D computed tomography (CT) scans were used to evaluate the spines for normal anatomy at the facet joints. Cervical spines with musculature were stored at -20 °C until specimen preparation.

Table 3.1: Donor information

Spine	Age	Gender	Height (in)	Weight (lbs)	Cause of Death
A	62	Male	74	115	Respiratory failure
B	33	Male	74	124	Complications of blunt force head injury
C	68	Male	71	134	Respiratory failure, lung cancer

An orthopaedic surgeon isolated the facet joints from the three donor cervical spines. Cervical spines were first thawed for 72 hours in a 5 °C fridge. Once thawed, the surgeon removed musculature with a scalpel, then carefully removed the remaining soft tissues and muscle insertions to expose the capsular ligament. Each spine was then sectioned into C2 - C3, C4 - C5, and C6 - C7 motion segments (Figure 3.1A). All spinal ligaments and intervertebral discs, except for the capsular ligaments, were then removed and motion segments cut through the vertebral bodies and spinous process along the midsagittal plane to create independent facet joint pillars. The spinous process of the superior vertebra was removed at the lamina and the vertebral body of the inferior vertebra was removed at the pedicle (Figure 3.1B). The superior vertebral body and inferior lamina were kept to aid in fixation to the potting fixture and had the additional benefit of being used as anatomical landmarks for alignment.

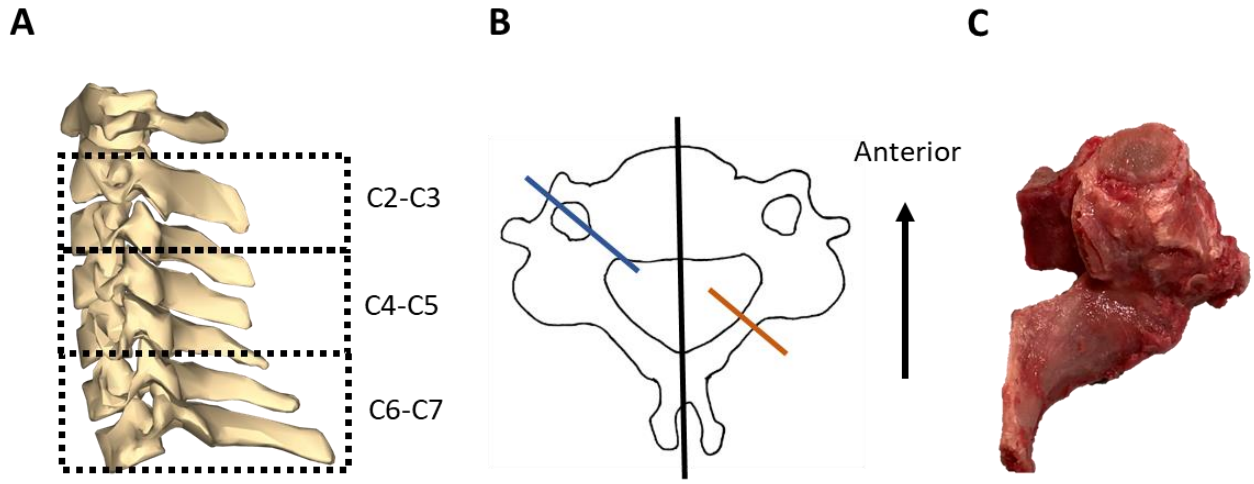

Figure 3.1: (A) Shows how spine was segmented into motion segments (sagittal view). (B) Shows isolation of specimen (axial view). Blue line indicates where inferior vertebrae was cut, and orange line shows where superior vertebra was cut. (C) Shows a representative cadaveric specimen (axial view). Arrow shows anterior direction for (B) and (C). Adapted from [93] and [94].

After isolation, the surgeon evaluated the tissue integrity of the facet joint. Where possible, location and approximate size of any tissue disruption was recorded. The isolated facet joints were subsequently divided into two groups: intact and disrupted. The isolated facet joint specimens were then wrapped in saline-soaked gauze and stored at -14 °C until testing.

A total of ten facet joints were isolated for testing (Table 3.2).

Table 3.2: Specimen information

Specimen	Spine	Level	Side	Disrupted
1	A	C6-C7	L	Yes
2	A	C6-C7	R	No
3	B	C6-C7	L	No
4	B	C6-C7	R	Yes
5	C	C2-C3	L	No
6	C	C2-C3	R	No
7	C	C4-C5	L	Yes
8	C	C4-C5	R	Yes
9	C	C6-C7	L	No
10	C	C6-C7	R	No

Before testing, specimens were thawed overnight in a 5 °C fridge, then at room temperature for approximately 1 hour. The specimen was sprayed approximately every 15 minutes with saline to maintain hydration, beginning when the specimens were thawed until the end of the final test, except for two 20-minute periods while the cement was hardening. Before potting the specimen in cement, the bone was patted dry with paper towel to improve fixation.

To increase fixation, three 1” M4 wood screws were placed in the lamina of the inferior vertebra and three in the vertebral body of the superior vertebra. After placing the screws, the facet joint was palpated and the joint manipulated to identify the facet joint plane. The AP direction (along the plane of facet joint in anterior-posterior direction) was marked using an India Ink marker on the capsule ligament, using a straight-edge as a reference for alignment. These marks were expanded to create a grid of marks that covered the outer capsular ligament. Marks were placed manually.

Specimens were potted in 3" ABS pipe using Modern Materials Denstone cement and aligned manually. To fix the specimen in cement, an articulating arm clamped the inferior vertebra in AP alignment (AP direction vertical) as the cement hardened around the superior vertebra for 20 minutes. After the cement hardened, the LT direction (perpendicular to AP direction in the plane of the facet joint) and tension directions were identified and marked. The specimen was then inverted and suspended such that the inferior vertebra could be potted in cement. The specimen was left for ~40 minutes to allow the cement to harden completely. As the cement hardened, a reference flag was placed in the cement in line with the capsular ligament direction (Figure 3.2).

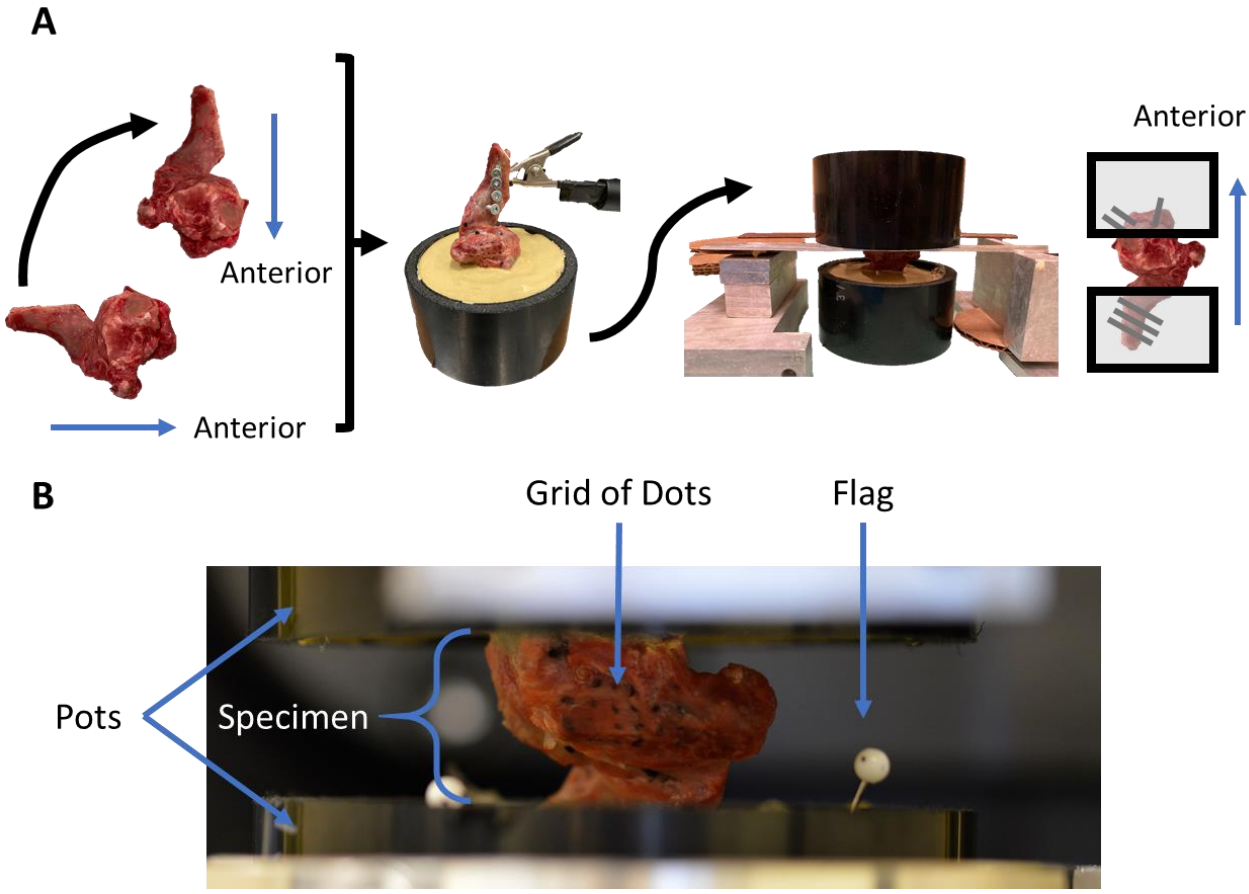

Figure 3.2: (A) Specimen potting workflow. From left to right - align specimen with AP direction vertical; clamp in position and pour cement into superior pot; flip sample over and support while pouring cement into inferior pot (bottom pot). (B) Final specimen setup.

3.1.2 Experimental Procedure

An AMTI VIVO six degrees-of-freedom (6DOF) joint motion simulator (VIVO) was used to apply loading to the facet joint specimens (Figure 3.3A). The VIVO servohydraulic apparatus is capable of 6DOF force and motion control about a defined reference pose. The VIVO load cell was initially zeroed with the baseplate and bottom fixture mounted. The potted facet joint specimens were then mounted to the VIVO using custom fixtures. The superior pot was clamped in the top fixture, with the specimen's tension direction manually aligned with the VIVO y-axis (Figure 3.3A), and then mounted on the VIVO upper actuator. The inferior pot was supported as the VIVO baseplate was raised until a non-zero axial compressive force was recorded in Fz. The inferior pot was fixed to the bottom fixture on the VIVO baseplate. The VIVO baseplate, which provides the three linear degrees-of-freedom, was used to displace the inferior pot during testing.

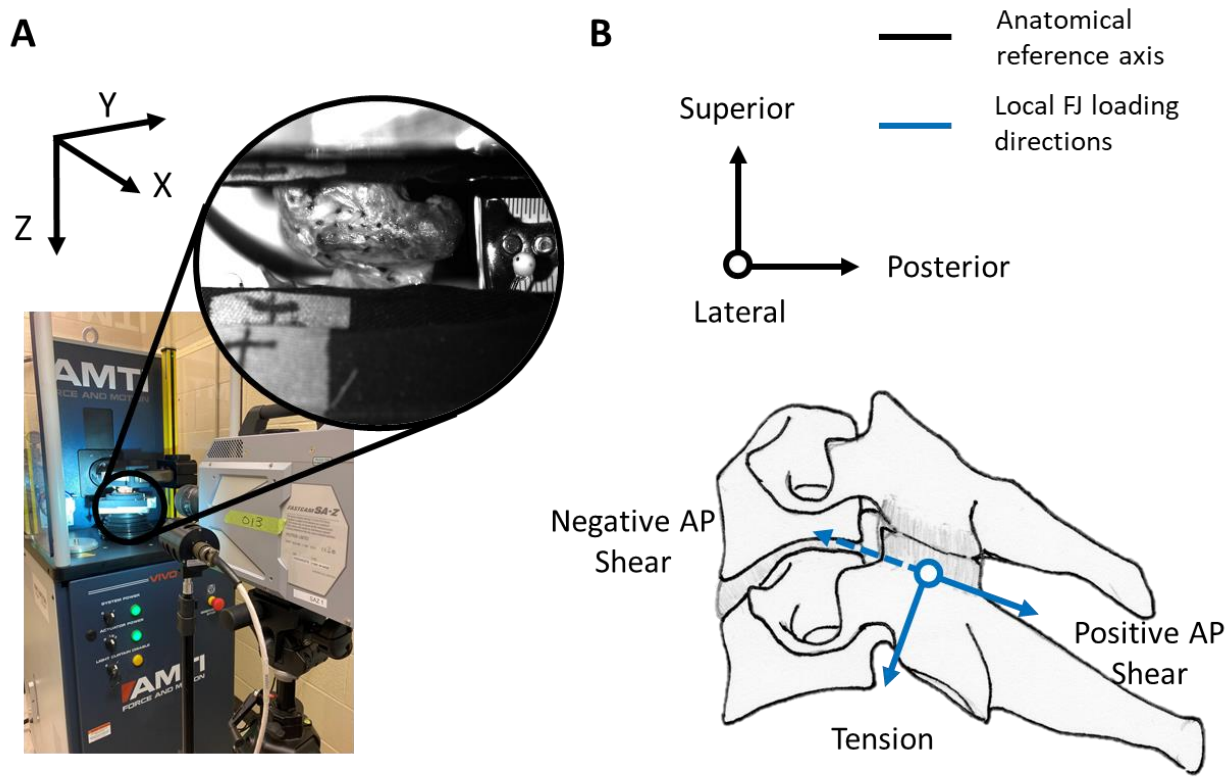

Figure 3.3: (A) Experiment setup highlighting a specimen mounted on the VIVO with respect to the VIVO coordinate system. (B) Anatomical reference axis for motion segment (black). Facet joint loading directions (blue) describing displacement of inferior vertebra. Positive LT shear is out of the page. Note that experiment loading was performed relative to the facet joint loading directions.

A Photron SA-Z high speed camera with a 105 mm lens and a resolution of 1024 pixels x 1024 pixels was used for optical tracking of the facet joint capsular ligament. A high-speed LED light was used for lighting. The camera was calibrated before every test, when the camera was moved, or when the lighting was changed. A calibration image was taken at the beginning of each test with a ruler placed just in front of the capsular ligament.

To record forces and moments about the centre of the facet joint, a Microscribe G2X was used to digitize the origin of the facet joint relative to the origin of the default VIVO coordinate system to define a "reference pose" input position, which defines where the VIVO 6DOF loads are calculated. The VIVO coordinate system was defined by taking three points on the VIVO base that aligned with the VIVO x, y and z coordinates. The VIVO origin was found using three points located on the two arms and center of the baseplate. The facet joint origin was approximated by averaging four points (top and bottom right and left points on the joint). A transformation matrix was then calculated to translate the coordinate system origin from the VIVO origin to the joint center and inputted to the VIVO software as the reference pose.

Loading was applied to the inferior vertebra in the facet joint loading directions (Figure 3.3B). With interest in testing multiple loading directions, the neutral joint position needed to be identified by cyclically loading each specimen in tension, AP shear, and LT shear. In AP and LT shear, the specimen was loaded $\pm$ 2 mm for five cycles at 0.025 Hz. In tension, the specimen was loaded $\pm$ 1 mm for five cycles at 0.025 Hz. Force displacement curves for each direction were then plotted. For AP shear and LT shear, the center of the neutral zone was considered the neutral position. The limits of the neutral zone were manually determined. For tension, the transition from compression to tension in the loading phase was taken as the neutral position (Figure 3.4). The VIVO starting position was then adjusted to match the identified facet joint neutral position for testing.

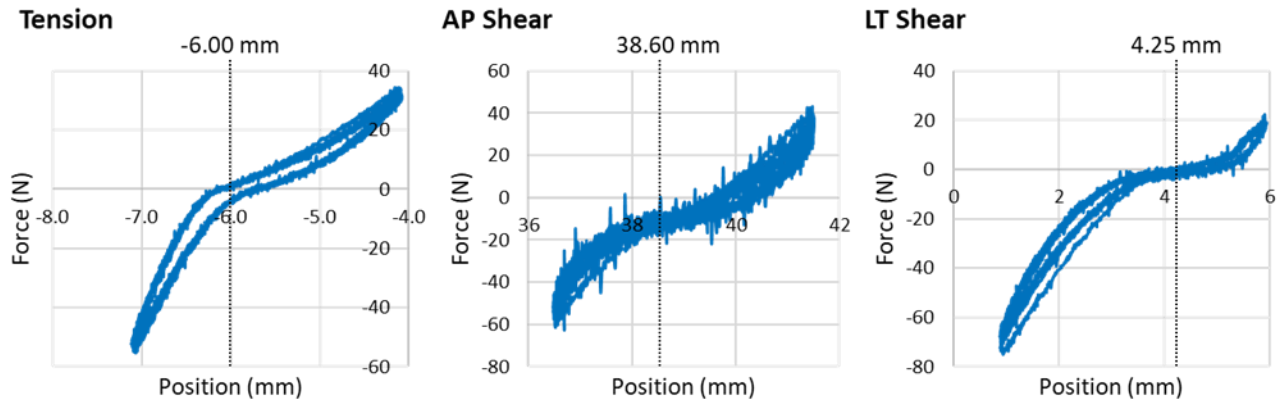

Figure 3.4: Representative example (specimen 10) to determine the neutral positions shown by the dotted lines in low-displacement cyclic loading.

The experimental loading protocol was designed with two factors: (1) direction of loading and (2) rate of loading. Each specimen was loaded in displacement controlled cyclical loading in tension, AP shear, and LT shear directions. Two rates of loading, quasi-static (0.1 mm/s) and high (10 mm/s), were selected based on literature for sub-catastrophic loading and the capabilities of the VIVO. For quasi-static tests, five displacement cycles were applied. For high-rate tests, iterative learning control (ILC) was first performed to identify the appropriate actuator response control settings. This was followed by ten displacement cycles.

In AP and LT shear, sinusoidal loading was applied around the neutral position, with loading starting in the positive VIVO axis directions (Figure 3.5). For AP shear, the VIVO baseplate displaced in the positive z direction (down) first, corresponding to positive AP shear (Figure 3.3B). For LT shear, the VIVO baseplate moved in the positive x direction (towards camera) first, corresponding to positive LT shear. For tension, sinusoidal loading was applied with the neutral position as the minimum displacement. Depending on whether the specimen was a right or left facet joint, loading was applied in the positive or negative y direction respectively, as the facet joint pairs were considered mirror images of each other. Displacements in the non-loading directions were constrained. Note that, due to the sinusoidal waveform, average rates of displacement were reported.

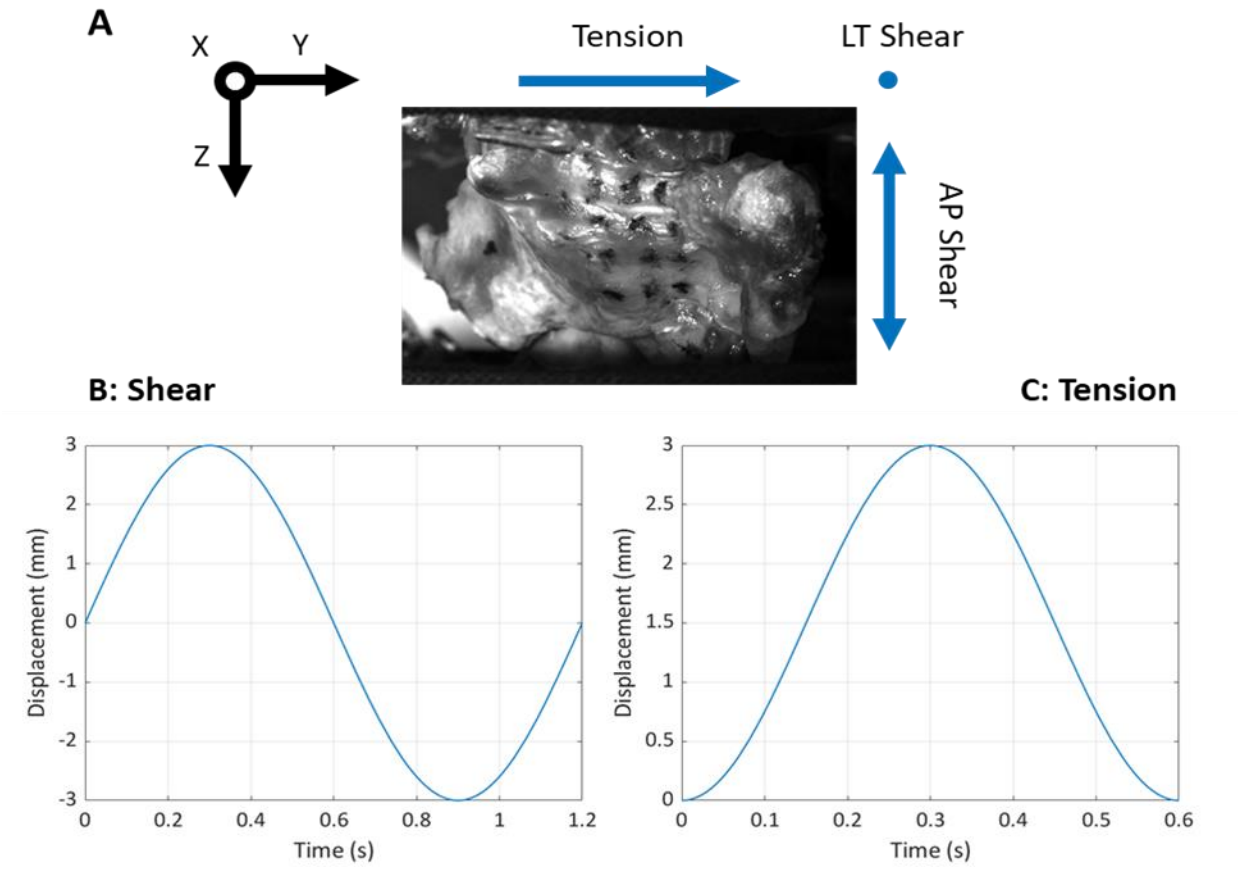

Figure 3.5: (A) AP Shear, LT Shear and Tension loading directions relative to the VIVO coordinate system and visualized on a representative specimen. The specimen is right facet joint so tension loading in positive y-direction. (B) Ideal single cycle for high-rate AP and LT shear and (C) tension to 3 mm. Zero position was the neutral position for the specimens, which is specimen-dependent. At the high-rate, specimens were loaded for 10 cycles. The magnitude was specimen-dependent.

For the testing sequence, each specimen was first tested in quasi-static AP shear and tension followed by high-rate AP shear and tension. The camera was then moved perpendicular to LT shear direction and the specimen tested in quasi-static LT shear followed by high-rate LT shear. The order of application of AP shear and tension was randomized for each pair (right and left) of facet joints. Displacements between 2 mm and 3.5 mm from the neutral position were applied based on sub-failure ranges in literature and refined using the neutral position data to ensure the displacement exceeded the ligament toe region for each specimen.

Following non-destructive loading, specimens were either disrupted or failed in AP shear. Specimens that were tested in AP shear loading first were failed in AP shear at the quasi-static rate (0.1 mm/s). The capsular ligament of specimens tested in tension first were resected in the plane of the joint using a scalpel. For both, the camera was repositioned to record the tests.

Force and position data were recorded by the VIVO at 1000 samples/s at the high-rate and 100 samples/s at the quasi-static rate, except for AP failure testing which was recorded at 500 samples/s. Optical data was captured at 500 fps at the high-rate and 60 fps as the quasi-static rate.

3.1.3 Data Analysis

VIVO force data was shifted to account for any initial offset using the average of the first 20 data points. Regions of compression in the tension loading direction were removed from the raw data by determining the displacements at which the specimens were in compression. Force and displacement data were then run through a Matlab script to separate into loading and unloading phases in the positive and negative directions by identifying maximum and minimum points and where the displacement crosses zero in the displacement vs time graph (Figure 3.6).

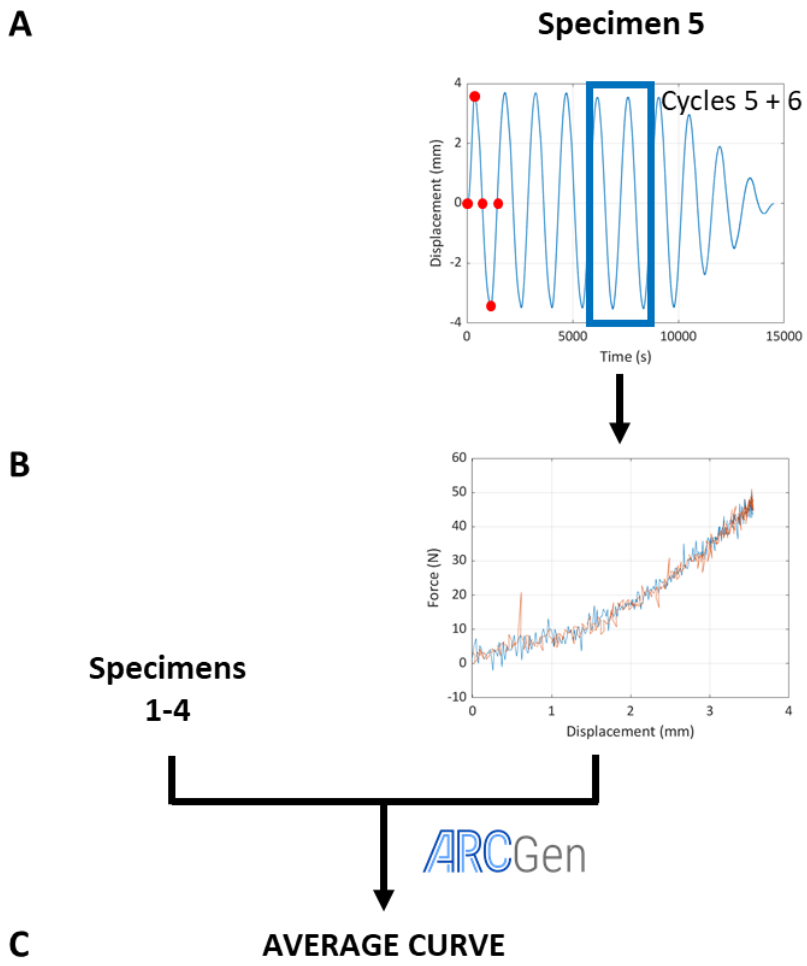

Figure 3.6: A representative example of the data analysis workflow for intact specimens in AP shear at high-rate. (A) Red dots show the identification of maximum and minimum points and where the displacement crosses zero in the displacement vs time graph. These points were used to separate curves into positive loading, positive unloading, negative loading and negative unloading phases. (B) Force-displacement curves for cycles five and six extracted and averaged with cycles five and six of the four other intact specimen using ARCGen to get (C) the average curve for the load condition from all of the tested specimens. The same process is applied for intact and disrupted specimens (separately) loaded in AP and LT shear at high-rate and quasi-static rate. At quasi-static rates, cycles four and five are extracted. For tension, the same process is followed but only have positive loading and unloading phases.

Two cycles from each test were used to calculate the average force-displacement curves. For quasi-static loading the last two cycles, cycles four and five, were used. For high-rate loading, cycles five and six (of ten total cycles) were used for cycle consistency as the VIVO control system ramped displacement in and out. ARCGen (R2023a) [19]was used to calculate the average force-displacement curves and corridors for each load condition (Figure 3.6).

ARCGen is a method developed by Hartlen and Cronin [19] to determine average curves and response corridors based on arc-length re-parameterization and signal registration. Individual signals were first scaled based on the total range of data then re-parametrized with respect to normalized arc-length, a monotonically increasing metric enabling complex signals to be averaged. Signal registration was then used to align signal features. Finally, the average and standard deviation was calculated at each registered point.

To estimate capsular ligament surface strains for high-rate tests in intact specimens during AP shear and tension, video data was first downsampled to 125 fps for fewer frames to digitize. Marker positions were digitized from video data using Tracker software [95] (Figure 3.7).

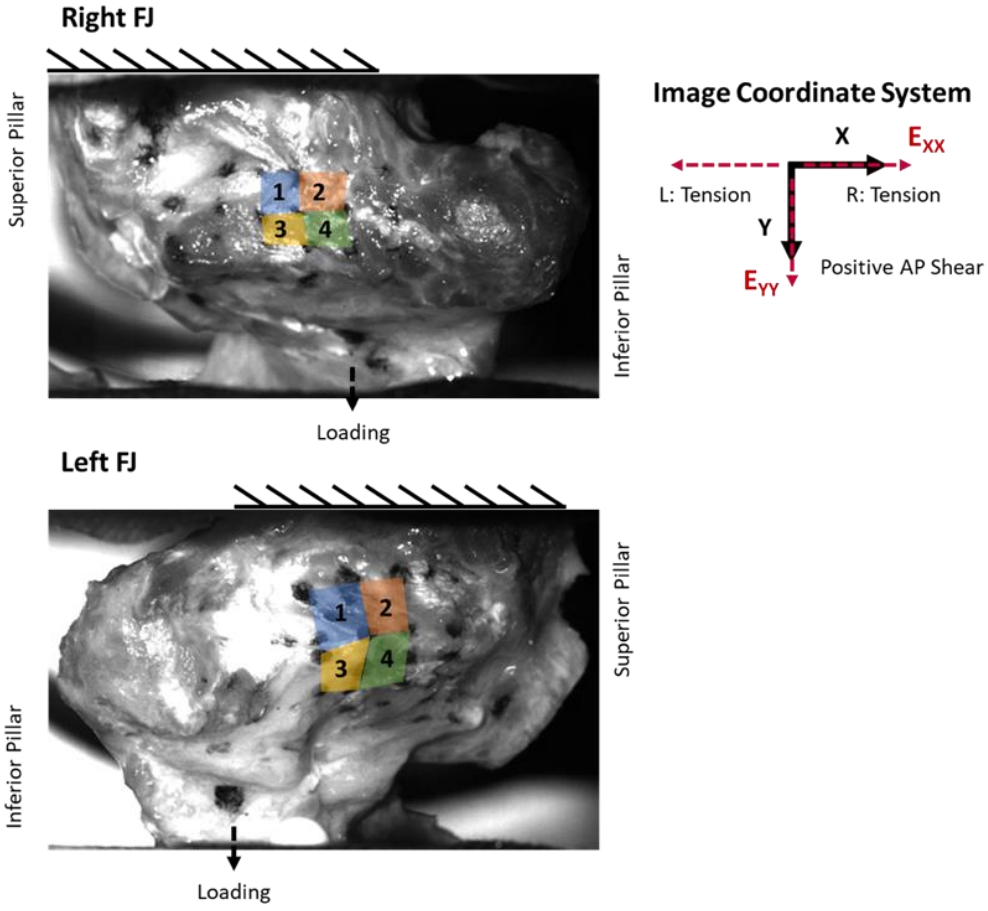

Figure 3.7: The four elements for which Green Strain is calculated shown on a representative right and left facet joint specimen. The right and left facet joints are mirror images; element 1 for the right facet joint is element 2 for the left facet joints and vice versa. In the image coordinate system, tension for the right facet joint is in the positive x-direction and for the left facet joint in the negative x-direction. AP shear is in the y-direction. The E_{XX} component of Green Strain is along the direction of tension and E_{YY} of AP shear.

A Matlab script was then used to create four elements from nine digitized markers on the capsular ligament and to calculate Green strain in each element from cycles one to seven. Green strain was calculated as $\frac{1}{2}(\boldsymbol{F}^T \cdot \boldsymbol{F} - \boldsymbol{I})$, where $\boldsymbol{I}$ is the identity matrix and $\boldsymbol{F}$ is the deformation gradient relative to the initial position of each of the nodes. Before calculating Green strain, the positions were filtered with a two-way 2nd order Butterworth filter with a low-pass cut-off frequency of 0.5 [96].

The cross-correlation function in Matlab was used to align video data with VIVO data using the VIVO displacement and the digitized flag marker in the video. The digitized flag marker position was converted from pixels to positions (mm) based on a calibration image analyzed in Fiji [97], an image processing package.

Fiji was used to estimate the length and width of the incision for the ligament resection test. Length was taken as the linear tip-to-tip length of the long axis of the incision and the width was taken as the largest distance of the incision perpendicular to the length.

3.2 Results

3.2.1 Specimen Preparation

Of the ten specimens prepared, four capsular ligaments were considered disrupted, with a tear through the width of the ligament. Specimen 1 was disrupted on the superior-medial aspect of the outer capsular ligament. Specimens 4 and 8 were disrupted between the laminae. The disruption was inaccessible, so dimensions were not recorded. Specimen 7 was disrupted on the superior right aspect of the outer capsular ligament, likely from being nicked during specimen preparation. The disruption was approximately 1.4 mm by 2.9 mm ellipse. During testing of specimen 5, an intact specimen, the VIVO software crashed. Therefore, only the quasi-static tension and AP shear data were considered for the specimen.

3.2.2 Average Force-Displacement Curves

Average force-displacement curves of intact specimens for the loading phase in the positive direction are shown in Figure 3.8. Tension had higher forces for the same displacement compared to AP and LT shear, which were similar.

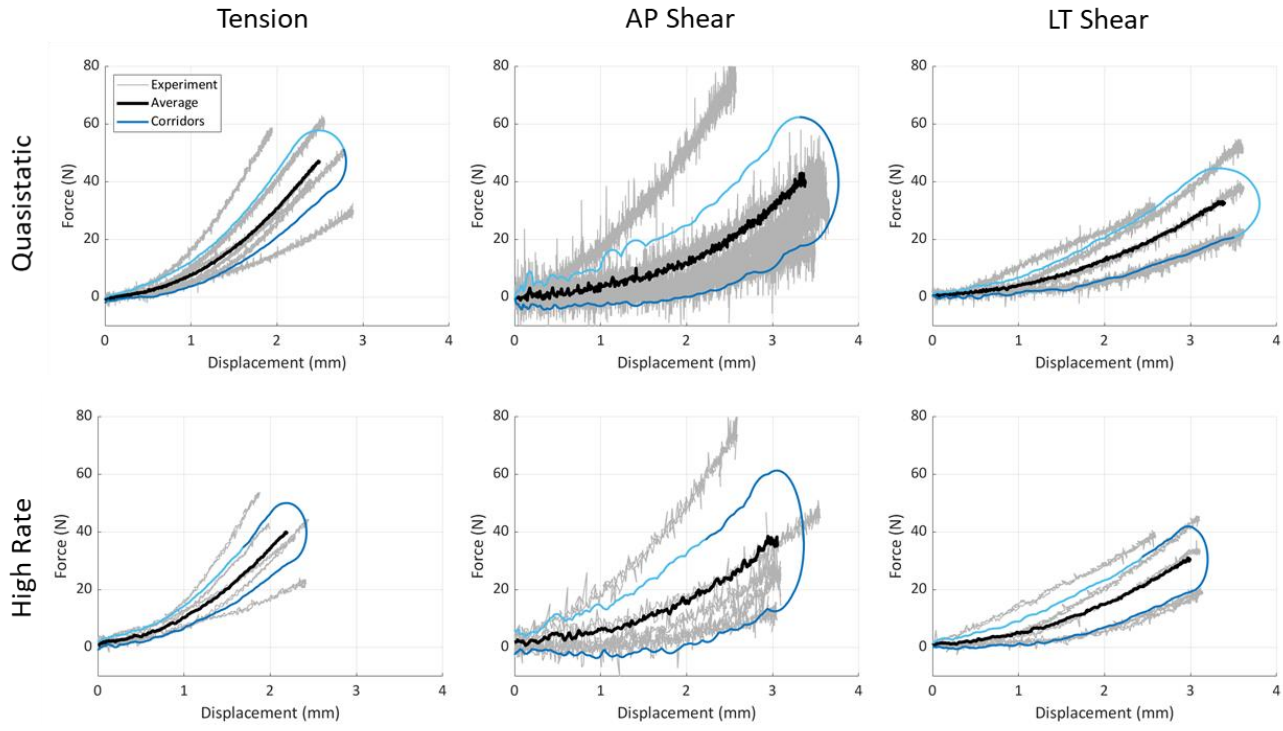

Figure 3.8: Average force-displacement curves and corridors. Original experimental data is shown in grey.

The following series of graphs compared average force-displacement curves under different load conditions (Figure 3.9). The magnitude of force for disrupted average curves was noticeably lower than intact average curves. There was little difference between high-rate and quasi-static loading. The positive and negative directions showed some asymmetry in both AP shear and LT shear and ligament hysteresis could be seen in the positive loading and unloading phases. Note that the AP shear loading direction had the most noise because it corresponded to the VIVO Fz load direction, which had the twice load capacity as the other directions. Analysis of VIVO performance and raw experimental data can be found in Appendix B.

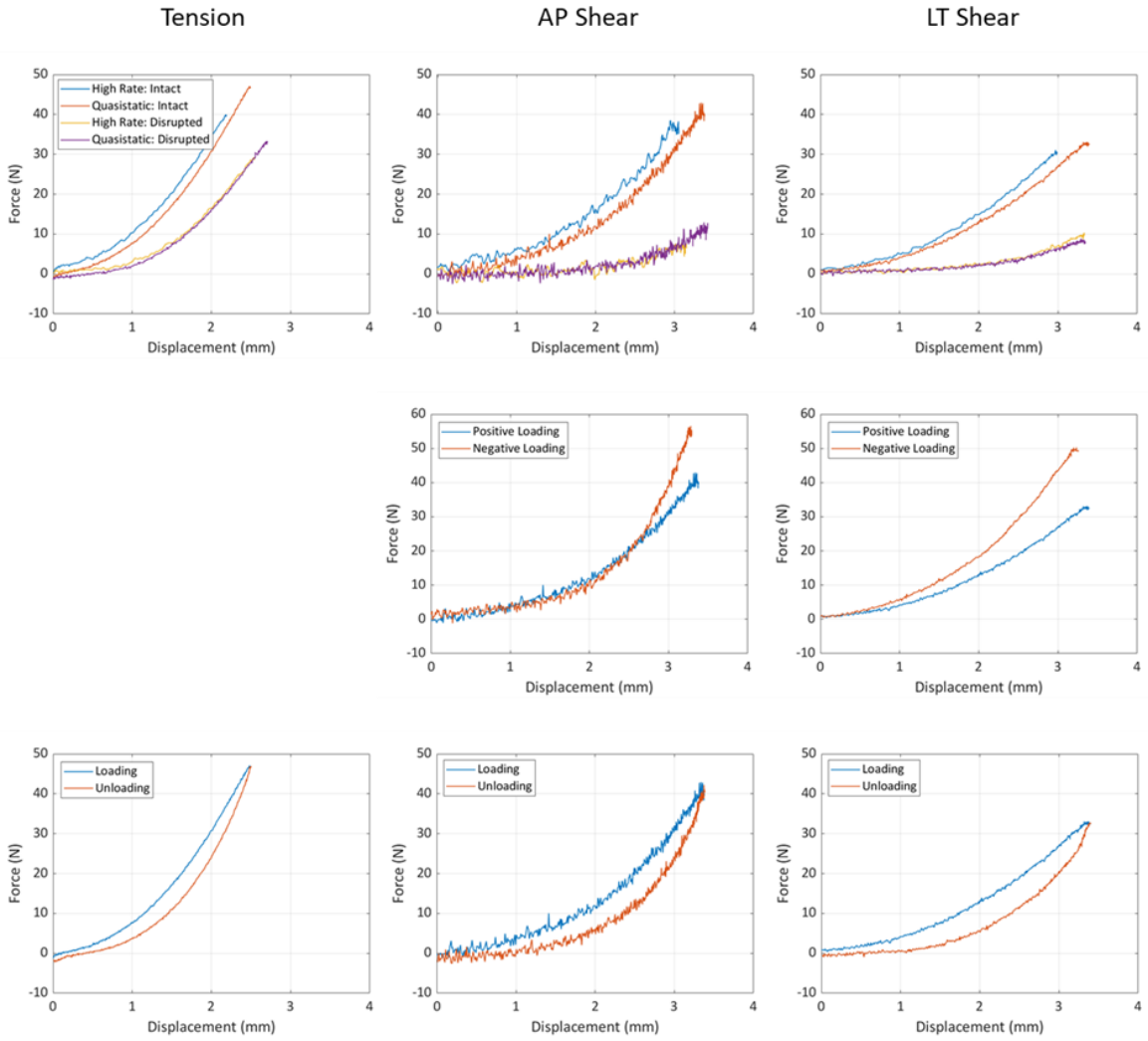

Figure 3.9: Comparing average force-displacement curves. (Top Row) Compares average curves for rate and intact vs disrupted. (Middle Row) Compares average curves for symmetry between positive and negative directions for intact specimen at quasi-static rates. (Bottom Row) Compares average loading and unloading.

3.2.3 Capsular Ligament Strain

Direct comparison of maximum strain between specimens was difficult because maximum displacement varied between specimens. However, trends could be extracted from the strain evolution. Figure 3.10 is a representative set of graphs showing the strain evolution over time.

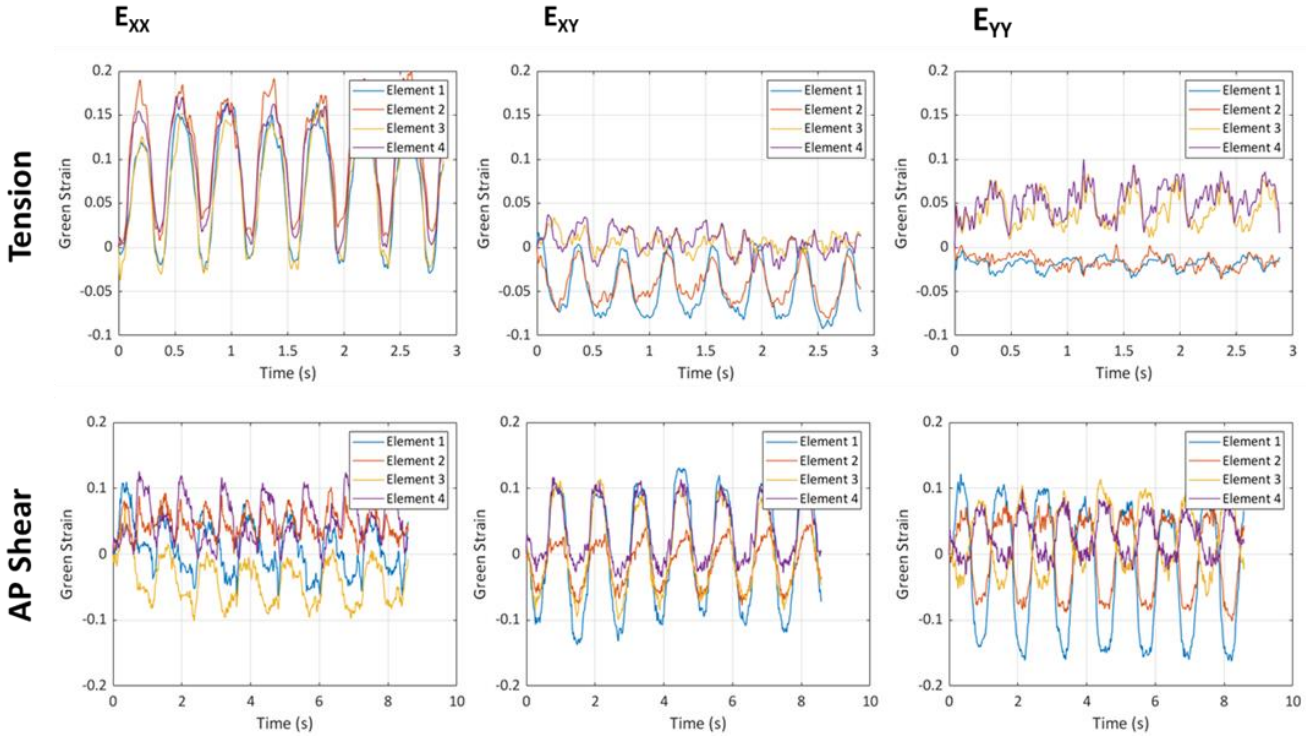

Figure 3.10: Strain evolution over time a representative sample for (Top) tension and (Bottom) AP shear loading.

In tension, elements 1 and 3 and elements 2 and 4 (Figure 3.10), corresponding to the superior and inferior regions, were generally paired; they were in-phase and had similar magnitudes across loading modality and Green strain components. The E_{xx} component of Green strain (aligned with direction of loading) was the most well-behaved; it was typically in-phase with well-defined cyclic behavior in all elements. The strain in E_{xx} was also greater than the other components when comparing the magnitude of the highest element in each component. In the E_{yy} and E_{xy} components, the cyclic behavior was less well defined in some or all of the elements, with greater variability between specimens.

In AP shear, the E_{xy} (shear) component of Green strain showed well defined cyclic behaviour. All elements were typically in-phase, although the shear magnitudes varied and the element with the greatest shear was different between specimens. In some specimens, the E_{yy} component displayed well defined cyclical behaviour. In the other specimens, there was either high variability or out-of-phase responses between elements. In the E_{xx} component, specimen typically displayed variable or out-of-phase responses between elements. The magnitude of shear in E_{xy} was not noticeably greater than E_{xx} and/or E_{yy}.

3.2.4 Capsular Ligament Resection

As an exploratory study, four of the specimens were resected to investigate capsular ligament prestrain. The average ratio of width to length of the incisions was 0.26 with a range of 0.22 to 0.28. Note the width was measured at the maximum width of the incision, usually at the mid-length.

3.3 Discussion

Scatter in the experimental data was observed between specimens in the same loading condition, even between specimens from the same donor. Several factors may have contributed to this, including differences in age of the specimens, inter-specimen variability (geometry, thickness of the capsular ligament, composition and orientation of collagen fibers), level differences [15] and anatomical asymmetry between right and left facet joints [98]. Data reported for the AP shear direction had more noise because the VIVO had a greater load capacity (lower sensitivity) in this direction. Note that specimens were loaded in the facet joint loading directions which would result in mixed loading of a motion segment relative to the anatomical reference axis.

There was very little difference between average force-displacement curves at quasi-static and medium rates for all loading directions. As ligament response was generally considered to be rate dependent, this result was unexpected but could be partially attributed to the application of sinusoidal load curves. The maximum rate of displacement was only achieved for a small portion of the cycle; for the shear load directions the maximum rate of displacement occurs in the neutral region of the ligament where it may not have as much effect. Sinusoidal load curves were used to reduce VIVO displacement error at the maximum and minimum displacements, where displacement changed direction.

The average tension force-displacement curve exhibited lower forces than have previously been reported by Mattucci et. al., with an average force at 2 mm of 34 N compared to Mattucci's 105 N for a strain rate of 0.5 s^{-1} (about 2 mm/s) and 195 N at 20 s^{-1} (about 60 mm/s) [15].

There were several factors that may have contributed to these discrepancies. The first was the age of the specimens, which was known to affect the tissue mechanical properties. Mattucci's study only included specimens below 50 years while the age of the specimens in this study were 33, 62, and 68. Secondly, different load regimes were investigated. While Mattucci tested the capsular ligament to failure, this study applied cyclical loading in the physiological range below sub-failure of the specimens. Additionally, the number of donors and the total number of specimens was much lower in this study than in Mattucci's study, covering a smaller subset of the populations and capturing less inter-specimen variability. Finally, the neutral position of the

specimens was defined differently. In literature, including the study by Mattucci et. al., the initial position of facet joints was defined by applying a small load to the joint, typically 5 N. In this study, the neutral position was found by applying a low magnitude load in all directions from the initial position to identify the neutral position. This could explain the horizontal shift in the curve compared to Mattucci's data.

To confirm, a supplementary study was performed on two additional specimens (Appendix C). First, the specimens were loaded in AP shear and tension at the quasi-static rate according to the methods reported in this study. The specimens were then loaded to failure in tension at a quasi-static rate to replicate Mattucci's study. The tension to failure data was lower than Mattucci's average but fell within Mattucci's spread of data. Considering the specimens were older than those used in Mattucci's study, this result indicated the response of the specimens agreed with the data reported by Mattucci. In cyclical AP shear, the results of the specimens were higher than the average force-displacement curve reported in the study but again fell within the range of curves. Notably, Mattucci reported higher forces than other sources in literature. Ivancic et. al. [82], for example, reported forces at 2 mm of displacement ranging from 25 N to 202 N when testing at a peak rate of 723 mm/s. Many reported specimens were clustered between 52 N and 100 N, which is more comparable to the 34 N reported in this study.

The AP shear average force-displacement curves were comparable to the series of studies by Winkelstein's group. In one study [10], isolated facet joints were loaded until failure in posterior shear at 0.01 mm/s, with reported force-displacement curves showing forces at 2.5 mm to be between 10 N and 51 N. The facet joint was positioned in the same orientation as a previous flexibility test of the motion segment and then loaded posteriorly, while in this study, the inferior facet pillar was loaded anteriorly and posteriorly relative to the superior facet pillar in the plane of the facet joint, so joint alignment may have contributed to discrepancies. In a subsequent study by Winkelstein's group [79], the average force at 2.5 mm was reported to be 16.08 N when the superior vertebra underwent posterior retraction. Finally, the superior vertebra was loaded at 0.5 mm/s until failure such that the inferior facet translated posteriorly relative to the superior facet [74]. At 2.5 mm, the average force-displacement curve reported a force of 22.8 N. These studies were performed at low rates in a single shear direction; however, both quasi-static and

high rates found in this study fell within their reported ranges. There is no data with which to compare LT shear; however, average force-displacement curves for AP and LT shear show similar force magnitudes.

Heterogeneous collagen fiber orientation has previously been reported for cervical capsular ligaments, with increased alignment in the stretch direction during tensile loading [8]. As collagen is the primary load-bearing structure in ligaments, collagen alignment across the joint in tension would suggest higher loads are supported in this direction, which was supported by the higher forces in average tension force-displacement curves compared to AP and LT shear. However, forces in AP and LT shear were shown to be of the same order of magnitude as tension, which may be attributed to the heterogeneous collagen fiber orientation. Considering the capsular ligament plays a role in guiding and restricting the complex motion of the facet joint, it is important for the capsular ligament to support relatively high loads in multiple modes of loading for joint stability.

Considering the symmetry between positive and negative loading directions, differences in the length and slope of the toe region and the slope in the linear region could be identified. The toe regions for AP and LT shear were similar in the positive and negative direction, although in AP shear the toe region in the positive loading direction had a steeper slope. This was consistent with individual specimen force-displacement curves. However, the slopes of the average curves outside the toe region were noticeably different. In AP shear, the negative loading direction had a much stiffer response, particularly after 2.5 mm. Video recordings of the tests show that the superior bone came into contact with the inferior potting cement for several specimens. This contact would contribute to the higher force, and therefore the higher stiffness seen for AP shear. In LT shear, the negative direction had a steeper slope than the positive direction, although the slopes were more comparable than in the AP shear direction. The ligament may stiffen (steeper slope) in the LT shear positive loading direction with greater displacement, however the displacements in this experiment were not large enough to establish this. Alternatively, there may be a physical asymmetry in the loading of the capsular ligament, potentially due to non-uniform geometry of the joint or heterogeneous mechanical properties around the ligament.

The average force-displacement curves did not go through zero force as would be expected. This may be due to forces that were applied when mounting the specimens. The VIVO load cell was zeroed before the specimens were mounted, as the top and bottom fixtures could not be in contact. When the specimens were mounted and fixed, small loads were applied. These small loads should have been addressed when the forces were shifted to account for offset in data analysis but may not have been entirely accounted for. For tension in particular, data when the joint was in compression was removed and forces not re-zeroed, which may have also contributed to non-zero loads.

The reported average force-displacement curves only considered forces recorded in the primary axis, however off-axis forces were also observed. For the intact specimens, off-axis forces were lowest for loading in tension, with off-axis forces between 2.5% and 40% of the maximum force in the tension direction. The off-axis force was usually higher in LT shear than AP shear direction. For LT and AP shear, off-axis forces were usually higher in the tension directions. For LT, the off-axis forces ranged from 15% to similar magnitudes to the LT direction (in specimen 3). In AP shear, the off-axis forces ranged from 4% to similar magnitudes as in the AP shear direction (in specimen 10). Generally, higher off-axis forces occurred in the positive loading direction.

Specimen alignment was one factor resulting in off-axis forces, as misaligned facet joints displaced in LT shear, for example, could load the ligament in tension (or compression if the opposing pillars come into contact). Other potential sources of off-axis forces include friction, the presence of osteophytes (which could cause redirection of loads), ligament geometry and insertion points, bone contact, and the morphology of the facet joint (not a flat plane). Off-axis forces could be considered in the analysis using a vector approach. With this approach, both the magnitude and the direction of the average force vector would change.

Isolating the facet joint was challenging, and disruption of the capsular ligament occurred in just under half of the specimens. However, the disrupted specimens provided the opportunity to investigate the impact of disrupted ligaments on the force-displacement response. In every load condition, the disrupted average was lower than the intact average force-displacement curve, as would be expected. In disrupted specimen, load transmission would be disrupted reducing the

recorded forces. The average force-displacement curve for disrupted specimens exhibited a shifted and extended toe region, suggesting load was not carried by the capsular ligament until higher displacements. Degree and position of disruption were not controlled so conclusions for specific types of disruption cannot be drawn. However, the observations of the effect of disruptions could have implications in joint stability after sub-catastrophic capsular ligament damage.

Comparisons between intact and disrupted specimens could be made based on individual specimen force-displacement curves. Two specimen pairs had one disrupted specimen and one intact specimen, allowing for direct comparison of the effect of disruptions. The first pair were specimen 1 and 2 from donor A, where specimen 1 was disrupted on the superior-medial outer capsular ligament. There is little effect in tension, but the force in the disrupted specimen in LT and AP shear was lower, particularly in the positive direction. In LT shear, the force at 3 mm of the disrupted specimen was 30% of the intact in the positive direction and 80% in the negative direction. In AP shear, the force at 3 mm of the disrupted specimen was 0.4 of the intact specimen in the positive direction and is similar in the negative direction. Note that in negative AP shear, the inferior bone made contact with the superior potting cement, so the contact force may dominate the response.

The second pair were specimens 3 and 4 from donor B, where specimen 4 was disrupted between the laminae. In tension, the force of the disrupted specimen at 2 mm was about 40% of the intact specimen. In LT shear, the force of the disrupted specimen at 2.5 mm was 10% of intact in the positive direction and 40% in the negative direction. Finally, in AP shear the force of the disrupted specimen at 2.5 mm was 10% of the intact specimen in the positive direction and 70% of the negative direction. This suggested the location of the disruption influenced the direction of loading that was compromised, with the disruption between the laminae decreasing the recorded force in all direction when compared to the disruption on the outer ligament.

The reported strain fields indicated subject-specific heterogeneous strain patterns. Heterogeneous collagen organization in cervical capsular ligaments [8] may have contributed to the strain gradient across the ligament. Non-uniform fiber alignment and capsular ligament

geometry may contribute strain being measured in the non-loading directions. Additionally, while the E_{xx} component of Green strain in the evaluated ligament region was relatively homogeneous in several specimens, the strain gradient between elements was generally heterogeneous in magnitude and/or direction. Heterogeneous magnitude was shown by the varying magnitude between elements in a single specimen and heterogeneous direction was shown by out-of-phase strain evolution between elements, particularly in components not along the primary loading direction. Non-uniform geometry, various insertion points, and interaction with underlying body anatomy may have also played a role in the strain gradient. Heterogeneous strains may have implications for inducing pain, with higher local strains potentially activating nociceptive neurons [8]. The strain fields reported here were too coarse to spatially determine maximum local strain. Markers were placed manually, however strains were not averaged so differences in marker placement between specimen would not affect observed trends.

The exploratory study on ligament resection suggested the capsular ligament was under prestrain in the neutral position, as the ligament pulled back when incised. This supports literature findings that the lumbar capsular ligament shrinks when a section was cut away from the joint. [73] The current setup was designed for ligament loading and was not conducive for the resection study. The location and length of incisions was not consistent between specimens and the ligament was not cleanly cut through on the first attempt. However, it did indicate ligament prestrain in the capsular ligament would be important to investigate further.

3.4 Limitations

Typical limitations of cadaveric studies also applied to this study, namely limited number of specimens and their older age. Each of the individual facet joint specimens were sourced from three donors, with 60% of the facet joints being from a single donor. Of the disrupted specimens, 67% were from a single donor. Additionally, tissue quality was a key concern. Tissue from elderly donors is likely to have degraded over time, which could result in micro-tears that were not detected.

The cause of death of the youngest donor (33-years-old) was complications from head trauma which likely disrupted capsular ligaments in levels above C6 - C7 and may also have resulted in undetected damage to the C6 - C7 levels used in testing. Specimen 3 was of particular concern, as a potential disruption was observed in the tension video post-processing, although it could be the outer layer of soft tissue separating from the capsular ligament. When considering the force-displacement data of this specimen, the AP shear force was lower than tension force, but quite similar in magnitude (about 50 N compared to 58 N at 2 mm). It was not possible to confirm whether the specimen was disrupted as it was destructively tested. This specimen was kept in the intact group because it recorded much greater forces in all loading directions compared to specimen 4, its pair that had a confirmed disruption between the laminae. However, the force in tension may be underestimated.

Limitations specific to this study included specimen preparation and experiment protocols. Firstly, testing was performed at room temperature, where literature has reported that ligament biomechanics are affected by temperature. On top of which, specimen preparation was a challenging and delicate process. During specimen preparation, disruption of the capsular ligament occurred most frequently during final modifications to the specimen before potting. Additional training with a larger number of specimens in future studies may reduce the frequency of these disruptions.

Specimen alignment during potting was one of the most challenging steps and was inconsistent due to inter-specimen variability and technical challenges. The facet joint was surrounded by the capsular ligament, making visual alignment impractical. Alignment was performed based on joint

movement but was subject to human error. Additionally, the structures used to clamp each specimen in alignment while potting had limited fine manipulation, increasing error in alignment. Developing a jig capable of consistently aligned specimen would be helpful.

The experiment protocol kept more of the bony structure (the superior vertebral body and inferior lamina and spinous process) to increase fixation of the specimen. However, this limited the line of site to the inner capsular ligament; the strain of the inner capsular ligament was not captured by the camera. Additionally, only one camera was used to record marker displacements, which meant only 2D strains could be approximated, although the capsular ligament is a 3D structure.

During experiment protocol development, sinusoidal loading was applied based on VIVO performance and capabilities. However, this mode of loading limited the target rate to a small portion of the cycle. To achieve extended displacements at a target rate, linear displacement would be more appropriate. However, the VIVO setting would have to be optimized and the performance investigated. With respect to the sinusoidal loading, VIVO performance was generally good; however, for the high-rate tests there was some error when ramping in and out and when changing direction. At rates nearing the limits of the VIVO, it may be necessary to pad test with cycles at the beginning and end such that the cycles for analysis have sufficiently low error.

Finally, reported displacements used actuator displacements of the VIVO rather than movement of the vertebral body itself. The error from using actuator displacements was about 0.4 mm (typically closer to 0.3 mm) in AP shear, corresponding to 11% of the maximum displacement. In tension, the maximum relative movement was about 0.5 mm, corresponding to about 17% of the maximum displacement (Appendix B). Meanwhile, error in the optical digitization used to estimate ligament strain was about 0.15 mm and was partly due to the semi-automatic tracking of markers (Appendix B).

3.5 Conclusion

Using the AMTI VIVO, six intact specimens and four disrupted specimens were tested in tension, AP shear and LT shear at two different rates. Further applications of the experimental force-displacement data, including disrupted specimens and unloading curves, could be applied to models in the future. Additionally, prestrain in the capsular ligament was experimentally observed, and identified as an important contribution that should be further evaluated.

Chapter 4 Evaluation of a Computational Human Body Model Facet Joint

Computational human body models (HBMs) can be useful tools to predict tissue response under different loading scenarios. The objective of this computational chapter was to examine and compare the response of the cervical facet joint implementation in the GHBMC 50th percentile male model (M50) and two proposed alternative capsular ligament implementations to experimental data.

4.1 Methods

4.1.1 Models

The GHBMC M50 right C4 - C5 facet joint was extracted from the full body model (Figure 4.1A). The first facet joint extraction was the isolated facet joint (FJ_{E1}) used to replicate the boundary conditions used in Mattucci's testing (Figure 4.1B). The second facet joint extraction was the facet joint with additional bony structures (FJ_{E2}) (Figure 4.1C) used to replicate the boundary conditions in Chapter 3. Two enhancements to the capsular ligament implementation were investigated using the FJ_{E2} model: (1) adding additional 1D elements in a diagonal formation (FJ_{E2_Di}) (Figure 4.1D); and (2) using 2D shell elements (FJ_{E2_Sh}) (Figure 4.1E).

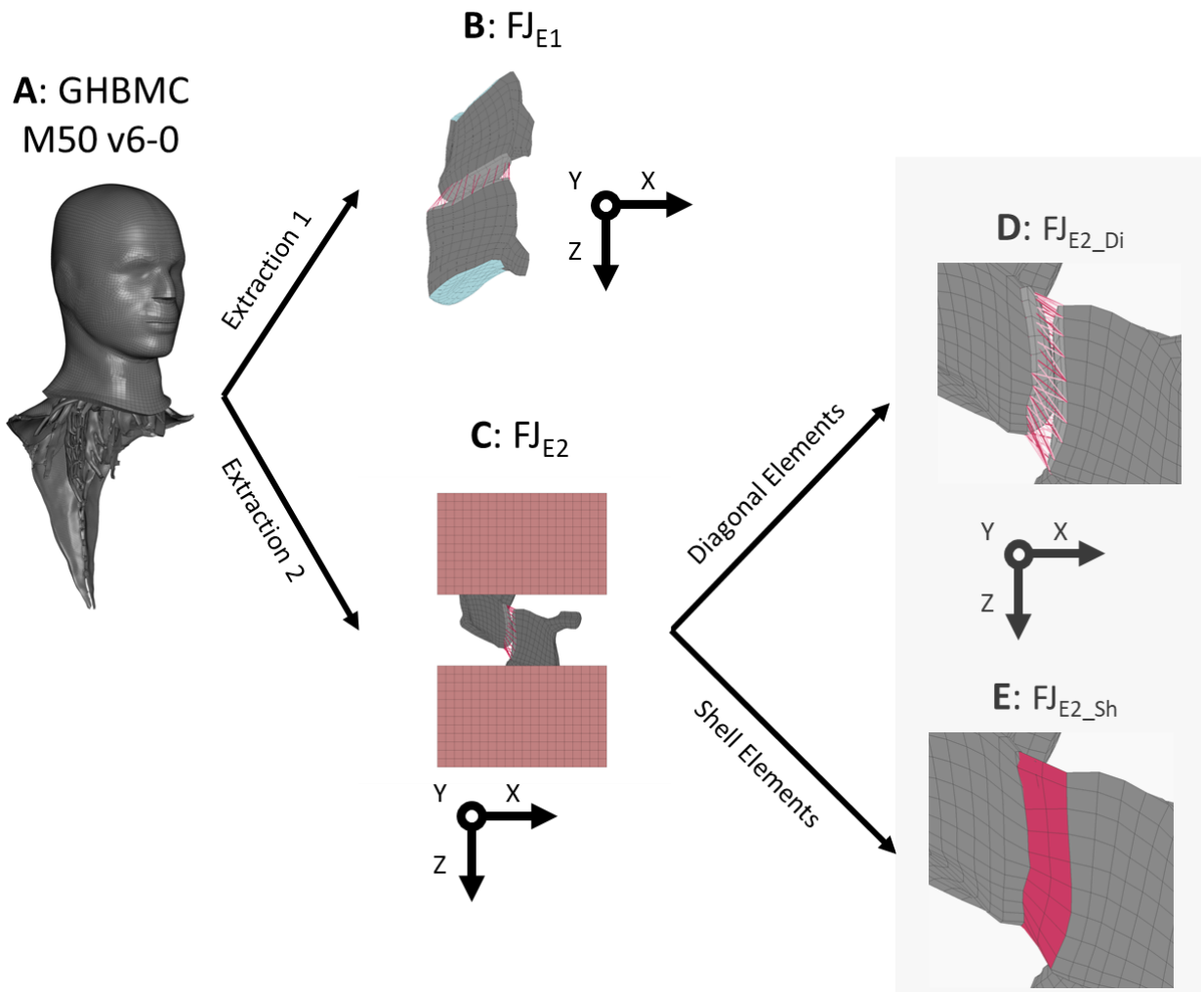

Figure 4.1: Facet joint models including: (A) the GHBMC M50 v6-0 model; (B) the FJ_{E1} model extracted from the GHBMC model used to compare to Mattucci's data in tension; (C) the FJ_{E2} model extracted from the GHBMC model, reoriented and potted to replicate the experiment from Chapter 3; (D) the FJ_{E2_Di} model with diagonal elements; and (E) the FJ_{E2_Sh} model with shell elements representing the CL. Models with enhancements to the GHBMC M50 v6-0 model bounded in grey box.

Extraction of the FJ_{E1} Model

The right C4 - C5 facet joint was extracted from the GHBMC M50 v6-0 model at the pedicle and lamina to replicate specimen preparation in the study by Mattucci [15]. The facet joint tissues from the GHBMC model (cortical and cancellous bone, cartilage and capsular ligament (CL)) were unchanged except for the endplates, which were converted to a rigid material model in order to apply boundary conditions to the facet joint. The orientation of the facet joint was not modified from its orientation in the GHBMC model. The FJ_{E1} model was solved using a commercial finite element code (LS-DYNA R12.0, double precision).

Extracting the FJ_{E2} Model

The right C4 - C5 facet joint was isolated from the GHBMC M50 v6-0 model. To recreate the experiment specimen preparation from Chapter 3, the left half of the C4 - C5 motion segment was deleted. The C5 vertebral body was then deleted at the pedicle and the C4 spinous process deleted at the lamina. Potting material was modelled with solid elements measuring 2.5 mm on each side, a similar size to the elements of the bony facet joint. A total of 4800 elements were used for the potting material. The material model for the potting was piecewise linear plastic with material properties given in Table 4.1.

Table 4.1: Material properties of the linear plastic potting material for FJ_{E2} Model. [99]

	Density (kg/mm^3)	Young's Modulus (GPa)	Poisson's Ratio	Yield Stress (GPa)
Baseline	2E-06	2.2	0.34	1E6

Rigid plates comprising of shell elements were added to the inferior surface of the C5 potting and the superior surface of the C4 potting, with the rigid plate sharing nodes with the potting material. Alignment was performed by manually rotating the facet joint to mimic the position of the experimental specimen in the potting material. The facet plane was vertical with the AP direction (along the plane of facet joint in anterior-posterior direction) aligned with the z-axis, the LT shear direction aligned with the x-axis, and the tension direction aligned with the y-axis. A solid-in-solid constraint was applied between the solid elements of the facet joint bone and the potting material. See Appendix D for details on model development. The model was solved using a commercial finite element code (LS-DYNA R12.0, double precision).

4.1.2 Evaluation of the FJ_{E1} Model in Global and Local Tension

The first step in evaluating the GHBMC facet joint was to compare the FJ_{E1} model to Mattucci's experimental data. To replicate Mattucci's experiment in the FJ_{E1} model, two coordinate systems were defined. The first coordinate system was the global coordinate system defined as in the GHBMC model. The second coordinate system was the local coordinate system defined in the plane of the facet joint. The local coordinate system x'-axis was defined by two nodes on the C5 facet pillar that were approximately in the anterior-posterior direction. The z'-axis was then

defined by the closest distance between the midpoint of two nodes on the C4 facet pillar and the x'-axis, and finally the y'-axis by the cross product between the two. Tension was then defined as the negative 'z' direction in either the global or local coordinate system (Figure 4.2).

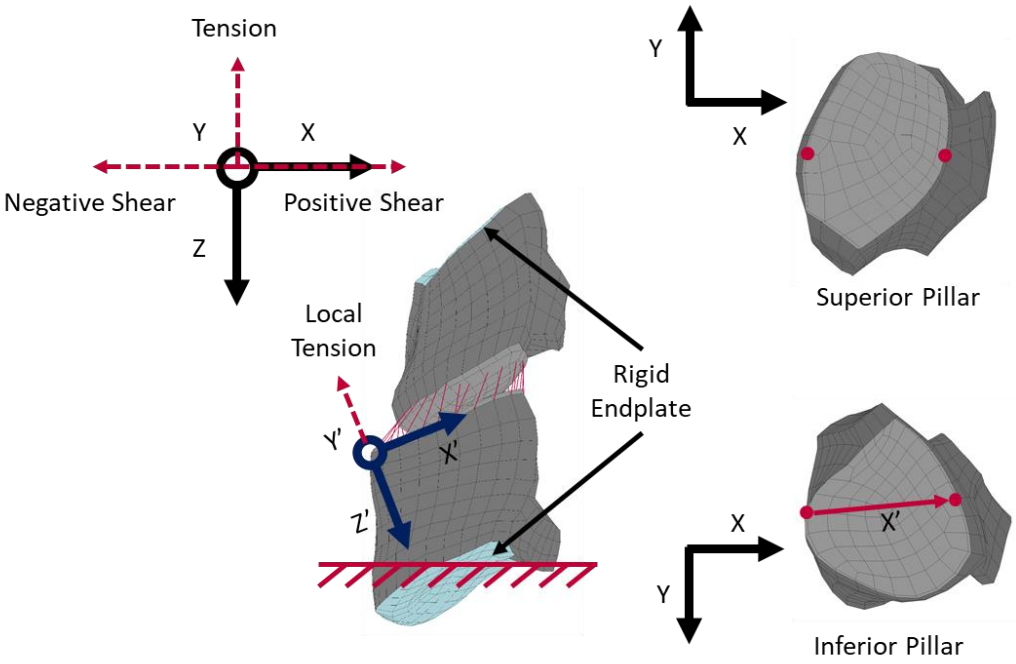

Figure 4.2: Global vs local coordinate systems for the FJ_{E1} Model. The global coordinate system is shown in black, with the red dashed arrows showing loading directions. The local coordinate system is shown in blue superimposed on the facet joint with local tension shown with the red dashed arrow. The axial views to the right show the nodes used to create the local coordinate system.

The boundary conditions were set up such that the C5 rigid endplate was constrained in all translational and rotational degrees of freedom and the C4 rigid endplate was constrained in all translational and rotation degrees of freedom except the translational tension direction (z-direction). Velocity-based loading was applied with a 0.5 ms ramp-up at 0.002 mm/ms based on the quasi-static strain rate reported by Mattucci (0.5 s^{-1}) and a ligament length of 4 mm.

The resultant displacement and resultant force of the C4 rigid endplate were extracted in the global coordinate system and compared to the average force-displacement curve reported by Mattucci at each rate.

4.1.3 Evaluation of the FJ_{E1} Model Capsular Ligament Elements in Joint Shear

The FJ_{E1} model was loaded in positive and negative shear, with shear defined as displacement in the global x-axis (Figure 4.2). The C5 rigid endplate was constrained in all translation and rotational degrees of freedom. The C4 rigid endplate was unconstrained in all degrees of freedom and was loaded separately in the positive and negative x-axis at 0.002 mm/ms.

The length and forces of a subset of capsular ligament elements distributed around the facet joint were monitored.

4.1.4 Evaluation of the FJ_{E2} Model Force-Displacement Response Compared to Chapter 3 Experimental Data

The FJ_{E2} model was loaded in AP shear, LT shear, and tension to replicate the experiment tests from Chapter 3 (Figure 4.3).

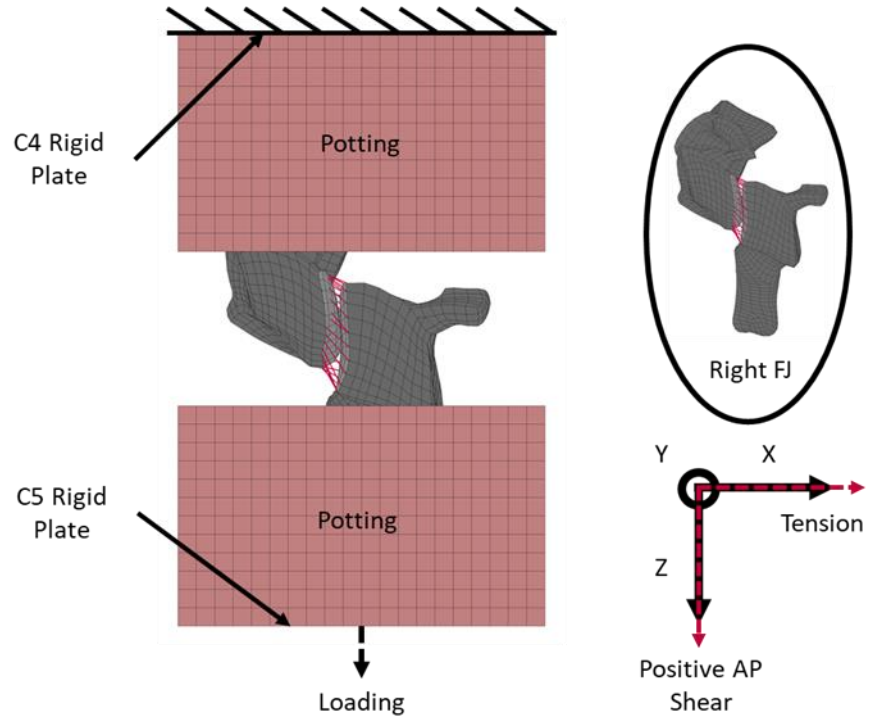

Figure 4.3: Boundary conditions of the FJ_{E2} model. The C4 rigid plate was fixed and the C5 rigid plate was loaded in AP shear, LT shear and tension as shown overlaid on the coordinate system. The circled region shows the orientation of the facet joint without potting.

To load the model, both the C4 and C5 rigid plates were constrained in all rotational degrees of freedom and two translational degrees of freedom, with the unconstrained degree of freedom being the loading direction. The C4 load curve in the unconstrained degree of freedom was set to 0 such that the C4 rigid plate was constrained in all degrees of freedom. Prescribed displacement was applied to the C5 rigid plate in the unconstrained degree of freedom to replicate the experimental boundary conditions. As the experimental data showed very little difference between the quasi-static (0.1 mm/s) and high rate (10 mm/s), only the high-rate loading was simulated in the model with displacements to 3 mm in AP and LT shear and 2.5 mm in tension (Figure 4.4). The C5 plate rigid body displacement and the C4 plate force in the loading direction was extracted. The C4 plate force was extracted rather than the C5 plate as it had a much cleaner signal, but the magnitude of the force was the same as the C4 plate (equal and opposite forces).

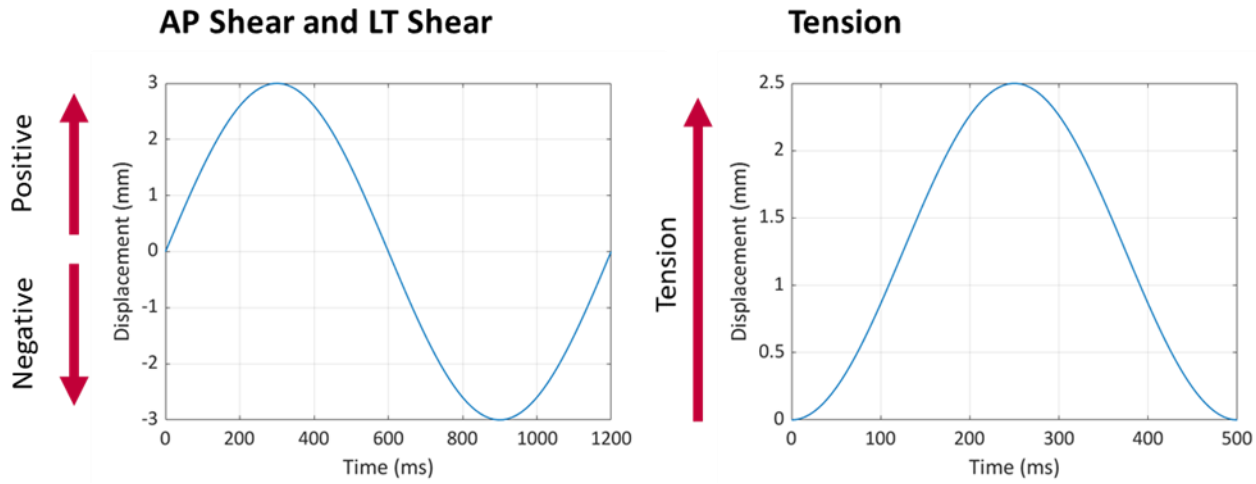

Figure 4.4: Prescribed displacement of C5 rigid plate to replicate Chapter 3 loading.

To evaluate the GHBMC facet joint in shear loading, the output force-displacement curve of the FJ_{E2} model was compared to the average force-displacement curves reported in Chapter 3. Note that only the loading phases were considered as the material model did not include hysteresis effects in unloading.

4.1.5 Integration of Diagonal Elements (FJ_{E2_Di}) to Enhance Capsular Ligament Response in Shear

The feasibility of implementing diagonal elements to alter the facet joint response was first investigated using ligament shear data to characterize the CL elements of the FJ_{E1} model (Appendix E). The FJ_{E2_Di} model was then developed by adding 1D tension only elements in a cross formation (referred to as diagonal elements) between neighbouring elements of the FJ_{E2} model (referred to as original elements) for a total of 50 diagonal elements (Figure 4.5).

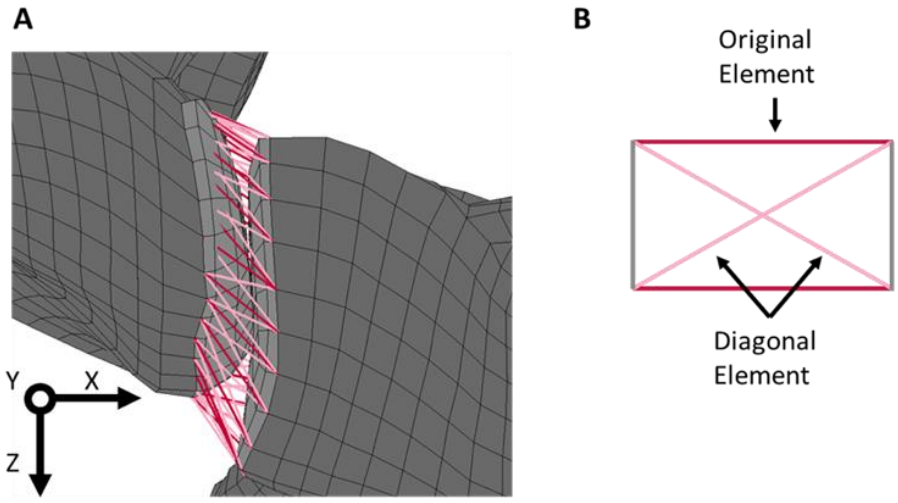

Figure 4.5: (A) FJ_{E2_Di} model showing original elements from the FJ_{E2} model in red and added diagonal elements in pink. (B) Idealized single unit showing implementation of diagonal elements in a cross formation between original elements.

The input curves for the CL elements were calculated to simultaneously fit the model force-displacement response to the experimental data in tension, AP shear and LT shear. The approach was to set the input curves of all CL elements (diagonal and original) to zero force and sequentially build up the force response (Figure 4.6). Starting in the positive AP shear direction allowed to force response to be built up; if the input curves were calculated for the LT direction first, the response in tension and AP shear were overestimated. R^2 values comparing the model output to experimental data were used to monitor changes in the model response during the process of fitting the CL elements.

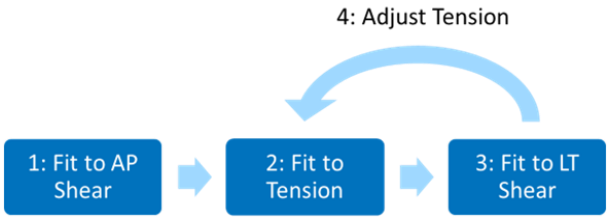

Figure 4.6: Sequence for fitting original and diagonal CL element input curves, starting with fitting to positive AP shear, tension and positive LT shear then adjusting the input to achieve greater agreement with experimental data from Chapter 3.

Each step in the fitting sequence followed a similar process as described in Figure 4.7, to account for the different contributions of the CL elements to the overall response: (A) the FJ_{E2_Di} model was loaded in the direction the CL elements were to be fit; (B) the change in length of the relevant CL elements were extracted; (C) the change in length of each element was normalized to the maximum change in length at each timestep and the sum of all normalized change in lengths calculated; (D) the force for the relevant CL element input curve was calculated by dividing the average experimental force (or difference in force compared to model output force) by the sum of normalized change in lengths. The input curve for the CL elements was defined as the maximum change in length vs. the CL element force at each timepoint.

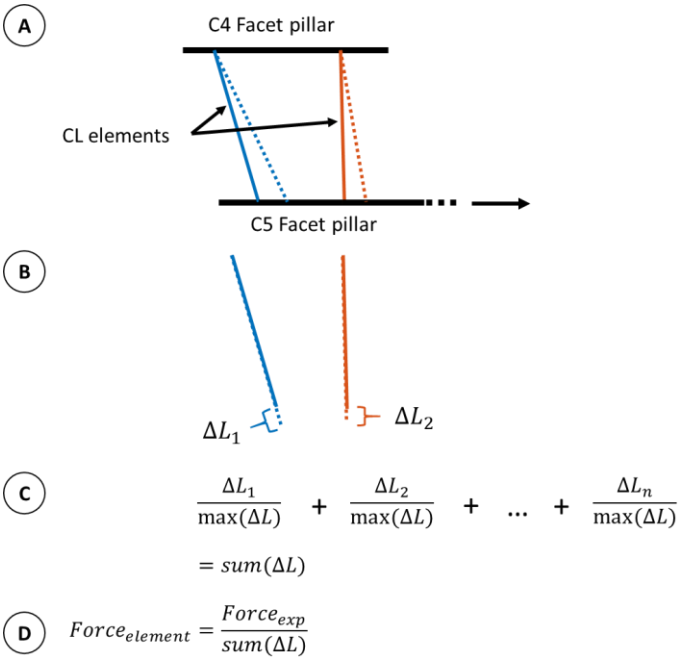

Figure 4.7: Process of fitting diagonal elements to experimental AP shear. (A) AP shear simulation. (B) Extracting the change in length of elements at a timestep during AP shear. (C) Normalize change in length to element with maximum change in length. (D) Divide experimental AP shear force at timepoint by the sum of normalized change in lengths.

After each step, the model was run in AP shear, LT shear and tension and the R^2 values were calculated for the force vs. displacement curves of the rigid plate compared to the experimental data. The average experimental force-displacement curves were linearly resampled to the same displacements as the model output and the R^2 value then calculated by the equation: $1 - \frac{SSE}{SST}$ where SSE is the sum of squared residuals between the experiment and model curves. SST is the total sum of squares for the experiment curve. R^2 is not intended as a metric for assessing similarity between curves; however, as the curves were monotonically increasing with a similar shape and magnitude, the R^2 values were used to evaluate changes in the model (as opposed to absolute goodness of fit).

There were several specifics to note on the fitting process. First, the experimental force and displacement data from Chapter 3 was filtered using a two-way 2nd order Butterworth filter with an effective cut-off frequency of 0.5 [96] before averaging the curves using ARCGen (Section 3.1.3). Secondly, the experimental data was resampled to 50 datapoints between 0 and 3 mm for AP and LT shear or between 0 and 2.5 mm for tension, and the first data point set at zero force and displacement. The model output was downsampled to 50 datapoints such that the experimental and model displacement data aligned. Thirdly, the input curves for the original and diagonal elements were manually modified to be monotonically increasing using linear interpolation. Note that, while filtered experimental data was used to develop model input curves, the model output force vs displacement curves were compared to the unfiltered experimental data.

After the fitting process, the FJ_{E2_Di} model was loaded in Mattucci quasi-static tension; the C4 potting rigid plate of the FJ_{E2_Di} model was loaded in tension at 0.002 mm/ms to replicate the loading of the tension model in Section 4.1.2. The output force vs displacement curve was compared to the FJ_{E2} model loaded under the same conditions.

Details on Steps of the Fitting Sequence

The capsular ligament elements were fit to the positive loading directions.

The first step used the experimental average force vs displacement in positive AP shear to calculate the input curve of the diagonal elements. Referring to the process in Figure 4.7, the details for the first step are: (A) the FJ_{E2_Di} model was loaded in positive AP shear; (B) the change in length of the diagonal CL elements were extracted; (C) the change in length of each element was normalized to the maximum change in length at each timestep and the sum of all normalized change in lengths calculated; and (D) the force for the diagonal CL element input curve was calculated by dividing the average experimental AP shear force by the sum of normalized change in lengths.

The second step used the experimental average force vs. displacement in tension to calculate the input curve of the original CL elements. Referring to the process in Figure 4.7, the details for the second step are: (A) the FJ_{E2_Di} model from step one was loaded in tension; (B) the change in length of the original CL elements were extracted; (C) the change in length of each element was normalized to the maximum change in length at each timestep and the sum of all normalized change in lengths calculated; and (D) the difference between the average experimental force in tension and the model output force in tension was calculated. The force for the diagonal CL element input curve was calculated by dividing the difference in force by the sum of normalized change in lengths.

The third step used the experimental average force vs. displacement in LT shear to adjust the input curve for a subset of two diagonal elements. Two single diagonal elements were identified that had the greatest change in length in LT shear and the least in AP shear and were not neighbouring elements (Figure 4.8).

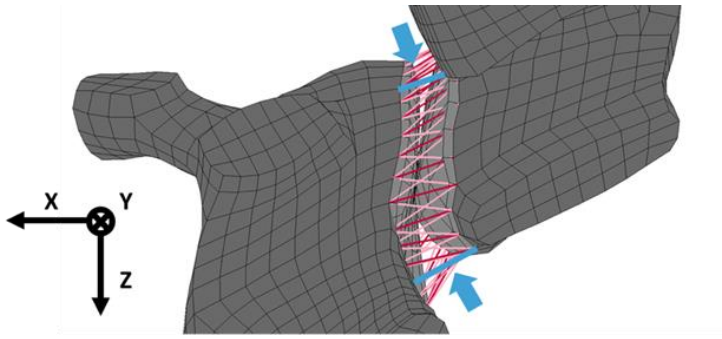

Figure 4.8: Location of diagonal beams for the FJ_{E2_Di} model. Red elements show the original elements, pink shows the diagonal elements fit to AP Shear and blue elements shows the subset of diagonal elements fit to LT Shear. Location of subset of diagonal elements highlighted by blue arrows.

Referring to the process in Figure 4.7, the details for the third step are: (A) the FJ_{E2_Di} model from step two was loaded in positive LT shear; (B) the change in length of the subset of two diagonal elements were extracted; (C) the change in length of each element was normalized to the maximum change in length at each timestep and the sum of all normalized change in lengths calculated; and (D) the difference between the average experimental force in positive LT shear and the model output force in LT shear was calculated. The force for the diagonal CL element input curve was calculated by dividing the difference in force by the sum of normalized change in lengths. The input curve for the subset of two diagonal elements from step one was modified by adding the force per element calculated in the current step. As the input curve for AP shear and LT shear had different intervals, the change in lengths were manually aligned such that the corresponding force per element could be added.

The fourth step used the experimental average force vs displacement in tension to adjust the input curve for the original elements. Referring to the process in Figure 4.7, the details for the fourth step are: (A) the FJ_{E2_Di} model from step three was loaded in tension; (B) the change in length of the original CL elements were extracted; (C) the change in length of each element was normalized to the maximum change in length at each timestep and the sum of all normalized change in lengths calculated; and (D) the difference between the average experimental force in tension and the model output force in tension was calculated. The force for the diagonal CL element input curve was calculated by dividing the difference in force by the sum of normalized change in lengths. The input curve for original elements from step two was modified by adding

the force per element in the current step at each timepoint. At small changes in length, the forces were negative and these values were modified to zero force.

4.1.6 Capsular Ligament Modeled with Shell Elements to Enhance Capsular Ligament Response in Shear

To overcome some of the limitations of 1D tension-only elements, including changing orientation without carrying load and lack of interaction with geometry, the capsular ligament was implemented using a shell element representation.

Capsular Ligament Geometry

The FJ_{E2} model was modified to create the FJ_{E2_Sh} model. The geometry of the capsular ligament was meshed with element size on the order of 2 mm by 2 mm and had a thickness of 1.1 mm. To prevent capsular ligament penetration of the cartilage, the outer ring of cartilage elements was removed from the C4 and C5 facet pillars to avoid interference with the ligament and a surface-to-surface contact between the C4 and C5 cartilage and capsular ligament was added (Figure 4.9).

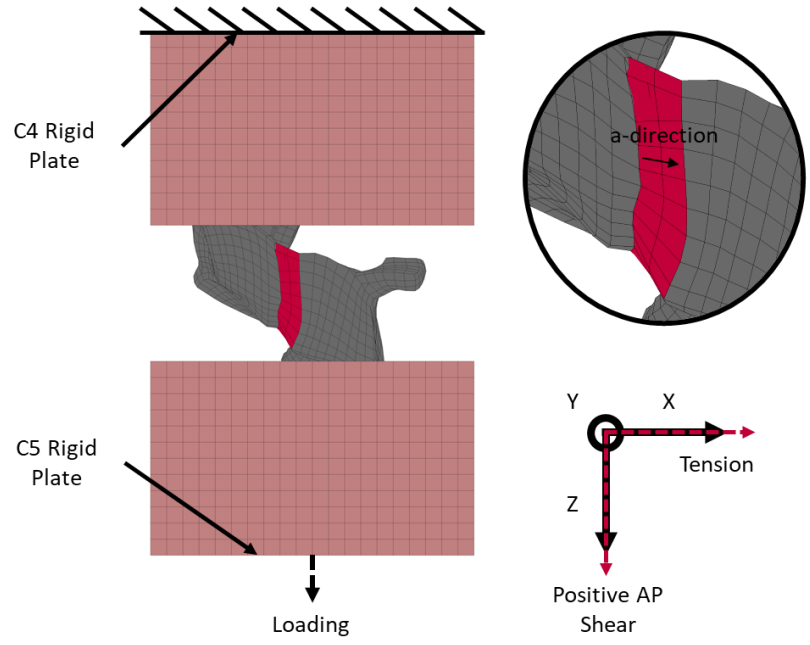

Figure 4.9: CL shell element mesh and loading of the FJ_{E2_Sh} model. The circled region shows the capsular ligament shell mesh and the a-direction of the material model.

Capsular Ligament Material Model

A nonlinear elastic orthotropic material model (Mat_Fabric) was used for the shell elements. The material model defined orthogonal properties separately, with Green strain vs 2nd Piola-Kirchhoff (PK) stress input curves defined for both a- and b-directions. The a-direction (Figure 4.9) was longitudinal along an axis defined by nodes 1 and 2 of each element and the b-direction was the transverse direction.

The a-direction material parameters were defined using the experimental data in tension from Chapter 3. The raw data in Chapter 3 was re-analyzed to remove data in regions where the joint went into slight compression during cyclical tension loading. The force and displacement data were filtered using a two-way 2nd order Butterworth filter with an effective cut-off frequency of 0.5 [96] before averaging the force-displacement curves using ARCGen (Section 3.1.3). The average force-displacement curve was converted to 2nd PK stress vs. Green strain using simplified geometry of the FJ_{E2} model geometry and by assuming uniform uniaxial tension and nearly incompressible material. The average displacement was converted to Engineering strain using the average length of original elements (4.14 mm) and then to Green strain by $E = \varepsilon + 0.5\varepsilon^2$. The average force was converted to Engineering stress using a ligament cross sectional area of 51.18 mm^2, based on the average of the superior and inferior circumference of the facet joint and a 1.1 mm ligament thickness, by $\sigma = force/51.18$. Engineering stress was converted to 2nd PK stress by $\sigma_{2nd\ PK} = \frac{\sigma}{1+\varepsilon}$. The resulting strain vs stress curve was downsampled to 50 points and modified to be monotonically increasing by linearly interpolating between neighbouring forces for every instance where the force decreased.

The b-direction input curve was defined perpendicular to the a-direction by scaling down the 2nd PK stress of the a-direction by a magnitude of 0.1 [85]. The remaining material input parameters were based on the VIVA model inputs [85] and are shown in Table 4.2.

Table 4.2: Input parameters for fabric material model.

Capsular Ligament (Fabric)			
Density (kg/mm^3)	**Poisson's Ratio (a-direction)**	**Poisson's Ratio (b-direction)**	**Shear Modulus (GPa)**
1E-06	0.3	0.49	2.427E-04

Single Element Simulation and Simulation of the FJ_{E2_Sh} Model in tension, AP shear and LT Shear

First, a single element test was performed using a 1 mm by 1 mm single shell element with a thickness of 1.1 mm. The single element was loaded in the x- and y- directions in displacement-based loading to 0.5 mm (50% engineering strain).

Then the FJ_{E2_Sh} model was loaded in tension, AP shear and LT shear as described in Section 4.1.4 (sinusoidally loaded at 10 mm/s).

4.2 Facet Joint Finite Element Results

4.2.1 Evaluation of the $\mathbf{FJ_{E1}}$ Model in Tension

Figure 4.10 compares the FJ_{E1} model force-displacement curve to Mattucci's average force-displacement curves. For quasi-static rates, the FJ_{E1} model closely followed Mattucci's experimental data. The orientation of the tension load vector for quasi-static loading (global and local tension) for the FJ_{E1} model was also compared. The model response showed noticeable differences between coordinate systems, with the model loaded in tension along the local axis exhibiting lower stiffness than in global tension.

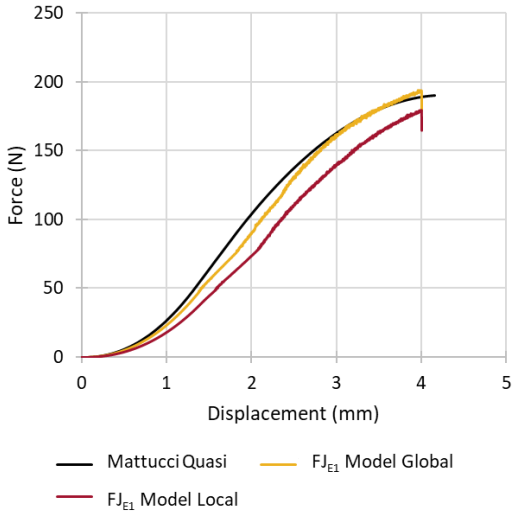

Figure 4.10: Comparing Mattucci's quasi-static experimental data and the FJ_{E1} model loaded in tension with two orientations of the load vector (global and local).

4.2.2 Evaluation of the Capsular Ligament Elements of the $\mathbf{FJ_{E1}}$ Model in Joint Shear

When the FJ_{E1} model was loaded in positive and negative shear, the 1D tension-only capsular ligament elements penetrated the cartilage (Figure 4.11A), with implications for the physiological representation of the facet joint. In the zero-displacement position, elements at the superior surface on the anterior aspect and, to a lesser extent, the superior surface of the medial aspect penetrated the cartilage. When the joint underwent shear, the 1D tension-only elements past through the articular cartilage as they changed orientation. In positive shear, the anterior elements and medial elements penetrated further into the superior cartilage while the posterior and lateral element started to penetrate the inferior cartilage. In negative shear, the anterior elements moved through the cartilage such that they were no longer penetrating the articular

cartilage while elements penetrated the cartilage at the superior surface on the posterior aspect of the joint.

Considering one element on the medial aspect of the facet joint and one on the anterior aspect, the behaviour of the elements was different between regions and between positive and negative loading (Figure 4.11B). In positive shear, the medial element began to increase in length around 200 ms while the anterior element did not increase beyond the initial length within the range of facet joint displacement of the simulation. In negative shear, the opposite occurred – the medial element did not increase beyond the initial length and the anterior element increased in length at about 800 ms. The anterior element engaged later in the simulation compared to the medial element in positive shear.

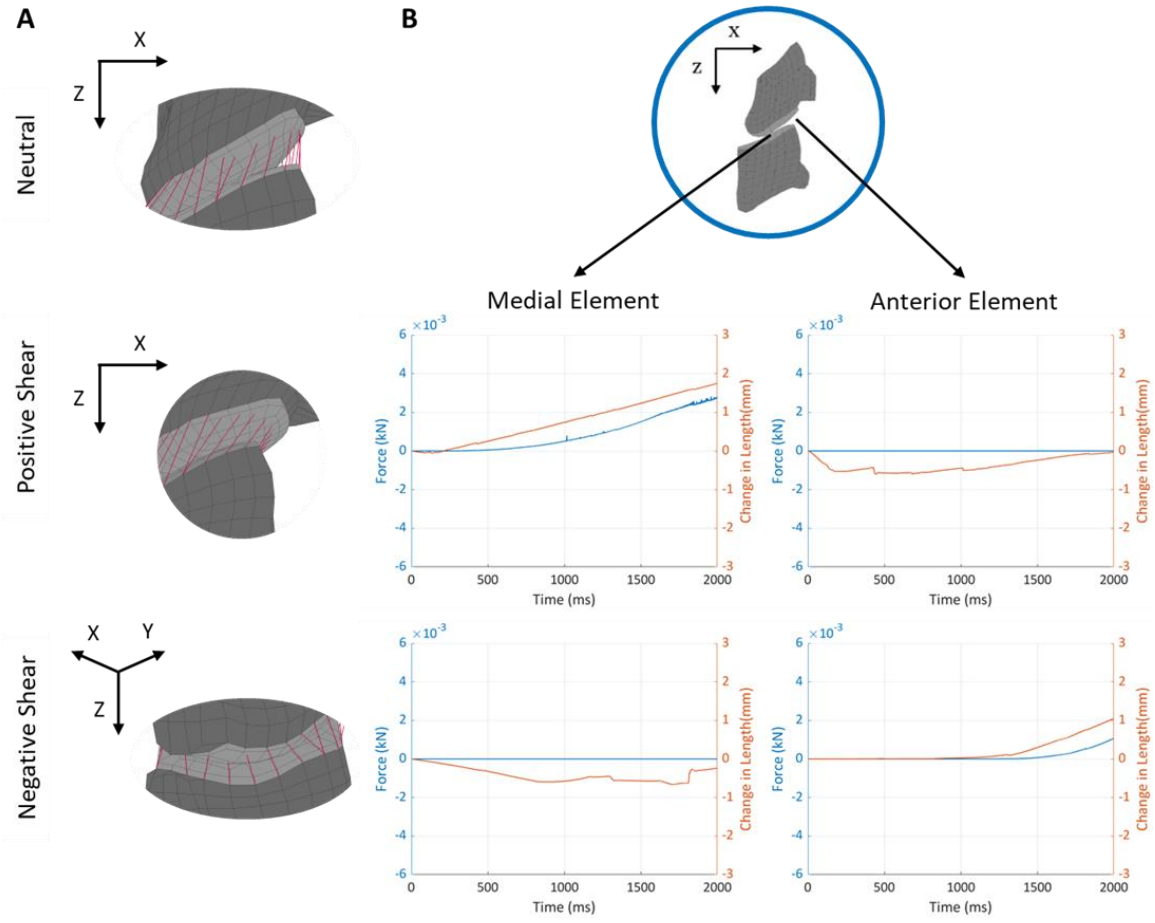

Figure 4.11: Limitations of 1D tension-only elements. (A) Shows element penetration of cartilage in the neutral position and during positive and negative shear. (B) Shows element change in orientation without load of two elements. The FJ_{E1} model was run in quasi-static shear in the global coordinate system.

The change in length of select capsular ligament 1D elements around the facet joint circumference was highly variable (Figure 4.12). In positive shear, five of the ten selected elements increased in length during facet joint displacement while the other five initially decreased in length. The rate at which the elements changed length differed for each element, and the change in length at the end of the simulation ranged from approximately 0 mm to 3 mm. Elements in negative shear showed a similar spread, but eight out of ten elements decreased in length during the simulation. Only two did not decrease in length, and those elements only begin the increase at about 1000 ms. The change in length at the end of the simulation ranged from approximately -3 mm to 1 mm.

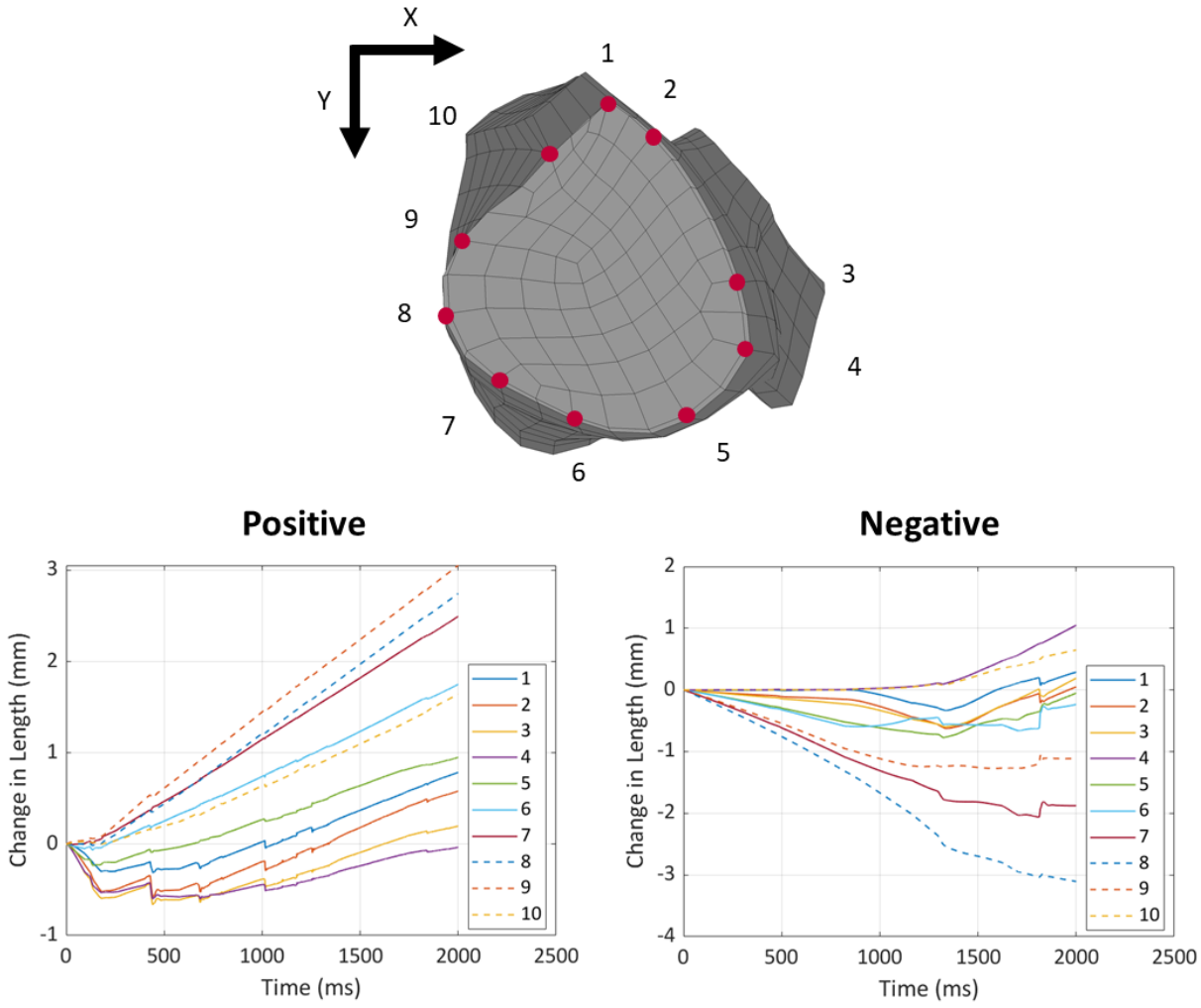

Figure 4.12: Change in length of select elements around circumference of facet joint during positive and negative shear. The FJ_{E1} model was run in quasi-static shear in the global coordinate system.

4.2.3 Evaluation of the FJ_{E2} Model Force-Displacement Response Compared to Chapter 3 Experimental Data

Figure 4.13 plots the force-displacement output of the FJ_{E2} model loaded in tension, AP shear and LT shear with the experimental data from Chapter 3. In the positive loading phase, the multi-loading model overestimated forces in AP shear and tension but underestimated forces in LT shear. In the negative loading phase, the model underestimated both LT shear and AP shear.

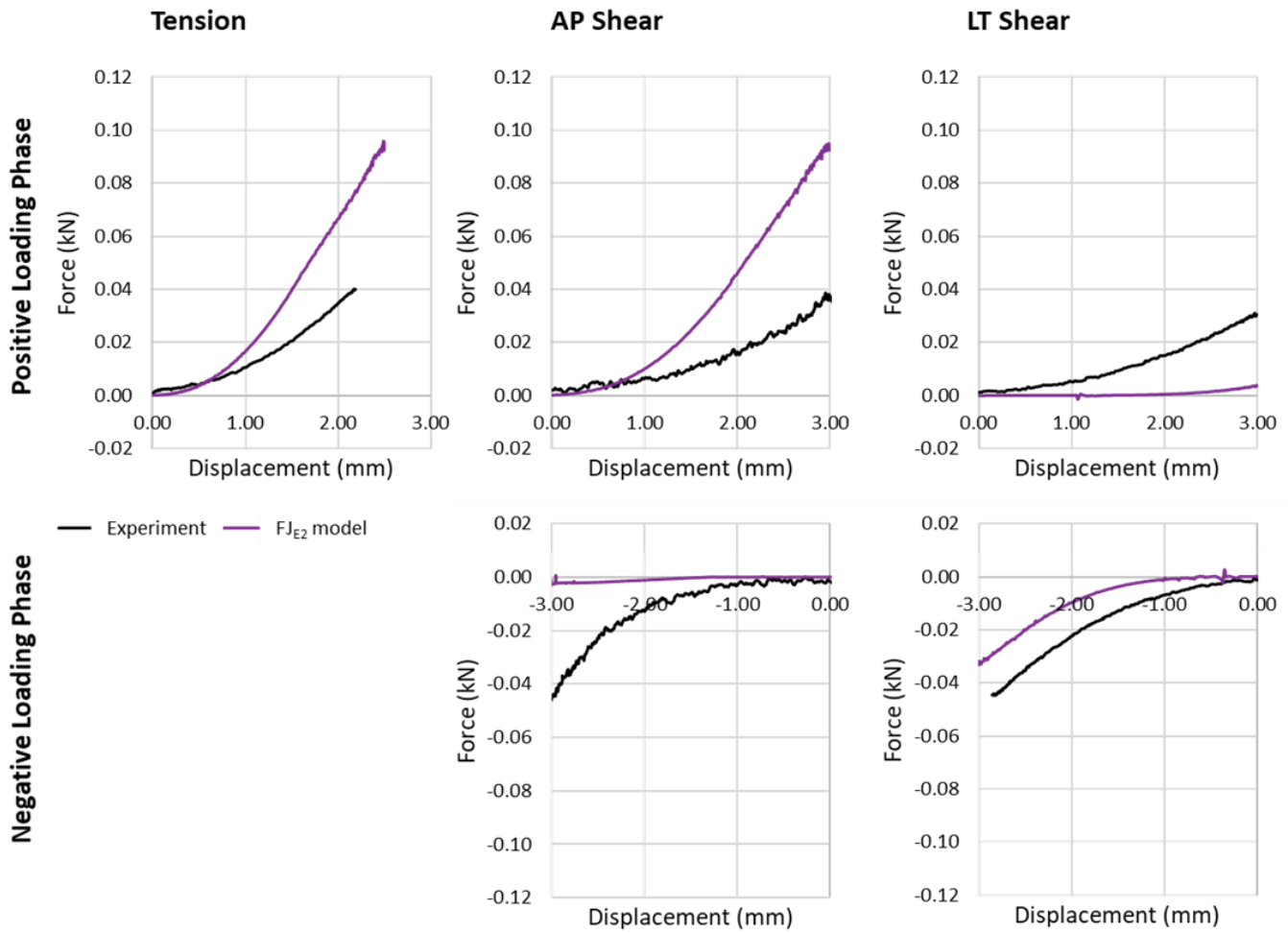

Figure 4.13: Comparing FJ_{E2} model output to experimental data from Chapter 3 in the positive loading phase (Top) and negative loading phase (Bottom).

4.2.4 Integration of Diagonal Elements (FJ_{E2_Di}) to Enhance Capsular Ligament Response in Shear

The CL element input curves for the FJ_{E2_Di} model (Figure 4.14) showed that the subset of diagonal elements fit to LT shear had a much higher force for the same change in length compared to the diagonal elements fit to AP shear and the original elements. The force carried by the diagonal elements increased as soon as the elements begin to increase in length while the original elements engaged at greater changes in length, with the force beginning to increase at 0.8 mm.

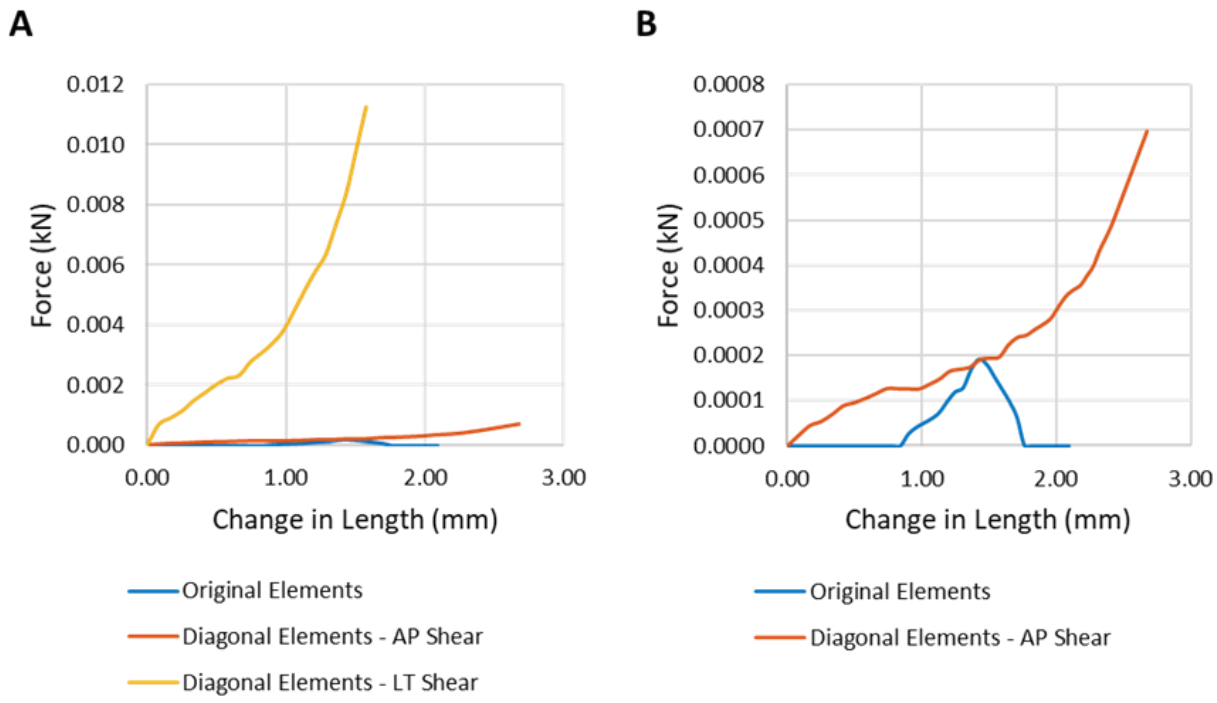

Figure 4.14: (A) Input curves for the original and diagonal elements for the FJ_{E2_Di} model. (B) Focusing on the original elements and diagonal elements fit to AP shear.

Figure 4.15 shows the output curves for the FJ_{E2_Di} model compared to the average experimental curves from Chapter 3 and the FJ_{E2} model. Together with the R^2 values in Table 4.3, these curves indicate the FJ_{E2_Di} model improved the response compared to the FJ_{E2} model, particularly in positive AP shear and tension. However, in the negative LT shear direction the FJ_{E2_Di} model performed poorly compared to the FJ_{E2} model.

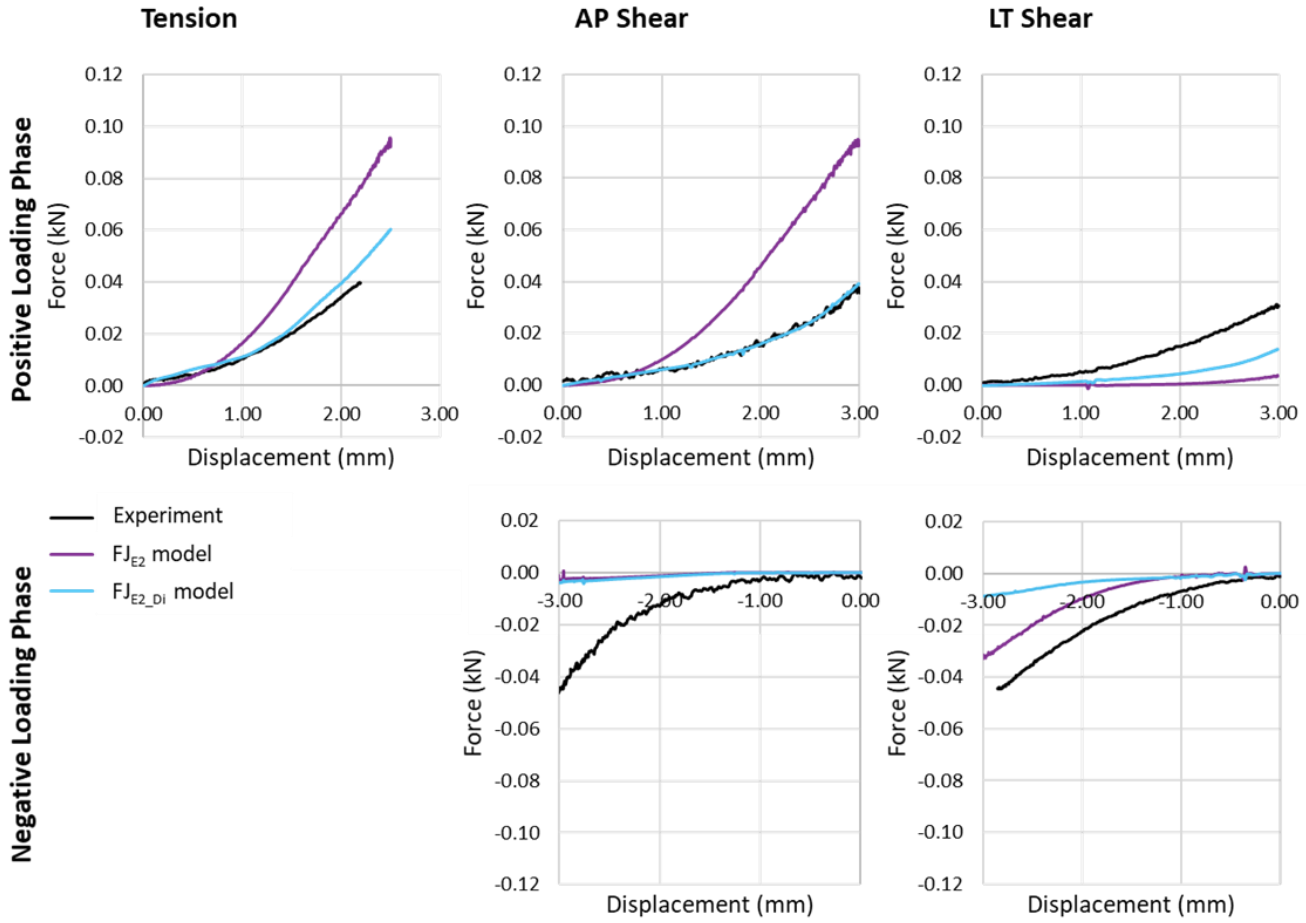

Figure 4.15: Output force-displacement curves in the positive and negative shear directions and tension for the FJ_{E2_Di} model in the positive loading phase (Top) and the negative loading phase (Bottom).

Table 4.3: Comparing R^2 values for the FJ_{E2} model and the FJ_{E2_Di} model. The R^2 values for the development of the FJ_{E2_Di} model are also shown. Green shows where the R^2 value of the FJ_{E2_Di} model is higher than the FJ_{E2} model; blue shows little change; and red shows a decrease.

	FJ_{E2} Model	FJ_{E2_Di} Model			
		Step 1	Step 2	Step 3	Step 4
POSITIVE LOADING PHASE					
AP Shear	<0.0 (-8.27)	0.04	0.07	<0.0 (-1.58)	0.99
LT Shear	<0.0 (-1.83)	<0.0 (-1.81)	<0.0 (-1.46)	<0.0 (-0.03)	<0.0 (-0.26)
Tension	<0.0 (-0.83)	<0.0 (-0.04)	0.97	<0.0 (-0.57)	0.95
NEGATIVE LOADING PHASE					
AP Shear	<0.0 (-1.10)	<0.0 (-1.02)	<0.0 (-1.00)	<0.0 (-0.97)	<0.0 (-0.99)
LT Shear	0.40	<0.0 (-1.14)	<0.0 (-0.13)	<0.0 (-0.11)	<0.0 -0.95)

When comparing the FJ_{E2_Di} model to the FJ_{E2} model, both loaded to replicate Mattucci's study, and Mattucci's quasi-static data (Figure 4.16), the FJ_{E2_Di} model had lower forces than the experimental data and the FJ_{E2} model after 1 mm and the slope did not decrease at higher displacements.

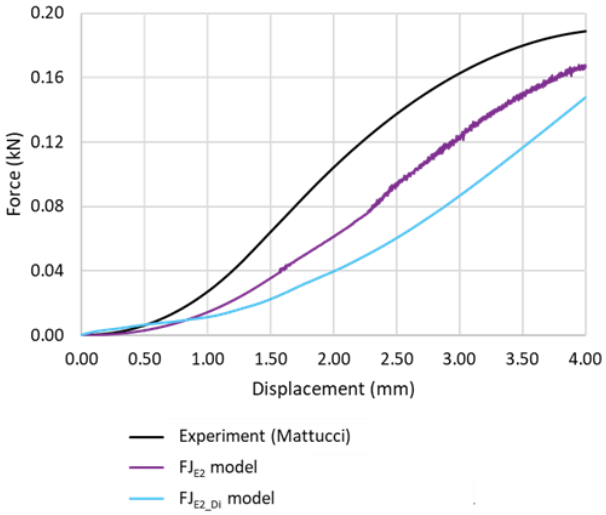

Figure 4.16: Comparing the output force-displacement curves from the FJ_{E2} model and the FJ_{E2_Di} model fit in positive shear direction.

4.2.5 Capsular Ligament Modeled with Shell Elements to Enhance Capsular Ligament Response in Shear

The single element case in the a-direction for the fabric material model behaved well, with the simulation output matching the input curve (Figure 4.17A). Buckling of elements was observed when the FJ_{E2_Sh} model was loaded in AP shear and there were two elements with initial penetration of the cartilage (Figure 4.17B). In tension there was a very close match between the model and the experimental data from Chapter 3 (Figure 4.17C). This is supported by the higher R^2 value (Table 4.4) when compared to the FJ_{E2} model. In positive AP shear, the model response closely matched the experimental data (Figure 4.17D). In positive LT shear, the response did not match the experimental data as closely but was an improvement on the FJ_{E2} model (Figure 4.17E). In the negative loading direction, the model was in poor agreement with the experimental data.

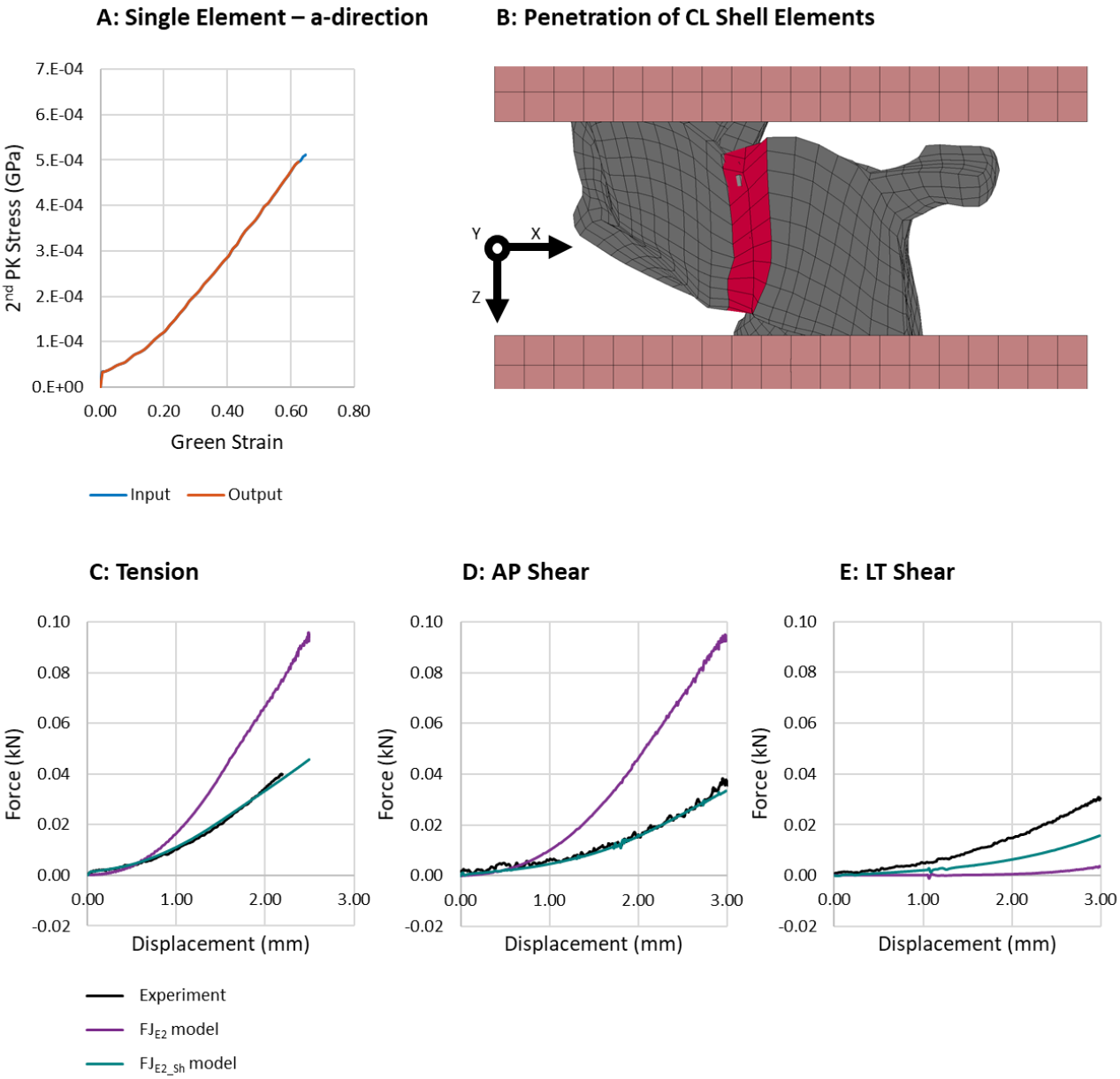

Figure 4.17: (A) Single element test for ligament shell element with fabric material model. (B) Buckling of shell elements during AP shear loading and penetration of cartilage through capsular ligament. (C-E) Comparing the FJ_{E2_Sh} model to experimental data from Chapter 3.

Table 4.4: Comparing R^2 values for the FJ_{E2}, the FJ_{E2+Di} model and the FJ_{E2_Sh} model.

	FJ_{E2} Model	**FJ_{E2_Di} Model**	**FJ_{E2_Sh} Model**
POSITIVE LOADING PHASE			
AP Shear	<0.0 (-8.27)	0.99	0.97
LT Shear	<0.0 (-1.83)	<0.0 (-0.26)	0.06
Tension	<0.0 (-0.83)	0.95	1.00
NEGATIVE LOADING PHASE			
AP Shear	<0.0 (-1.10)	<0.0 (-0.99)	<0.0 (-0.27)
LT Shear	0.40	<0.0 (-0.95)	0.01

4.3 Discussion

Model Performance

The FJ_{E1} model performed well in tension, with a response that closely followed Mattucci's quasi-static experimental data and captured the expected ligament behaviour of increasing stiffness with increasing strain rate. The GHBMC facet joint was characterized using Mattucci's data, which tested ligaments in tension to ligament failure, so it follows that the FJ_{E1} model in tension would be in good agreement with Mattucci's data.

However, when the FJ_{E2} model output in tension was compared to the cyclic sub-failure tension data reported in Chapter 3, there were noticeable differences. The experimental data had a longer toe region and less steep linear region than the model. Additionally, the FJ_{E2} model overestimated the force response in positive AP shear but underestimated it in negative AP shear and LT shear.

It was important to note the distinction between the FJ_{E1} model compared to Mattucci's tension data and the FJ_{E2} model compared to the Chapter 3 experimental data. Firstly, the specimen orientation of the FJ_{E2} model with respect to the tension loading direction was different than the FJ_{E1} model. The difference in FJ_{E1} model force vs displacement output in the global and local coordinate system demonstrated that the GHBMC model was sensitive to changes in loading direction, suggesting the differences in orientation between the FJ_{E1} model and the FJ_{E2} model influenced their response. Additionally, there were notable differences between the data collected in Chapter 3 and Mattucci's data. These differences were explored in Section 3.3. Briefly, the loading regimes, age, and number of specimens were different between the datasets. While Mattucci tested a greater number of younger specimens in tension to failure with a constant strain rate, the experiment in Chapter 3 tested fewer older specimens in cyclic loading to sub-failure displacements.

The current GHBMC implementation was capable of replicating Mattucci's tension to failure tests; however, it may be limited in representing other loading modes, including cyclical loading within sub-failure levels.

Model Limitations

The current GHBMC implementation of the facet joint capsular ligament had several limitations when considering the performance of the FJ_{E1} and FJ_{E2} models in shear. Evaluation of the FJ_{E1} model in shear highlighted two key points: the 1D tension only elements used to represent the capsular ligament did not interact with the hard-tissue geometry resulting in non-physiological load paths; and the capsular ligament elements changed orientation before carrying load.

The asymmetry in FJ_{E1} model and FJ_{E2} model response between the positive and negative shear directions was likely a consequence of the capsular ligament elements changing orientation before carrying load and the initial orientation of capsular ligament elements relative to the loading direction. For instance, an element angled towards the anterior direction would engage early in the simulation if extended in the anterior direction but would engage later if extended in the posterior direction; the element first reoriented towards posterior direction without an increase in length (Figure 4.18). However, the initial orientations of the elements were not modified in this study, as that would require a reconfiguration of the original setup. Capsular ligament elements in the FJ_{E1} model and FJ_{E2} model had non-uniform initial orientation and length, exacerbated by the irregular geometry of the facet joint.

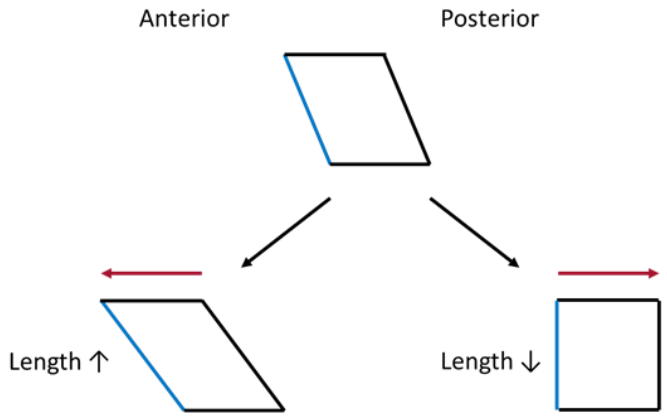

Figure 4.18: Demonstration of an element loaded in the direction it is angled (anterior) and in the opposite direction (posterior). In the posterior direction, the element changes orientation before increasing length and carrying load.

The change in lengths of individual capsular ligament elements in the FJ_{E1} model in positive and negative shear also demonstrated asymmetry. In positive shear, the monitored subset of capsular ligament elements engaged earlier and had greater change in lengths. In contrast, in negative shear the selected elements decreased in length to a greater degree and engaged later to a lesser change in length. The change in length of capsular ligament elements was a function of location around the circumference of the facet joint and the element's initial orientation. The FJ_{E2} model also displayed asymmetry between positive and negative shear in both the AP and LT shear direction. The initial orientation of CL elements in the current implementation was biased towards the positive shear direction in AP shear and negative shear direction in LT shear. While the average curves from Chapter 3 showed some asymmetry between positive and negative AP shear, it was considerably less than the asymmetry in both the FJ_{E1} and FJ_{E2} models.

The lack of interaction with hard-tissue geometry and changing orientation before carrying load were key limitations of using 1D tension-only elements to represent a complex three-dimensional tissue. A consequence of using 1D elements was that shear strain in the capsular ligament was not properly represented. Additionally, local strains in the capsular ligament itself could not be extracted, which could impact future work on local injury prediction. Injury occurs at the tissue level while current injury prediction relies on intervertebral kinematic measurements. However, 1D tension-only elements are computationally efficient, stable and provide a methodology for modelling progressive failure. Additionally, the input material parameters (force-displacement curves) are simple compared to the geometric information and assumptions that would be required to determine stress and strain for more complex shell element material models.

Model Capsular Ligament Modifications with Diagonal Elements or Shell Elements

Negative R^2 values were reported for the FJ_{E2} model and FJ_{E2_Di} model. R^2 values are typically between 0 and 1; however, if the sum of squared residuals is greater than the total sum of squares, R^2 can be negative. A negative R^2 indicates the sum of squared error between a horizontal line at the experimental average and the experimental data is lower than the sum of squared error between the model output and the experimental data. The R^2 values of the FJ_{E2} model were all negative with the exception of negative LT shear. In contrast, the R^2 value for AP

shear and tension in the FJ_{E2_Di} model were above 0.8, showing an improvement over the FJ_{E2} model.

The FJ_{E2_Di} model improved the response in tension and positive AP shear relative to the FJ_{E2} model. While the positive LT shear response was also improved, it remained in low agreement with the experimental data. The response in negative AP shear was similar to the FJ_{E2} model; however, the response in LT shear was inferior. Both models were compared to the experimental data in Chapter 3. The capsular ligament input curves were calculated to fit each direction (tension, AP shear and LT shear) simultaneously but was unable to achieve good fit in all directions.

LT shear was the most difficult loading direction to fit. The FJ_{E2} model reported very low force output in LT shear and fitting the diagonal elements to agree with the positive LT shear would result in highly overestimating the force in other directions. This is, once again, likely due to the initial orientation of the beams relative to the direction of loading, where few elements were engaged immediately so the force per element was high. To attempt to address this, a small subset of elements was selected that lengthened most in LT shear but least in AP shear. In this way, the force response in LT shear was increased without negatively impacting the positive AP shear and tension directions.

To put the model outcomes in context, the kinematics of the right C4 - C5 facet joint was extracted from the full head and neck model in several vehicle impact scenarios (Appendix F). The magnitude of LT shear was found to be less than AP shear in all impact scenarios. The FJ experienced the highest LT shear relative to AP shear in the 7g lateral impact scenario, with maximum LT shear being 0.44 times the maximum AP shear. The lowest was 8g frontal impact, where maximum LT shear was only 0.02 times the maximum AP shear. As such, considering the FJ_{E2_Di} model was only able to replicate the experimental data for two loading direction, LT shear was the loading direction with the most leeway for lower agreement with experimental data.

After development, the FJ_{E2_Di} model was simulated to replicate Mattucci's quasi-static tension data. The magnitudes were similar until about 1.00 mm, but the FJ_{E2_Di} model had a longer toe region than the FJ_{E2} model, although the linear region slope was similar. The force vs

displacement curve of the FJ_{E2_Di} model did not start to plateau at higher loads, unlike the experimental data or the FJ_{E2} model. Overall, the model modifications increased agreement with the experimental data in Chapter 3, but consequently reduced the agreement with the data reported by Mattucci.

Fitting the capsular ligament element input curves was not a unique solution. Different approaches to the fitting sequence could be taken; for instance, the changing the order of the fitting sequence (AP shear then tension then LT shear) or selecting a different subset of diagonal elements. Several variations on the FJ_{E2_Di} model were developed. In the FJ_{E2_Di} model, the input curve for the subset of two diagonal elements fit for LT shear had a force per element that was an order of magnitude higher than other capsular ligament elements. The load concentrations in these elements may affect the FJ response under more complex modes of loading when integrated with the full head and neck model. To address this, a subset of eight elements was selected, distributing the load and reducing the force of the input curve by threefold. While the R^2 values for the output force-displacement curves were similar to the FJ_{E2_Di} model, the fitting process took more iterations, and the shape of the curves were farther from the experimental data.

Additionally, the process was attempted using the negative loading directions (negative AP shear and negative LT shear) as inputs; however, the diagonal beam implementation was unable to improve the force-displacement response. Due to the bias in the initial beam orientation towards positive AP shear, the force vs displacement output of the FJ_{E2} model in the negative AP shear direction was very low. The model was only able to replicate either the response in negative AP shear or tension.

Shell elements were considered as an alternative implementation of the capsular ligament. When an orthotropic material model was applied to the FJ_{E2_Sh} model, the response was improved compared to the FL_{E2} model in all loading directions except negative LT shear. Good agreement between the model and experimental force-displacement curves was achieved in tension and AP shear. The FJ_{E2_Sh} model performed as well as or slightly better than the FJ_{E2_Di} model, without requiring iteratively fitting 1D tension only elements. Although this implementation used

previously published method to determine b-direction material properties, the next step would be to characterize the b-direction material properties using the experimental data in Chapter 3.

The agreement between the model output and experimental data in positive AP shear supported the assumption that the b-direction properties of the capsular ligament was one order of magnitude less than the a-direction properties, as reported by Osth et. al. [84]. It also suggested the assumptions used to convert force-displacement to stress-strain were appropriate in this scenario.

4.4 Study Limitations

The applied boundary conditions were one limitation of the modelling methods. The data provided from Chapter 3 was the crosshead displacement, with the implication being the models were simulated using crosshead displacement rather than actual displacement of the facet pillars. These errors were quantified in Chapter 3. Additionally, the FJ_{E1} model was also unconstrained during positive and negative shear to address the pillar-to-pillar contact that occurred in the global coordinate system simulations. As a result, the displacements in the off-loading-axis directions were uncontrolled and forces were extracted as resultant forces. As this implementation was not compared to experimental data, these points do not affect the conclusions drawn from the simulations. Finally, both the FJ_{E1} model and FJ_{E2} model were simulated in specific modes of loading. Although this is a good first step in evaluating the response of the facet, the response under more complex modes of loading (e.g. axial rotation and flexion-extension bending), including impact scenarios, are also important to consider.

In terms of the material model inputs, while the FJ_{E1} model included rate effects, when comparing the FJ_{E2} to experimental data from Chapter 3 and when developing the diagonal element models only a single rate was considered. As ligaments are rate-dependent structures, the material characterization would need to be extended to capture this behaviour.

While the methodology for determining material model inputs of the diagonal beam implementation was applicable to all spinal levels, the specific input curves for the FJ_{E2_Di} model is limited to the C4 - C5 level. The change in length of individual elements were used to determine the input force vs change-in-length curves, and the change in length depends on the initial orientation and the geometry of the facet joint. Additionally, the diagonal element models are only applicable to displacements before element failure, as the failure behaviour was not considered, and before the opposing diagonal elements are significantly engaged, otherwise the response would stiffen.

Using shell elements to capture tissue level behaviour of the capsular ligament brought different challenges. To develop the simplified FJ_{E2_Sh} model, a simplified geometry of the capsular ligament was applied, where the ligament was defined as the shortest distance between nodes

on opposing articular pillars. The thickness of the shell elements representing the capsular ligaments approached a one-to-one ratio with the shell length, where the thickness should ideally be less than $1/10^{th}$ of the shell length. This would have affected the calculated stress, particularly for bending modes of deformation. Additionally, the outer ring of cartilage elements was removed to avoid interference with the ligament, which would need to be re-meshed to be compatible with the new ligament implementation. Further work would be required to both implement and validate the shell implementation.

Finally, the experimental average force-displacement curves used to characterize the material properties of both the diagonal elements and the shell elements did not cross the origin. In order to define the input parameters of the material models, the initial point in the force-displacement curve was forced to zero; however, this resulted in an initial jump in force in the input curves which is non-physiological.

4.5 Conclusions

The current GHBMC facet joint model, characterized using tension to failure data, performed well compared to Mattucci's tension data. While it is important to be aware of the differences between the models and experimental data, the study demonstrated the current GHBMC facet joint was limited in its ability to recreate experimental response in AP and LT shear. The addition of diagonal elements, fit to simultaneously modify the response in tension, AP shear and LT shear, was able to reproduce the experimental force vs displacement response in positive AP shear and tension, but did not have good agreement in LT shear or negative AP shear. Using shell elements to represent the capsular ligament showed promise as an alternative to 1D tension-only elements.

Chapter 5 Conclusions and Recommendations

5.1 Significance

The hybrid experimental-modelling approach of this study facilitated the translation of new experimental data to the computational GHBMC model, combining knowledge of the model requirements and experimental limitations. Access to the VIVO simulator enabled facet joints to be loaded in multiple modes of loading at two rates without repositioning the specimen. Using this data, the average force-displacement curves for tension, AP shear (positive and negative directions) and LT shear (positive and negative direction) at average rates of 0.1 mm/s and 10 mm/s were calculated for cyclic sub-failure loading. This enabled GHBMC facet joint evaluation in AP and LT shear, which has not previously been performed.

The GHBMC full body model is used by the automotive industry to test vehicle safety systems, amongst other applications. Gaining a better understanding of the strengths and limitations of the GHBMC facet joint can inform appropriate applications of the GHBMC model. Using diagonal elements to enhance the capsular ligament improved the model response in positive AP shear while maintaining a good model response in tension. However, the capability of 1D tension-only elements to represent the capsular ligament is limited, both in the behaviour of the 1D elements themselves (non-physiological load path and reorientation without carrying load) and in their ability to simultaneously recreate the experimental joint response in all load directions. Using shell elements to implement the capsular ligament is one alternative, however future work is required to implement and validate the shell implementation.

The knowledge gained with this study can inform the direction for further improvements to facet joint modelling as the modelling community works towards tissue-level injury prediction.

5.2 Limitations

Limitations of both the experimental study and the modelling study were identified within their chapters, however there are several additional limitations to address. Due to the small sample size comprising of all-male specimens, potential sex effects were not considered experimentally. Although the computational model represents the 50th percentile male, the GHBMC has also developed a small stature female model and the experiment data may not translate directly to the female model. As male and female anatomy and physiology are different, and, considering the role of these models to evaluate safety systems, it will be important to consider these differences when advancing the models.

Although CT scans were used for initial evaluation of the cadaver specimens, the images did not have high enough resolution or soft tissue contrast to clearly determine the geometry of the capsular ligament. This had implications for calculating stress-strain response curves from force-displacement curves and when meshing the 2D shell elements for the capsular ligament. The experimental average force-displacement curves were converted to stress-strain curves using the model geometry of the capsular ligament. However, even if the initial geometry of the capsular ligament was known, the same assumptions (uniform uniaxial tension and nearly incompressible material) would be required to convert to 2nd PK stress and Green strain.

In vivo, the cervical facet joints are oriented at an angle relative to the vertebral body endplates and spinal loads are typically considered relative to this vertebral body orientation. However, in this study, displacements were prescribed around the centre of the excised facet joints. The facet joint loading scenarios in the study were non-physiological, given the excised and oriented nature of the facet joint.

5.3 Future Work

Several key limitations in the experiment methodology should be addressed in future work. The first is refining the technique used to record the displacement of the specimen itself, rather than using crosshead displacement. Several groups have drilled flags into the bony anatomy, enabling optical tracking of vertebral displacement directly. Due to the small size of the excised facet joints and the setup used in this study, this would have been difficult to do without damaging the capsular ligament.

Secondly, the potting method, both in terms of fixation and alignment, should be improved. Alignment of the specimen was perhaps the most challenging step in the experimental protocol. Determining a feasible way to consistently align specimens would be invaluable moving forwards. Recent studies have used 3D printed molds or combinations of molds and cement to fix specimens. Imaging modalities such as x-ray or CT could potential be applied for specimen alignment; however, this would require access to such equipment and appropriate training. A jig used to align each specimen based on joint motion could be a feasible alternative.

Finally, increasing the resolution of the strain measurements and measuring strain around the circumference of the facet joint would provide valuable information on tissue-level behaviour to validate the computational model as it develops further. Using multiple cameras and improving the marker pattern would be a first step. Using 3D digital image correlation (DIC) would provide full strain field information during loading. Previous studies have used Verhoeff stain [78] [73] to speckle the capsular ligament for strain analysis and could be a promising option. However, 3D-DIC would significantly complicate the experiment set-up and data analysis.

Beyond improvements to current experimental techniques, there are opportunities to further characterize the facet joint. The VIVO enables more complex loading scenarios that could supplement the existing experimental data. Of particular interest would be to experimentally evaluate the effect of specimen alignment. During the sensitivity study of the FJ_{E2} model orientation, the force vs displacement curve was found to be highly sensitive to the facet joint orientation. While some differences may reflect physiological responses, there is currently no experimental data to assess the degree to which this response is physiological. The VIVO would

allow the same specimen to be loaded at a range of angles without repositioning, providing data to establish physiological sensitivity to facet joint orientation compared to model sensitivity. Additionally, while the simple modes of loading provided valuable information for model evaluation and development, using the VIVO to simulate rear impact and other complex, multi-modal loading of the facet joint based on outputs from the GHBMC model would provide additional information with which to validate the model.

On the computational modelling side, the next step would be to implement the diagonal elements in the motion segment model and the head and neck model. Further work is also needed to enhance the implementation of the capsular ligament.

To continue developing the 1D tension-only element implementation of the facet joint, which would maintain the computational efficiency and numerical stability of the capsular ligament, the capsular ligament elements may need to be reoriented. For example, tie-contacts could be used to join the capsular ligament elements to the facet joint articular pillar rather than connecting elements node-to-node. This approach may remove the element bias towards positive AP shear, allowing the capsular ligament elements to be fit in tension, AP shear and LT shear in both the positive and negative direction.

In the 2D shell implementation of the capsular ligament, a coarse mesh was applied. However, the shell elements experienced buckling at free nodes during AP shear. To improve the stability and behaviour of the capsular ligament shell elements, the facet joint should be modelled in greater detail. This would include a more representative capsular ligament geometry as well as introducing the meniscoids and synovial fluid. The enclosed volume effect of the synovial fluid would maintain outward pressure on the 2D shells. The cartilage would also need to be re-meshed to be compatible with the new ligament implementation.

Experimentally, the capsular ligament and meniscoid geometry could be determined from micro-CT scans. The capsular ligament was found to be under prestrain in this study. Further experimental work would be needed to formalize this data and apply ligament prestrain to the computational model. For the synovial fluid characterization, a study similar to the one performed by Gacek et. al. [73] on the lumbar facet joint could be performed.

In both the 1D tension-only element implementation and the 2D shell implementation, another consideration would be to represent collagen fiber alignment in the capsular ligament. For 1D tension-only elements, this may involve adding additional elements and orienting them according to trends in collagen alignment. In the 2D shell implementation, the fiber alignment could be incorporated in the selected material model or by applying multi-scale modelling.

Letter of Copyright Permission

CCC Marketplace

This is a License Agreement between Gwennyth Carroll/University of Waterloo ("User") and Copyright Clearance Center, Inc. ("CCC") on behalf of the Rightsholder identified in the order details below. The license consists of the order details, the Marketplace Permissions General Terms and Conditions below, and any Rightsholder Terms and Conditions which are included below.

All payments must be made in full to CCC in accordance with the Marketplace Permissions General Terms and Conditions below.

Order Date	25-Oct-2023	Type of Use	Republish in a thesis/dissertation
Order License ID	1410311-1		
ISSN	1528-8951	Publisher	A S M E INTERNATIONAL
		Portion	Chart/graph/table/figure

LICENSED CONTENT

Publication Title	Journal of biomechanical engineering	Rightsholder	American Society of Mechanical Engineers ASME
Article Title	Strain Response in the Facet Joint Capsule During Physiological Joint Rotation and Translation Following a Simulated Impact Exposure: an in Vitro Porcine Model	Publication Type	e-Journal
		Issue	5
		Volume	144
		URL	http://ojps.aip.org/ASMEJournals/Biomechanical
Author/Editor	American Society of Mechanical Engineers.		
Date	01/01/1977		
Language	English		
Country	United States of America		

REQUEST DETAILS

Portion Type	Chart/graph/table/figure	Distribution	Canada
Number of Charts / Graphs / Tables / Figures Requested	1	Translation	Original language of publication
		Copies for the Disabled?	No
Format (select all that apply)	Electronic	Minor Editing Privileges?	No
Who Will Republish the Content?	Academic institution	Incidental Promotional Use?	No
Duration of Use	Life of current and all future editions	Currency	CAD
Lifetime Unit Quantity	Up to 499		
Rights Requested	Main product and any product related to main product		

NEW WORK DETAILS

Title	Experimental Characterization and Finite Element Modelling of Cervical Facet Joint Mechanics	**Institution Name**	University of Waterloo
		Expected Presentation Date	2023-11-10
Instructor Name	Professor Stewart McLachlin		

ADDITIONAL DETAILS

Order Reference Number	N/A	**The Requesting Person / Organization to Appear on the License**	Gwennyth Carroll/University of Waterloo

REQUESTED CONTENT DETAILS

Title, Description or Numeric Reference of the Portion(s)	Figure 1	**Title of the Article / Chapter the Portion Is From**	Strain Response in the Facet Joint Capsule During Physiological Joint Rotation and Translation Following a Simulated Impact Exposure: an in Vitro Porcine Model
Editor of Portion(s)	Fewster, Kayla M.; Guo, Joyce; Zehr, Jackie D.; Barrett, Jeff M.; Laing, Andrew C.; Callaghan, Jack P.	**Author of Portion(s)**	Fewster, Kayla M.; Guo, Joyce; Zehr, Jackie D.; Barrett, Jeff M.; Laing, Andrew C.; Callaghan, Jack P.
Volume / Edition	144		
Page or Page Range of Portion	2	**Issue, if Republishing an Article From a Serial**	5
		Publication Date of Portion	2022-05-01

SPECIAL RIGHTSHOLDER TERMS AND CONDITIONS

Permission is granted for the specific use of the ASME Figure 1 ONLY as stated herein and does not permit further use of the materials without proper authorization. As is customary, we request that you ensure proper acknowledgment of the exact sources of this material, the authors, and ASME as original publisher.

ELSEVIER LICENSE
TERMS AND CONDITIONS

Oct 25, 2023

This Agreement between Gwennyth Carroll ("You") and Elsevier ("Elsevier") consists of your license details and the terms and conditions provided by Elsevier and Copyright Clearance Center.

License Number	5651381027645
License date	Oct 17, 2023
Licensed Content Publisher	Elsevier
Licensed Content Publication	Journal of the Mechanical Behavior of Biomedical Materials
Licensed Content Title	Planar biaxial extension of the lumbar facet capsular ligament reveals significant in-plane shear forces
Licensed Content Author	Amy A. Claeson,Victor H. Barocas
Licensed Content Date	Jan 1, 2017
Licensed Content Volume	65
Licensed Content Issue	n/a
Licensed Content Pages	10
Start Page	127
End Page	136

Type of Use	reuse in a thesis/dissertation
Portion	figures/tables/illustrations
Number of figures/tables/illustrations	1
Format	electronic
Are you the author of this Elsevier article?	No
Will you be translating?	No
Title of new work	Experimental Characterization and Finite Element Modelling of Cervical Facet Joint Mechanics
Institution name	University of Waterloo
Expected presentation date	Nov 2023
Order reference number	2
Portions	1e
Requestor Location	Gwennyth Carroll 70 King Street S St Marys, ON N4X 14A Canada Attn: Gwennyth Carroll
Publisher Tax ID	GB 494 6272 12
Total	0.00 CAD
Terms and Conditions	

ELSEVIER LICENSE
TERMS AND CONDITIONS

Oct 25, 2023

This Agreement between Gwennyth Carroll ("You") and Elsevier ("Elsevier") consists of your license details and the terms and conditions provided by Elsevier and Copyright Clearance Center.

License Number	5651380894491
License date	Oct 17, 2023
Licensed Content Publisher	Elsevier
Licensed Content Publication	Journal of Biomechanics
Licensed Content Title	The failure response of the human cervical facet capsular ligament during facet joint retraction
Licensed Content Author	Derek J. Lee,Beth A. Winkelstein
Licensed Content Date	Sep 21, 2012
Licensed Content Volume	45
Licensed Content Issue	14
Licensed Content Pages	5
Start Page	2325
End Page	2329

Type of Use	reuse in a thesis/dissertation
Portion	figures/tables/illustrations
Number of figures/tables/illustrations	1
Format	electronic
Are you the author of this Elsevier article?	No
Will you be translating?	No
Title of new work	Experimental Characterization and Finite Element Modelling of Cervical Facet Joint Mechanics
Institution name	University of Waterloo
Expected presentation date	Nov 2023
Order reference number	1
Portions	Figure 1 A-D
Requestor Location	Gwennyth Carroll 70 King Street S St Marys, ON N4X 14A Canada Attn: Gwennyth Carroll
Publisher Tax ID	GB 494 6272 12
Total	0.00 CAD
Terms and Conditions	

SM

Stephen Mattucci <smattucci@uoguelph.ca>

To: Gwennyth Alexandra Carroll

Wed 2023-10-25 3:09 PM

HI Gwennyth,

Of course. Feel free to use any figures you like from my thesis. Just keep in mind, if they aren't my images, you'll need to request from the original source. Ah, this brings back memories from requesting permission for both of my theses. You're in the home stretch! Good luck!

Steve

Stephen Mattucci, PhD, PEng (he / his)
Assistant Professor | Engineering Education | Design and Core
THRN 2411 | +1-519-824-4120 x52431
University of Guelph, School of Engineering

I live and work on the traditional land of the Mississaugas of the Credit First Nations, Anishinaabek and Haudenosaunee Peoples. I acknowledge the harms of the past, and in the spirit of reconciliation and collaboration, I am committed to learning and unlearning about Indigenous peoples and ways of knowing.

References

[1] N. Jaumard, W. Welch and B. Winkelstein, "Spinal Facet Joint Biomechanics and Mechanotransduction in Normal, Injury and Degenerative Conditions," *Journal of Biomechanical Engineering,* vol. 133, 2011.

[2] G. C, M. P, M. Pitcher, H. Chambers, S. Mansfield, M. Madden, C. Jordon, A. Kinsella and M. Hodson, "Neck sprains after road traffic accidents: a modern epidemic," *Injury,* vol. 24, no. 3, pp. 155-157, 1993.

[3] K. Quinlan, J. Annest, B. Myers, G. Ryan and H. Hwardd, "Neck strains and sprains among motor vehicle occupants - United States, 2000," *Accident Analysis and Prevention,* vol. 36, pp. 21-27, 2004.

[4] J. Fice, D. Cronin and M. Panzer, "Cervical Spine Model to Predict Capsular Ligament Response in Rear Impact," *Annals of Biomedical Engineering,* vol. 29, no. 8, pp. 2152-2162, 2011.

[5] M. Corrales and D. Cronin, "Importance of the cervical capsular joint cartilage geometry on head and facet joint kinematics assessed in a Finite element neck model," *Journal of Biomechanics,* vol. 123, 2021.

[6] H. Wang, C. Zhou, Y. Yu, C. Wang, T.-u. Tsai, C. Han, G. Li and T. Cha, "Quantifying the range of relative motions of the intervertebral discs and facet joints in the normal cervical spine," *Journal of Biomechanics,* vol. 112, 2020.

[7] S. O'Leary, N. Paschas, J. Link, E. Klingenberg, J. Hu and K. Athanasiou, "Facet Joints of the Spine: Structure-Function Relationships, Problems and Treatments, and the Potential for Regeneration," *Annual Review of Biomedical Engineering,* vol. 20, pp. 145-170, 2018.

[8] E. Ban, S. Zhang, V. Zarei, V. Barocas, B. Winkelstein, Picu and Catalin, "Collagen Organization in Facet Capsular Ligaments aries with Spinal Region and with Ligament Deformation," *Journal of Biomechanics,* vol. 139, 2017.

[9] G. Siegmund, B. Winkelstein, P. Ivancic, M. Svensson and A. Vasavada, "The Anatomy and Biomechanics of Acute and Chronic Whiplash Injury," *Traffic Injury Prevention,* vol. 10, pp. 101-112, 2009.

[10] G. Siegmund, B. Myers, M. Davis, H. Bohnet and B. Winkelstein, "Mechanical Evidence of Cervical Facet Capsule Injury During Whiplash," *Spine,* vol. 26, no. 19, pp. 2095-2101, 2001.

[11] B. Stemper, N. Yoganandan and F. Pintar, "Validation of a head-neck computer model for whiplash simulation," *Med Biol Eng Comput,* vol. 42, no. 333-338, pp. 333-338, 2004.

[12] M. Correia, S. McLachlin and D. Cronin, "Optimization of muscle activation schemes in a finite element neck simulating volunteer frontal impact scenarios," *Journal of Biomechanics,* vol. 104, 2020.

[13] Y. H. Kim, B. Khuyagbaatar and K. Kim, "Recent advances in finite element modeling of the human cervical spine," *Journal of Mechanical Science and Technology,* vol. 32, no. 1, 2018.

[14] M. Panzer and D. Cronin, "C4-C5 segement finite element model development, validation and load-sharing investigation," *Journal of Biomechanics,* vol. 42, no. 4, pp. 480-490, 2009.

[15] S. Mattucci, *Strain Rate Dependent Properties of Younger Human Cervical Spine Ligament,* University of Waterloo, 2011.

[16] K. Quinn and B. Winkelstein, "Vector correlation technique for pixel-wise detection of collagen fiber realignment during injurious tensile loading," *Journal of Biomedical Optics,* vol. 14, no. 5, 2009.

[17] N. Yoganandan, S. Kumaresan and F. Pintar, "Geometric and Mechanical Properties of Human Cervical Spine Ligaments," *Journal of Biomechanics Engineering,* vol. 122, 2001.

[18] D. Cronin, D. Singh, D. Gierczycka, J. Barker and D. Shen, "Chapter 13," in *Basic Finite Eleemtn method as Applied to Injury Biomechanics*, Elsevier Inc, 2018.

[19] D. Hartlen and D. Cronin, "Arc-Length Re-Parameterization and Signal Registration to Determine a Characteristic Average and Statistical Response Corridors of Biomechanical Data," *Frontiers in Bioengineering and Biotechnology ,* vol. 10, 2022.

[20] B. Radanov, M. Sturzenegger and D. Stegano, "Long-Term Outcome after Whiplash Injury. A 2-year Follow-up Considering Features of Injury Mechanism and Somatic, Radiologic and Psycosocial Findings," *Medicine,* vol. 74, pp. 281-297, 1995.

[21] K. Watanabe and e. al, "The Long-term Impact of Whiplash Injuries on Patient Symptoms and the Associated Degenerative Changes Detected Using MRI," *Spine,* vol. 46, no. 11, pp. 710-716, 2021.

[22] D. Zuby and A. Lund, "Preventing Minor Neck Injuries in Rear Crashes - Forty Years of Progress," *JOEM,* vol. 52, no. 4, 2010.

[23] L. Barnsley, S. Lord and N. Bogduk, "Comparative local anaesthetic blocks in the diagnosis of cervical zygapophysial joint pain," *Pain,* vol. 55, no. 1, pp. 99-106, 1993.

[24] N. Bogduk and A. Marland, "The Cervical Zygapophysial Joints as a Source of Neck Pain," *Spine,* vol. 13, no. 6, 1988.

[25] S. Lord, L. Barnsley, B. Wallis and N. Bogduk, "Chronic Cervical Zygapophysial Joint Pain After Whiplash: A Placebo-Controlled Prevalence Study," *Spine,* vol. 21, no. 15, pp. 1737-1744, 1996.

[26] A. Dwyer, C. Aprill and N. Bogduk, "Cervical Zygapophyseal Joint Pain Patterns I: A Study in Normal Volunteers," *Spin,* vol. 15, no. 6, 1990.

[27] M. C. J. Panjabi, K. Nibu, J. Frauer and V. Michael, "Capsular LIgament Stretches During In Vitro Whiplash Simulations," *Journal of Spinal Disorders,* vol. 11, no. 3, pp. 227-232, 1998.

[28] M. Panjabi, A. Pearson, S. Ito, P. Ivancic, E. Fimenez and Y. Tominaga, "Cervical Spine Ligament Injury During Simulated Frontal Impact," *Spine,* vol. 29, no. 21, pp. 2395-2403, 2004.

[29] B. Deng, P. Begeman, K. Yan, S. Tashman and A. King, "Kinematics of Human Cadaver Cervical Spine During Low Speed Rear-End Impacts," *Stapp Car Crash Journal,* vol. 44, 2000.

[30] G. Siegmund, M. Davis, K. Quinn, E. Hines, B. Myers, S. Ejima, K. Ono, K. Kamiji, T. Yasuki and B. Winkelstein, "Heat-Turned Postures Increases the Risk of Cervical Facet Capsule Injury During Whiplash," *Spine,* vol. 33, no. 15, pp. 1643-1649, 2008.

[31] A. Pearson, P. Ivancic, S. Ito and M. Panjabi, "Facet Joint Kinematics and Injury Mechanism During Simulated Whiplash," *Spine,* vol. 29, no. 4, pp. 390-397, 2004.

[32] R. McLain, "Mechanoreceptor Endings in Human Cervical Facet Joints," *Spine,* vol. 19, no. 5, pp. 495-501, 1994.

[33] Y. Lu, C. Chen, S. Kallakuri, A. Patwardhan and J. Cavanaugh, "Neural Response of Cervical Facet Joint Capsule to Stretch: A Potential Whiplash Pain Mechanism," *Stapp Car Crash Journal,* vol. 49, no. 49-65, 2005.

[34] K. Lee, M. Davis, R. Mejilla and B. Winkelstein, "In vivo cervical facet capsule distraction: Mechanical Implications for Whiplash and Neck Pain," *Stop Car Crash Journal,* vol. 48, pp. 373-395, 2004.

[35] R. Nightingale, B. Myers and N. Yoganandan, "Neck Injury Biomechanics," in *Accidental Injury: Biomechanics and Prevention* , Springer, 2015.

[36] D. Cronin, D. Singh, D. Gierczycka, J. Barker and D. Shen, "Modeling the Neck for Impact Scnearios," in *Basic Finite Element Methods as Applied to Injury Biomechanics*, Elsevier, 2018.

[37] Arcadian and Pixelsquid, "Wikimedia Commons," 6 December 2020. [Online]. Available: https://commons.wikimedia.org/wiki/File:Illu_vertebral_column.svg. [Accessed June 2023].

[38] O. College, "Wikimedia Commons," 19 June 2013. [Online]. Available: https://commons.wikimedia.org/wiki/File:723_Cervical_Vertebrae.jpg; License: https://creativecommons.org/licenses/by/3.0/deed.en. [Accessed June 2023].

[39] B. Clinic, "Cervical Facet Joint Syndrome," 20 March 2012. [Online]. Available: https://www.blackberryclinic.co.uk/articles/cervical-facet-joint-syndrome/. [Accessed June 2023].

[40] Pal, Routal and Saggu, "The orientation of the articular facets of the zygapophyseal joints at the cervical and upper thoracic region," *J Anat,* vol. 198, pp. 431-441, 2001.

[41] M. Panjabi, T. Oxland, K. Takata, G. Vijay, J. Duranceau and M. Krag, "Articular Facets of the Human Spine: Quantitative Three-Dimensional Anatomy," *Spine,* vol. 18, no. 10, pp. 1298-1210, 1993.

[42] W. Womack, D. Woldtvedt and Puttlitz, "Lower cervical spine facet cartilage thickness mapping," *Osteoarthritis and cartilage,* vol. 16, no. 9, pp. 1018-1023, 2008.

[43] N. Yoganandan, S. Knowles, D. Maiman and F. Pintar, "Anatmoic Study of the Morphology of Human Cervical Facet Joint," *Spine,* vol. 28, no. 20, pp. 2317-2323, 2003.

[44] J. Hughes, C. Chan, S. Polamalu, R. Debski and M. Voker, "Chapter 3: Biomechanics of Ligaments," in *Orthopaedic Biomechanics in Sports Medicine*, ISAKOS, 2021.

[45] J. Zitnay and J. Weiss, "Load Transfer, Damage, and Failure in Ligaments and Tendons," *Journal of Orthopaedic Research,* 2018.

[46] T. Siebert, H. Screen and C. Rode, "Chapter 8," in *Computational Modelling of Biomechanics and Biotribology in the Musculoskeletal System - Biomaterials and Tissues*, 2021.

[47] C. Chen, Y. Lu, S. Kallakuri, A. Patwardhan and J. Cavanaugh, "Distribution of A-Delta and C-Fiber Receptors in the Cervical Facet Joint Capsule and Thier Response to Stretch," *Journal of Bone and Joint Surgery,* vol. 88, no. 8, 2006.

[48] B. Winkelstein, R. McLendon, A. Barbir and B. Myers, "An anatomic investigation of the human cervical facet capsule quantifying muscle insertion area," *J. Anat,* vol. 198, no. 455-461, 2001.

[49] N. Yoganandan, S. Kumaresan and F. Pintar, "Biomechanics of the Cervical Spine Part 2. Cervical Spine Soft Tissue Responses and Biomechanical Modelling," *Clinical Biomechanics,* vol. 16, pp. 1-27, 2001.

[50] Cowin and Stephen, "Tendon and Ligament," in *Tissue Mechanics*, 2007.

[51] R. Kelc, J. Naranda, M. Kuhta and M. Vogrin, "The Physiology of Sports Injuries and Repari Processes," in *Current Issues in Sports and Exercise Medicine*, InetchOpen, 2013.

[52] J. Freeman, "Tissue Engineering Options for Ligament Healing," *Bone and Tissue Regeneration Insights,* vol. 2, no. 71, 2009.

[53] H. Henninger, C. Underwood, S. Romney, G. Davis and J. Weiss, "Effect of Elastin Digestion of the Quasi-Static Tensile Response of Medial Collateral Ligament," *Journal of Orthopaedic Research,* 2013.

[54] K. Quapp and J. Weiss, "Material Characterization of Human Medial Collateral Ligament," *Journal of Biomechanical Engineering,* vol. 120, 1998.

[55] H. Henninger, W. Valdes, S. Scott and J. Weiss, "Elastin governs the mechanical response of medial collateral ligament under shear and transverse loading," *Acta Biomaerialia,* vol. 25, pp. 304-312, 2015.

[56] J. Weiss, J. Gardiner and C. Bonifasi-Lista, "Ligament material behavior is nonlinear, viscoelastic and rate-independent under shear loading," *Journal of Biomechanics,* vol. 35, no. 7, pp. 943-950, 2002.

[57] J. Yao, Z. Lian, B. Yang and Y. Fan, "Chapter 3: Biomechanics of Ligaments," in *Frontiers in Orthopaedic Biomechanics*, Springer, 2020.

[58] B. Ellis and J. Weiss, "Effects of Aging on the Cellular Function, Healing and Mechanical Properties of Ligaments," *Mechanical Properties of Aging Soft Tissues,* pp. 167-185, 2014.

[59] S. Woo, J. Hollis, D. Adams, R. Lyon and S. Takai, "Tensile properties of the human femur-anterior cruciate ligament-tibia complex. The effects of speicmen age and orientation.," *AM J Sports Med,* vol. 19, no. 23, pp. 217-25, 1991.

[60] S. Woo, M. Hollis, D. Adams, R. Lyon and S. Takai, "Tensile properties of the human femur-anterior cruciate ligament-tibia complex," *The American Journal of Sports Medicine,* vol. 19, no. 3, 1991.

[61] C. Bass, C. Planchak and S. Lucas, "The Temperature-Dependent Viscoelasticity of Porcine Lumbar Spine Ligaments," *Spine,* vol. 42, 2007.

[62] S. Woo, T. Le, M. Gomez, S. Sato and F. Field, "Temperature Dependent Behavior of the Canine Medial Collateral Ligament," *Journal of Biomechanical Engineering,* vol. 109, no. 1, pp. 68-71, 1987.

[63] S. Hasberry and M. J. Pearcy, "Temperature dependence of the tensile properties of interspinous ligaments of shee;," *Journal of Biomedical Engineering,* vol. 8, no. 1, pp. 62-66, 1986.

[64] A. Hoffman, D. Robichaud, J. Duquette and P. Grigg, "Determining the effect of hydration upon the properties of ligaemnts using pseudo Gaussian stress stimuli," *Journal of Biomechanics,* vol. 38, pp. 1636-1642, 2005.

[65] T. Haut and R. Haut, "The state of tissue hydration determines the strain-rate sensitive stiffness of human patellar tendon," *Journal of Biomechanics,* vol. 30, no. 1, pp. 79-81, 1997.

[66] M. Ekiert, J. Karbowniczek, U. Stachewicz and A. Mlyniec, "The effect of multiple freeze-thaw cycles on the viscoelastic properties and microstructure of bovien superficial digital flexor tendon," *Journal of the Mechanical Behaviour of Biomedical Materials,* vol. 120, 2021.

[67] H. Huang, J. Zhang, K. Sun, X. Zhang and S. Tian, "Effects of repetitive multiple freeze-thaw cycles on the biomechanical properties of human flexor digitorum superficialis and flexor pollicis longus tendons," *Clinical Biomechanics,* vol. 26, pp. 419-423, 2011.

[68] K. Suto and e. al., "Repeated freeze-thaw cycles reduce the survival rate of osteocytes in bone-tendon constructs without affecting the mechanical properties of tendons," *Cell Tissue Bank,* vol. 13, pp. 71-80, 2010.

[69] A. Lee and D. Elliott, "Freezing does not alter multiscale tendon mechanics and damage mechanisms in tension.," *Annals of the New York Academy of Sciences - Musculoskeletal Repair and Regeneragion,* pp. 85-94, 2018.

[70] S. Woo, C. Orlando, J. Camp and W. Akeson, "Effects of postmortem storage by freezing on ligament tensile behaviour," *Journal of Biomechanics,* vol. 19, no. 5, pp. 399-404, 1986.

[71] M. Hongo and e. al, "Effect of Multiple Freeze-Thaw Cycles on Intervertebral Dynamics Motion Characteristics in the Porcine Lumbar Spine," *Journal of Biomechanics,* vol. 41, no. 4, pp. 916-920, 2008.

[72] S. Maas, A. Erdemir, J. Halloran and J. Weiss, "A general framework for application of prestrain to computational models of biological materials," *Journal of the Mecanical Behavior of Biomedical Materials ,* vol. 61, pp. 499-510, 2016.

[73] E. Gacek, A. Ellingson and V. Barocas, "In Situ Lumbar Facet Capsular Ligament Strains Due to Joint Pressure and Residual Strain," *Journal of Biomechanical Engineering,* vol. 144, 2022.

[74] D. Lee and B. Winkelstein, "The failure response of the human cervical facet capsular ligament during facet joint retraction," *Journal of Biomechanics,* vol. 45, pp. 2325-2329, 2012.

[75] F. Pintar, N. M. T. Yoganandan, A. Elhagediab and A. Cances, "Biomechanical Properties of Human Lumbar Spine Ligament," *Journal of Biomechanics,* vol. 25, no. 11, pp. 1351-1356, 1992.

[76] K. Fewster, J. Guo, J. Zehr, J. Barrett, A. Laing and J. Callaghan, "Strain Response in the Facet Joint Capsule During Physiological Joint Rotation and Translation Following a Simulated Impact Exposure: An In Vitro Porcine Model," *Journal of Biomechanical Engineering,* vol. 144, 2022.

[77] R. Quarrington, J. Costi, B. Freeman and C. Jones, "The effect of axial compression and distraction on cervical facet mechanics during anterior shear, flexion, axial rotation, and lateral bending motions," *Journal of Biomechanics,* vol. 83, pp. 205-213, 2019.

[78] A. Claeson and V. Barocas, "Planar biaxial tension of the lumbar facet capsular ligament reveals significant in-plane shear forces," *Journal of the Mechanical Behaviour of Biomedical Materials,* vol. 65, pp. 127-136, 2017.

[79] K. Quinn and B. Winkelstein, "Detection of Alterend Colalgen Fiber Alignment in the Cervical Facet Capsule After Whiplash-Like Joint Retraction," *Annals of Biomedical Engineering,* vol. 39, no. 8, pp. 2163-2173, 2011.

[80] J. Little and P. Khalsa, "Material Properties of the Human Lumbar Facet Joint Capsule," *Journal of Biomechanical Engineering,* vol. 127, 2005.

[81] B. Winkelstein, R. Nightingale, W. Richardson and B. Myers, "The Cervical Facet Capsule and Its Role in Whiplash Injury: A Biomechanical Investigation," *Spine,* vol. 25, no. 10, pp. 1238-1246, 2000.

[82] P. Ivancic, M. N. A. ,. T. Y. Coe, E. Carlson, W. Rubin, Dipl-ling and M. Panjabi, "Dynamic Mechanical Properties of Intact Human Cervical Spine Ligament," *Spine,* vol. 7, no. 6, pp. 659-665, 2007.

[83] Toyota, "About THUMS," Toyota Motor Corporation, [Online]. Available: https://www.toyota.co.jp/thums/about/. [Accessed September 2023].

[84] J. Osth, K. Brolin, M. Svensson and A. Linder, "A Female Ligamentous Cervical Spine Finite Element Model Validated for Physiolgoical Loads," *Journal of Biomechanical Engineering,* vol. 138, 2016.

[85] J. Osth, M. Mendoza-Vazquez, F. Sato, M. Svensson, A. Linder and K. Brolin, "A female head-neck model for rear impact simulations," *Journal of Biomechanics,* vol. 51, pp. 49-56, 2017.

[86] GHBMC, "About Us," [Online]. Available: http://www.ghbmc.com/. [Accessed September 2023].

[87] M. Iwamoto and Y. Nakahira, "Development and Validation of the Total HUman Model for Safety (THUMS) Version 5 Containing Multiple 1D Muscles for Estimating Occupant Motions with Muscle Activation During Side Impacts," *Stapp Car Crash Journal ,* vol. 59, pp. 53-90, 2015.

[88] M. Iwamoto, Y. Nakahira and H. Kimpara, "Development and Validation of the Total HUman Model for Safety (THUMBS) Toward Further Understanding of Occupant Injury Mechanisms in Precrash and During Crash," *Traffic Injury Prevention,* vol. 16, pp. 36-48, 2015.

[89] S. Mattucci and D. Cronin, "A method to characterize average cervical spine ligament response based on raw data sets for implementtaion into injury biomechanics models," *Journal of Mechanical Behaviour of Biomedical Materials,* vol. 41, pp. 251-260, 2015.

[90] J. Barker, D. Cronin and R. Nightingale, "Lower Cervical Spine Motion Segment Computational Model Validation: Kinematic and Kinetic Response for Quasi-static and Dynamic Loading," *Journal of Biomechanical Engineering,* vol. 139, no. 6, 2017.

[91] J. Barker and D. Cronin, "Multilevel Validation of a Male Neck Finite Element Model With Active Musculature," *Journal of Biomechanical Engineering,* vol. 143, no. 1, 2021.

[92] J. DeWit and D. Cronin, "Cervical spine segment finite element model for traumatic injury prediction," *Journal of the mechanical Behavior of Biomedical Materials,* vol. 10, pp. 138-150, 2012.

[93] Anatomography, "Cervical Vertebrae - close-up - lateral view," January 2013. [Online]. Available: https://commons.wikimedia.org/wiki/File:Cervical_vertebrae_-_close-up_-_lateral_view.png License: https://creativecommons.org/licenses/by-sa/2.1/jp/deed.en. [Accessed June 2023].

[94] M. Wedel, "Neural spine bifurcation in sauropod dinosaurs of the morrison formation: Ontogenetic and phylogenetic implications," *PalArch's Journal of Vertebrate Paleontology,* vol. 1, no. 1-34, p. 10, 2013.

[95] D. Brown, W. Christian and R. Hanson, "Tracker: Video Analysis and Modeling Tool," [Online]. Available: https://tracker.physlets.org/. [Accessed August 2023].

[96] J. Zehr, J. Barrett, K. Fewster, A. Laing and J. Callaghan, "Strain of the facet joint capsule during rotation and translation range-of-motion tests: an in vitro porcine model as a human surrogate," *The Spine Journal,* vol. 20, pp. 475-487, 2020.

[97] J. Schindelin, I. Arganda-Carreras and e. al, "Fiji: an open-source platform for biological-image analysis.," *Nature Methods,* vol. 7, no. 676-682, p. 9, 2012.

[98] X. Rong, Z. Liu, B. Wang, H. Chen and H. Liu, "The Facet Orientation of the Subaxial Cervical Spine and the Implications for Cervical Movements and Clinical Conditions," *Spine Anatomy,* vol. 42, pp. E320-E325, 2016.

[99] C. Rampersadh, A. Agnew, S. Malcom, D. Gierczycka, J. Iraeus and D. Cronin, "Factors affecting the numerical response and fracture location of the GHBMC M50 rib in dynamic anterior-posterior loading," *Journal of the Mechanical Behavior of Biomedical Materials,* vol. 136, 2022.

[100] R. Quarrington, J. Costi, B. Freeman and C. Jones, "Quantitative evaluation of facet deflection, stiffness, strain and failure load during simulated cervical spine trauma," *Journal of Biomechanics,* vol. 72, pp. 116-124, 2018.

Appendix A: Test Day Protocol

Experiment Date:
Sample Details:

- *Identifier:*
- *Level:*
- *Side:*

Day 1

- ☐ Remove sample from freezer and move to fridge to thaw overnight
  - *Time to fridge:*
- ☐ Cut 3” pots down to 1.75” (x2)

Day 2

Note: Spray sample every 5-10 min with saline
Measure temperature periodically

- ☐ Record start time
  - *Start time:*
- ☐ Remove sample from fridge
  - *Time removed:*
- ☐ Turn on VIVO to warm up (see VIVO SOP)
  - Ensure all controls are set to their neutral position.
- ☐ Measure length of capsular ligament (CL) with digital calipers
  - *Length (Yoganandan):*
  - *Length (Insertion Points):*

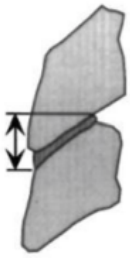
CL

- ☐ Dry ligament with paper towel (temporarily)
- ☐ Drill seven pilot holes with 1/64 drill bit:
  - Superior vertebral body (endplate) x3
  - Superior facet pillar x1
  - Inferior posterior elements x2
  - Inferior facet pillar x1
- ☐ Screw M4 1” wood screws into pilot holes
- ☐ Palpate and mark vertical line (in plane of facet pillar) with India Ink
  - When manipulating, compare movement to vertical on metal block
- ☐ Expand vertical to grid of dots on CL using India Ink
  - *Size of grid:*
- ☐ Mark facet pillar
- ☐ Spray with saline then dry bone with paper towel
- ☐ Prepare pots
  - Cellophane lining over cardboard false bottom
- ☐ Clamp screw on inferior vertebrae and position articulating arm over pot so articulating surface is vertical

- ☐ Prepare cement, then pour into pot.
- ☐ Wait about 20 minutes
- ☐ Put base fixture on VIVO and zero load cell
- ☐ Use pencil to mark line of lateral translation on cement while manipulating sample.
    - Use set square to find perpendicular line and extend to mark pot.
    - Ensure it aligns with VIVO AP
- ☐ Spray with saline then dry bone
- ☐ Prepare cement, then pour into second pot with cellophane lining.
    - Support potted side with 'bridge'
- ☐ As cement hardens, add flag to pot
- ☐ Wait 20 minutes, then wrap in saline soaked gauze
- ☐ Wait another 20 minutes
- ☐ Fix superior pot to superior fixture
    - Ensure the grid is facing the fixture adaptor and the mark on the pot is aligned with VIVO AP (the flat face of the superior fixture)
- ☐ Attach superior fixture to VIVO
- ☐ Support inferior pot as the base is brought up until in contact (~5N force) then fix bottom fixture
- ☐ **Mark pot**
- ☐ Take picture with DSLR camera
- ☐ Set VIVO to force mode
    - Apply load in tension, AP shear, and LT shear until ~ 3mm displacement and
    - Measure load
- ☐ Set VIVO to displacement mode.
    - Apply amount of displacement determined in previous step
    - Use to find '0' position
- ☐ Digitize VIVO origin and coordinate system
    - VIVO origin
        i. Point 1: FE arm
        ii. Point 2: Ab/Ad arm
        iii. Point 3: Base
    - Axis System (block on base)
        i. Point 4: BL
        ii. Point 5: BR
        iii. Point 6: TR
- ☐ Digitize 4 points on Facet Joint

Transformation Matrix			

- ☐ Set up camera and lighting.
- ☐ **Take snapshot with calibration piece (ruler) each time move camera**
    - *Length of calibration piece:*
- ☐ Load sample – 5 rounds of each in sin waveform.
    - Quasi-static – sample at 100 Samples/s; camera at 60fps
    - High rate – sample at 1000Hz; camera at 500 fps

	Loading	**Max Displacement**	**Waveform**	
			Max	**Min**
Quasi-static Rate 0.1 mm/s 5 cycles	Tension (AP)			
	AP (Tension)			
	LT			
	AR			
High Rate 10 mm/s 10 cycles	Tension (AP)			
	AP (Tension)			
	LT			

    - Do Tension and AP, then move camera
    - Do LT and AR, then move camera
    - Do AP failure OR resection
    - Record video
        i. Quasi - Every other frame (30fps) → then every 3 (10fps)
        ii. Medium – Every frame (500fps) → then every 3 (167fps)
- ☐ If no failure:
    - (1) If sample started in tension
        i. VIVO in displacement control with 0 displacement (should be rigid)
        ii. Start recording
        iii. Use scalpel to cut CL (along line of dots)
    - (2) If sample started in AP
        i. Fail sample in AP shear at quasi-static rate.

Camera Protocol:

- ☐ Turn on camera, then software
- ☐ Set resolution to 1024 x 1024 and frame rate to 60fps
- ☐ "Shade" camera
    - Re-"shade" whenever change rate or lighting
- ☐ Set to "Start" trigger mode
- ☐ Set where to save snapshot
- ☐ Shutdown: software, lens, power off

Appendix B: Verification of Experimental Methods

VIVO Performance

The VIVO positions closely matched the input positions (Figure B.1), particularly during quasi-static loading where the VIVO position closely matched the input waveform with an error generally less than 0.06 mm. Off-axis position held stable with an error generally less than 0.05 mm.

For high-rate loading in the primary loading direction, the VIVO position tended to undershoot the waveform for the first cycle or two and overshoot the waveform for the last two or three cycles while the waveform ramped down the displacement. In some load scenarios, typically LT shear, the VIVO position undershot the input waveform until the fourth cycle. By the fifth and sixth cycles, those used for data analysis, the VIVO position closely matched the input waveform with an error less than 0.1 mm. Off-axis position held stable with an error typically less than 0.1 mm.

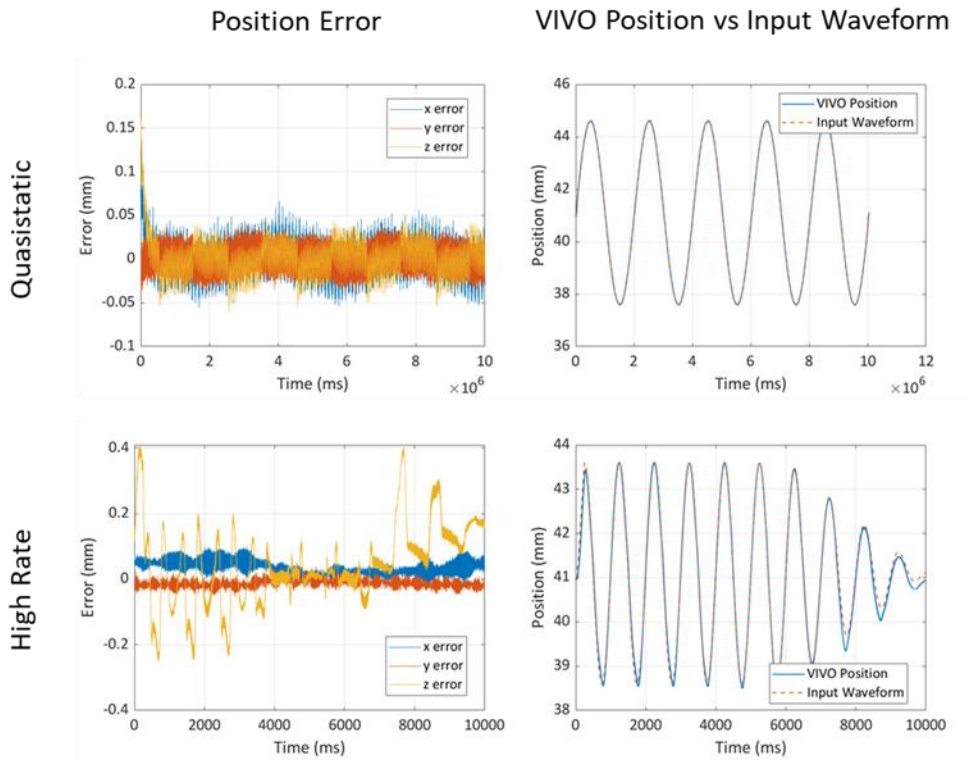

Figure B.1: VIVO performance for representative specimen (specimen 1) in AP shear. (Top) Quasi-static. (Bottom) High-rate. (Left) error signals reported by VIVO in all translational degrees of freedom. (Right) Comparing the input waveform and the position reported by the VIVO.

VIVO Raw Data

Raw VIVO data provides valuable insight into the experiment performance. The position data, together with error data reported by the VIVO, indicates the VIVO performed well at the quasi-static rate of loading but at the high rate, errors in the primary loading direction at the beginning and end of the test are observed. For both rates, the VIVO positions closely follow the input positions for the cycles used for analysis.

VIVO raw data was reported as a force vs time curve. As loading was displacement-controlled, the displacement was related to time by the input position curve. In the high-rate force vs time raw data, the maximum force increased at the beginning of the test and decreased at the end of the test, corresponding with the VIVO displacement ramping in and out. For both high-rates and quasi-static tests, after the first cycle, not including the ramp-up in the high-rate curves, the force decreased over the first few cycles approaching an asymptote. In tension, the force for several specimen went compression (Figure B.2).

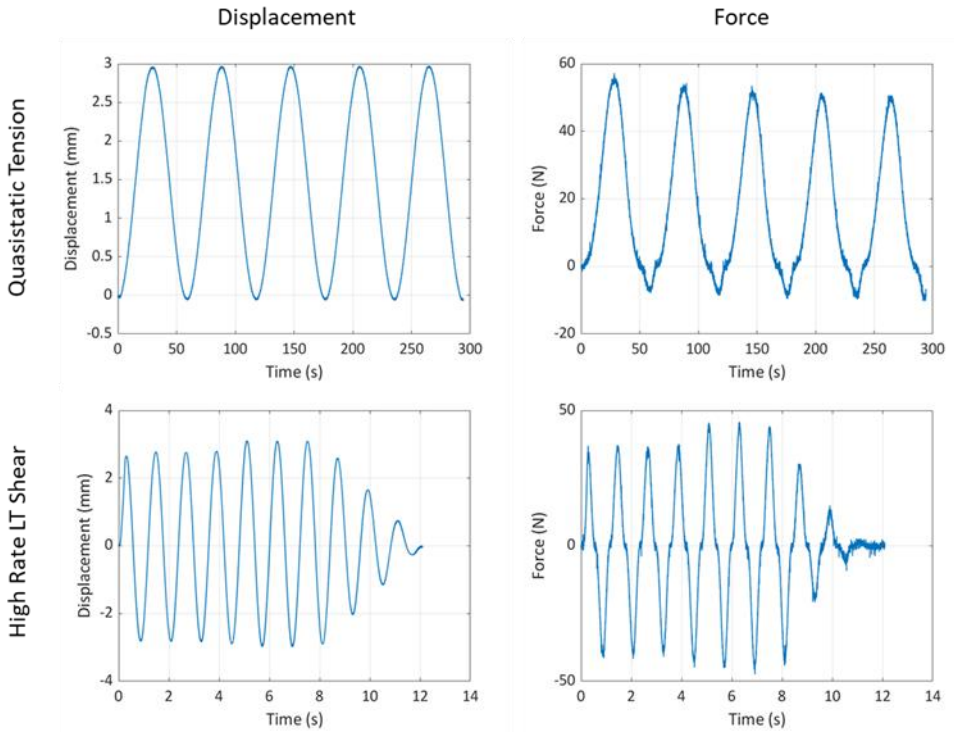

Figure B.2: Representative raw data graphs plotting displacement vs time and force vs time. (Top) Quasi-static tension with force vs time graph showing the peak force leveling off by the fourth cycle and compression near zero displacement. (Bottom) High-rate LT Shear showing VIVO ramp-up in displacement and corresponding forces.

The force data provided information to evaluate the experiment methodology. By cycles four and above of the force vs time curve, force approached an asymptote, indicating the ligaments were conditioned before the cycles extracted for analysis (Figure B.2). Force vs time raw data also indicated several of the specimens went into compression during tension loading at both rates (Figure B.2). The regions of compression were removed (Section 3.1.3) before the average force-displacement curves were calculated.

Compression during tension loading, where the initial neutral position was not in compression, may be explained by the ligament hysteresis curve. When determining the neutral position in tension, the loading curve was used to determine the neutral position, however the same displacement in the unloading curve put the joint into slight compression. As the initial neutral position was not in compression, this should not affect the AP and LT loading. The methodology for determining the neutral zone worked quite well in the AP and LT shear directions – the length of the toe region is typically similar in the negative and positive directions. Although some specimens displayed bias in the toe region (longer toe region) towards the positive or negative direction.

Displacement used for analysis used cross-head displacement of the VIVO rather than movement of the vertebral body itself. This assumed a perfect rigid coupling between the VIVO and the specimen, which was not the case. The vertebral bone was usually covered by soft tissue or periosteum, making it difficult to mark the bone itself. Additionally, the India Ink pen used was not able to create sharp, clear marks on the periosteum or bone. As a result, the displacement of the bony anatomy could not be tracked optically, so the cross-head displacement was used instead. Other groups working on the facet joint have drilled flags into the bony anatomy, enabling optical tracking of vertebral displacement directly.

For this study, the error from using cross-head displacement was quantified using the specimen with the clearest markers on the superior and inferior bone and a flag marker (used as a surrogate for the fixture displacement as it was rigidly potted in the cement). The maximum relative movement between the marker on the inferior bone and the flag was about 0.4 mm (typically closer to 0.3 mm) in AP shear which corresponds to 11% of the maximum displacement, not

considering the negative AP direction during which contact occurred between the inferior bone and superior cement. In tension, the maximum relative movement was about 0.5 mm, which corresponds to about 17% of the maximum displacement.

Several important factors should be noted. First, error in optical digitization may have increased the estimated error in tension as the error in tension was exasperated by the difficulty in marking exposed bone (some relative movement between bone and bone marker). Second, only the relative movement of the inferior bone and flag was reported as there was no corresponding flag in the superior pot, only a marker on the fixture. Third, the flag was not perfectly in line with the capsular ligament which would influence the magnitude of relative displacement due to depth perception of the camera. For example, a mark on the fixture in the foreground reported a peak displacement up to 0.5 mm greater than the flag, which was approximately aligned with the capsular ligament. Finally, the error estimation was based on a single specimen. The specimens, and specimens' potting, were highly variable, as previously noted, so relative movement between bone and fixtures would be different between specimens.

Capsular Ligament Strain

Before digitizing the capsular ligament markers to calculate capsular ligament strain, a calibration image was used to confirm that the parallax effect was not observed in the image within the region of interest.

An image of the specimen with a ruler aligned with the capsular ligament was taken as a calibration image and the distance between marks was measured using Fiji [97]. On the left side, center, and right side of the image, 5 mm (distance between ruler marks) corresponded with 13.7 pixels/mm. The error in digitizing the optical data was about 0.15 mm, based on variation in the digitized displacement in the non-loading direction of the flag marker, which should have only be displaced in the loading direction.

The Matlab implementation used to calculate Green strain from the digitized markers was verified using a simple unit element tested in uniaxial x elongation, uniaxial y elongation, and shear compared to theoretical calculations. The Matlab output exactly matched the theoretical

calculations for the simple loading modes. Additionally, a representative experimental element under uniaxial x elongation, uniaxial y elongation, shear loading, and multi-modal loading was compared to FEA software (LS-Dyna) output. A second test with the representative element was performed to verify the Matlab script could calculate strain when the initial element was not a right-angled rectangle. Positions for a representative experimental element were taken from the video digitization. In the multidirectional loading, each node in the element was displaced separately in the x- and y-directions.

The Matlab output was within 1% strain of the LS-Dyna output, so the Matlab implementation was used to calculate ligament strain (Table B.1).

Table B.1: DYNA verification of Matlab script to calculate Green Strain

	Uniaxial Tension in X			Uniaxial Tension in Y			Shear			Multidirectional		
	Exx	Eyy	Exy	Exx	Eyy	Exy	Exx	Eyy	Exy	Exx	Eyy	Exy
Matlab Implementation	1.27	0.00	-0.05	0.03	0.56	0.17	0.26	0.10	0.28	0.80	0.21	0.04
Dyna Implementation	1.28	0.00	-0.04	0.03	0.56	0.17	0.27	0.10	0.28	0.81	0.22	0.05

Error in the optical digitization used to estimate ligament strain was about 0.15 mm and was partly due to the semi-automatic tracking of markers. The irregular shapes of the markers, with indistinct boundaries and changes in morphology over time, made it difficult to track the makers – the tracking software jumped between points within the markers during analysis. Additionally, light reflecting off the tissue, exacerbated by the saline solution sprayed on the tissue for hydration, changed the intensity of marker pixels, potentially shifting the location of the tracker. At times, reflections covered parts of the marker, obscuring it from view.

Ensuring regular markers, with clear boundaries, are applied to specimens could help mitigate these errors. However, preventing reflections from hydration is more difficult as the specimen must remain hydrated during experimentation for more accurate representation of the in vivo mechanical properties.

Appendix C: Supplementary Study – Mattucci Tension to Failure

The purpose of this supplementary study was to replicate Mattucci's tension to failure experiment as an anchor point for the current methodology.

Two specimens, the right and left C2 - C3 facet joint pair from a male donor aged 62 years, were isolated for the supplementary study. The specimens were prepared and loaded in sub-catastrophic quasi-static tension as described in Chapter 3. To replicate Mattucci's study, each specimen was then preconditioned in tension by 20 cycles to 0.5 mm at a frequency of 1 Hz. Subsequently, a preload of 5 N was applied and the specimens were loaded to failure in tension at a rate of 1 mm/s (specimen 1) or 4 mm/s (specimen 2).

The sub-catastrophic results were plotted against the average tension force-displacement curve from Chapter 3 (Figure C.1) and the tension to failure response was plotted against Mattucci average and Mattucci spread of data (Figure C.2).

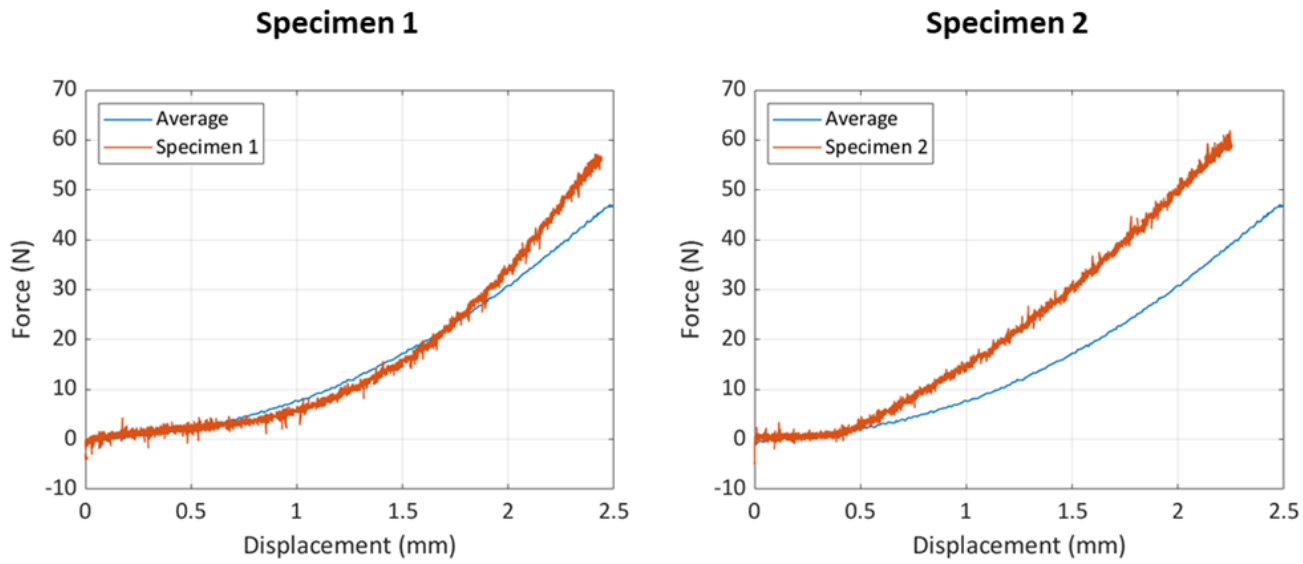

Figure C.1: Comparing specimen sub-catastrophic tension data from the supplementary study to the average tension force-displacement curve from Chapter 3.

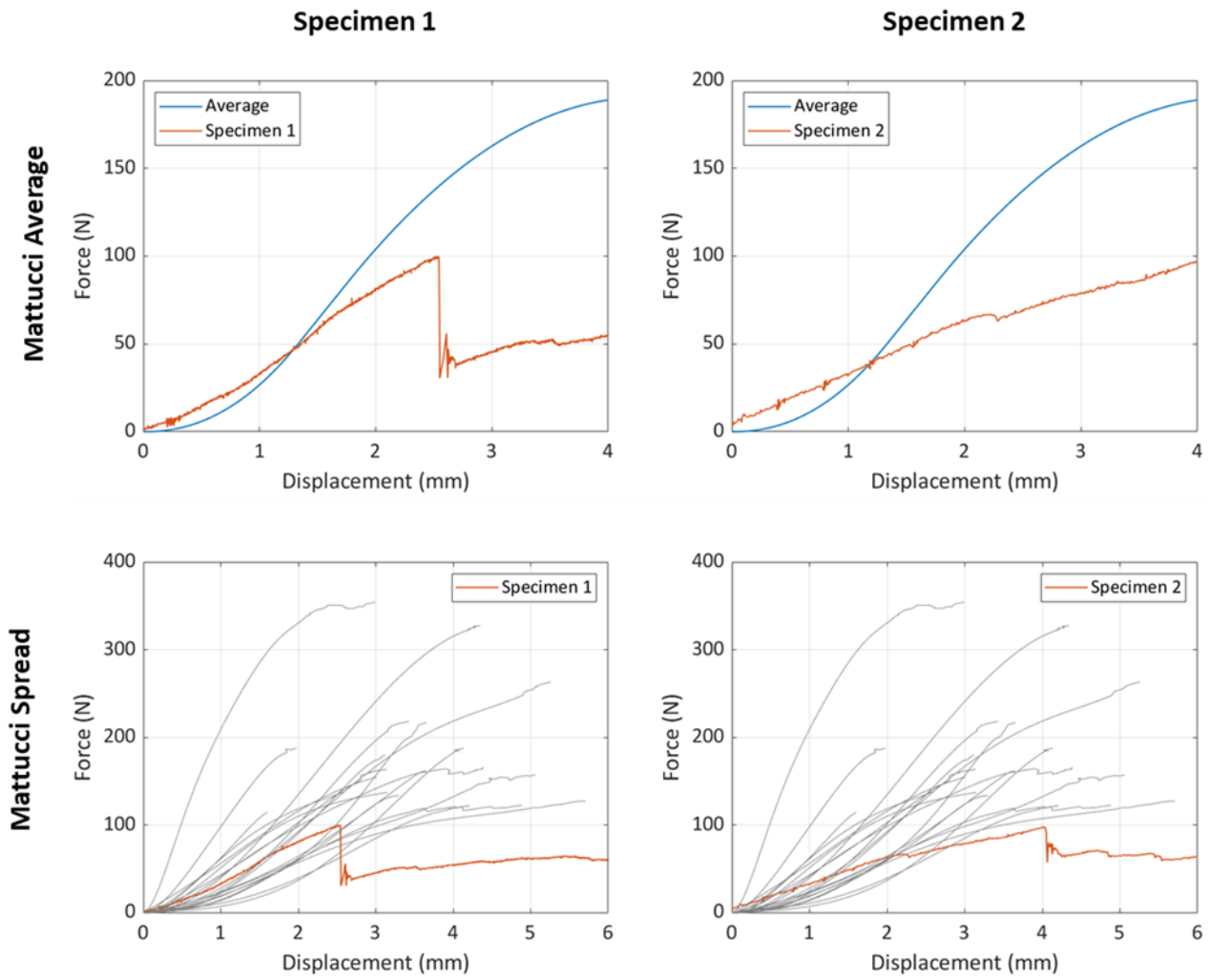

Figure C.2: Comparing specimen tension-to-failure data from the supplementary study to the average (Top) and spread (Bottom) of Mattucci data.

The specimens' responses in sub-catastrophic tension were similar to those found in Chapter 3. Note that, during the failure test, the first specimen bone failed at the lamina where the screws were placed before the ligament failed and in the second specimen, the cement failed on the superior pot before the ligament failed. Therefore, the curves can only be compared until the first dip in force.

Taking this into account, the specimens fell within the range of data reported by Mattucci. Therefore, the new setup was able to replicate Mattucci's results, providing an anchor point for the new methodology.

Appendix D: Developing the FJ_{E2} Model

The FJ_{E2} model in Section 4.1.1 was loaded in AP shear, LT shear, and tension to replicate the experiment in Chapter 3 as in Section 4.1.4.

Methods

Initially, the baseline FJ_{E1} model was solved in AP shear, LT shear, and tension in LS-DYNA R.12 with single and double precision. The force-displacement response was almost identical in the positive loading phase (from 0 ms to 300 ms) for all modes of loading. The force output was almost identical throughout the simulation; however, the displacement accumulated an error of about 4% maximum displacement by the end of the negative loading phase (600 ms to 90 mm) for AP shear and LT shear. As most of the analysis was performed in the loading phase or by comparing forces, single precision was used for the model development.

In developing the FJ_{E1} model potting and boundary conditions, two sensitivity studies were performed on the potting of the FJ_{ML} model. The first study evaluated the effect of element size on the output force-displacement curve of the C5 potting rigid plate. Each solid element of the potting material was split into 8, resulting in 38 400 elements with 1.25 mm side lengths. The rigid plates were resized to share the same nodes as the potting. The baseline FJ_{E2} model and the FJ_{E2} model with smaller potting elements were loaded in AP shear and tension and solved in LS-DYNA R12 with single precision. The second study evaluated the effect of the potting material parameters on the output force-displacement curve of the C5 potting rigid plate. The Young's modulus, Poisson's ratio, and Yield Stress were modified using values shown in Table D.1 One parameter was modified at a time, with the other parameters being held at the baseline values. The FJ_{E2} model in tension was solved using LS-DYNA R12.0, single precision.

Table D.1: Values for the sensitivity study on potting material parameters

	Density (kg/mm^3)	Young's Modulus (GPa)	Poisson's Ratio	Yield Stress (GPa)
Low	2E-06	0.5	0.49	1E4
Baseline		2.2	0.34	1E6
High		200	0.20	1E8

A sensitivity study was also performed on the FJ_{E2} model facet joint orientation. Using a transformation of the facet joint nodes, the facet joint was rotated ± 10 degrees around the x-, y-, and z-axis from baseline. One direction was changed at a time while the other directions were maintained at the baseline orientation. The model was loaded in AP Shear, LT shear, and tension and solved in LS-DYNA R12 with single precision. The output C5 rigid plate force-displacement curve was extracted for each simulation.

To confirm the FJ_{E2} model did not change the response of the GHBMC facet joint, the C4 potting rigid plate of the FJ_{E2} model was loaded in tension at 0.002 mm/ms to replicate the loading of the FJ_{E1} model in Section 4.1.2. Additionally, the FJ_{E1} model was manually rotated to the same orientation as the multi-loading model and the C5 rigid endplate loaded in AP shear as outline at the beginning of this section. The simulations were solved in LS-DYNA R12 with single precision and the output C5 rigid plate force-displacement curve extracted.

To address the spike in force seen in the LT shear positive loading direction, the contact between the opposing surfaces was modified to accommodate a sliding option.

Results and Discussion

As shown in Figure D.1, the potting size and potting material have very little effect on the output force-displacement curve.

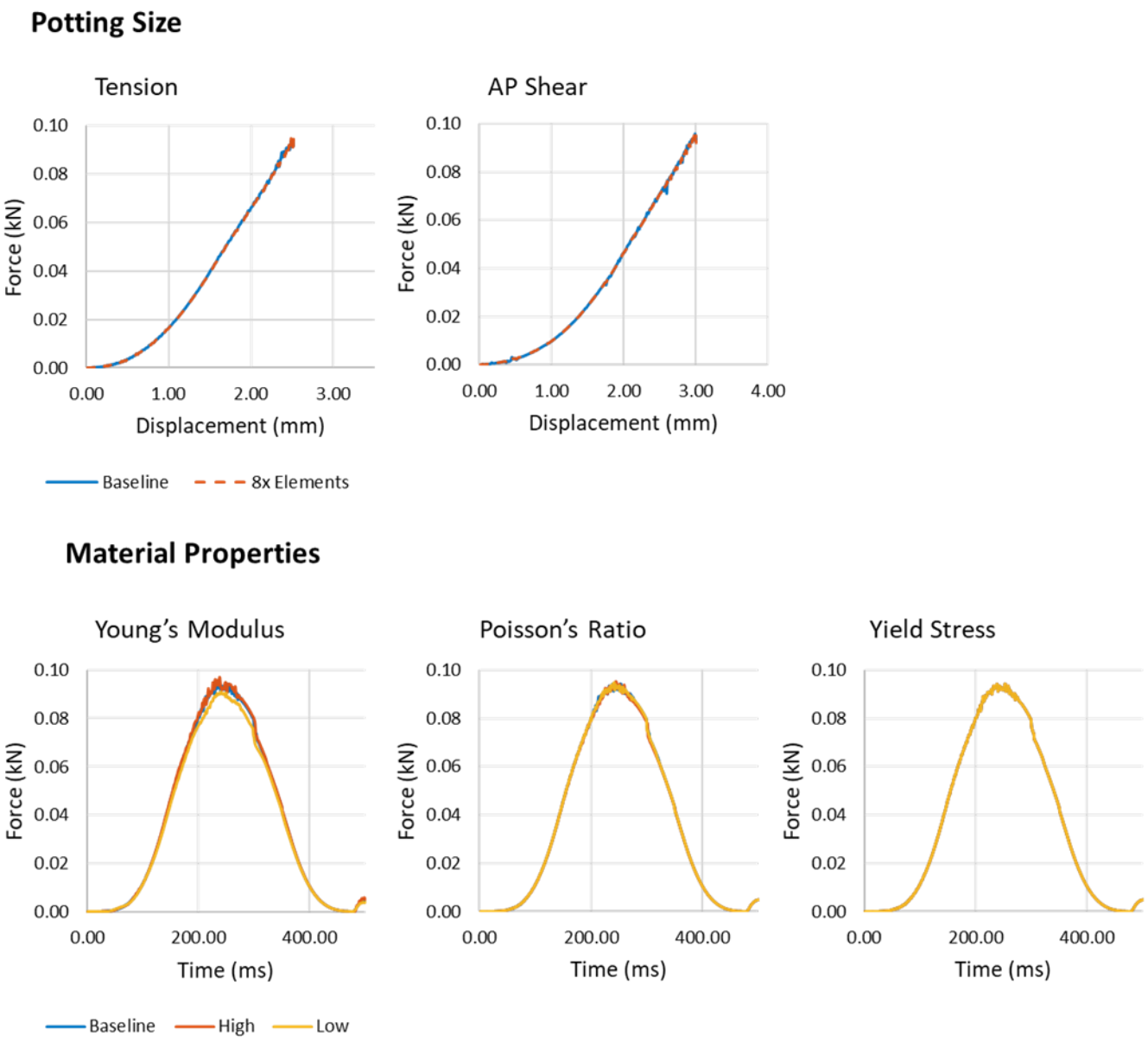

Figure D.1: Potting sensitivity study of the FJ_{E2}. (Top) Shows sensitivity of the output force-displacement curve to potting element size and (Bottom) shows the sensitivity of force vs time curve to material properties. All tests for material properties are in tension.

The facet joint orientation has a greater effect on the force-displacement curve (Figure D.2). In AP and LT shear, the positive direction loading and unloading occurs from 0 ms to 600 ms and negative loading and unloading from 600 ms to 1200 ms. In tension, positive loading and unloading occurs from 0 to 500 ms.

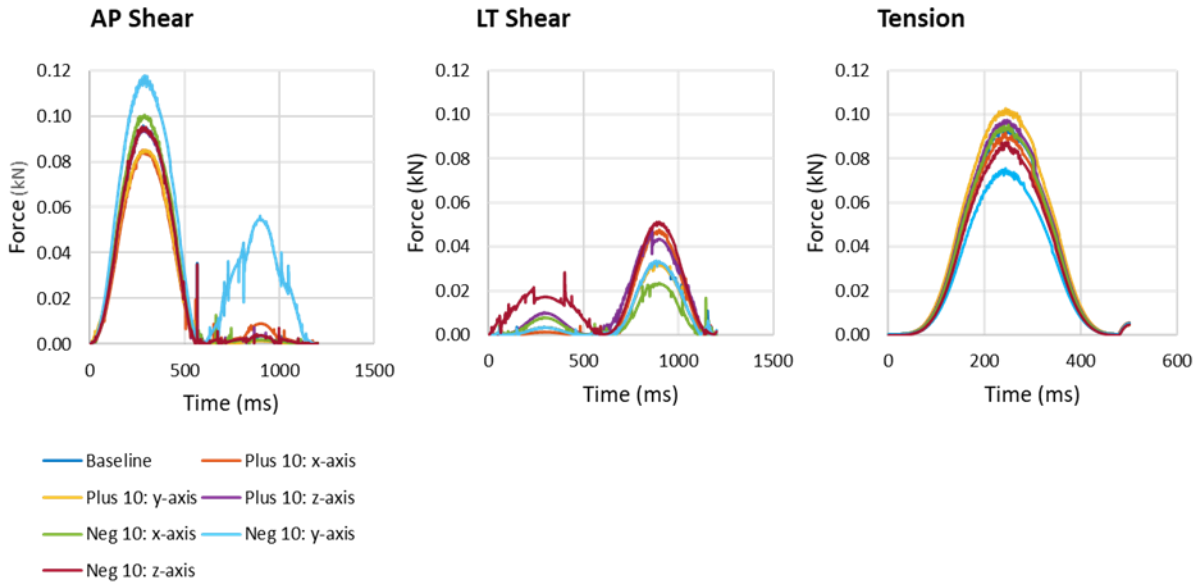

Figure D.2: Sensitivity of multi-loading model force-displacement curves to orientation of facet joint.

In AP Shear, rotations around the z-axis have little effect on the force vs time curve while rotating around the x- and y-axis change the peak load in positive and negative loading. A negative 10-degree rotation about the y-axis has the greatest effect on peak load, increasing the peak force particularly in negative loading. In LT shear, rotation around the y-axis has little effect on the force vs time curve while negative rotation around the z-axis has the greatest effect of peak load, with an increase in peak load seen in positive and negative loading directions. Finally, in tension, negative rotation around the x-axis has little effect on the force vs time curve. Negative rotation around the y-axis has the greatest effect on peak force, decreasing the peak force from about 0.09 kN to 0.075 kN.

When considering positive shear in the FJ_{E1} model and AP shear in the FJ_{E2} model, a difference in response was noted – shear in the FJ_{E1} model had a longer toe region and lower force compared to the FJ_{E2} model. The two models had different boundary conditions in terms of coordinate systems – loading rate and constrained vs unconstrained – however these differences prompted

further investigation as both FJ_{E1} and FJ_{E2} were extracted from the GHBMC M50 model, so a similar response was expected.

Under similar boundary conditions, the results are similar between the models. The force vs displacement curve for the FJ_{E1} model reoriented to the FJ_{E2} model orientation and loaded in AP shear was the same as the FJ_{E2} model during the loading phase (Figure D.3).

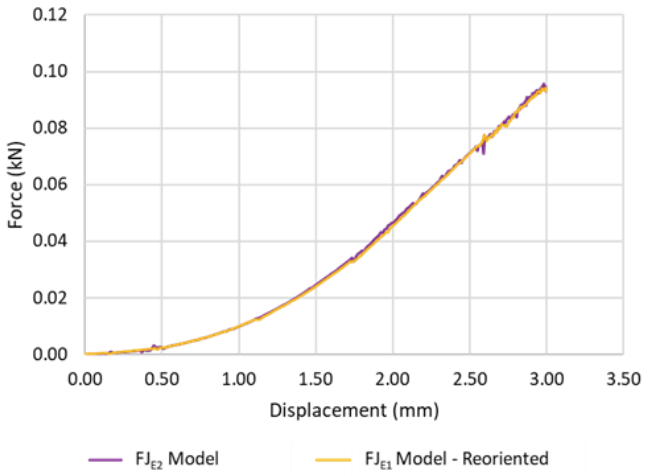

Figure D.3: FJ_{E1} model oriented in FJ_{E2} model orientation and loaded in AP shear.

The FJ_{E2} model in Mattucci quasi-static tension was lower than the FJ_{E1} model in global and local coordinate system (Figure D.4). Similar differences are seen between FJ_{E1} model in global and local coordinate systems as between FJ_{E1} model in local coordinate system and FJ_{E2} model.

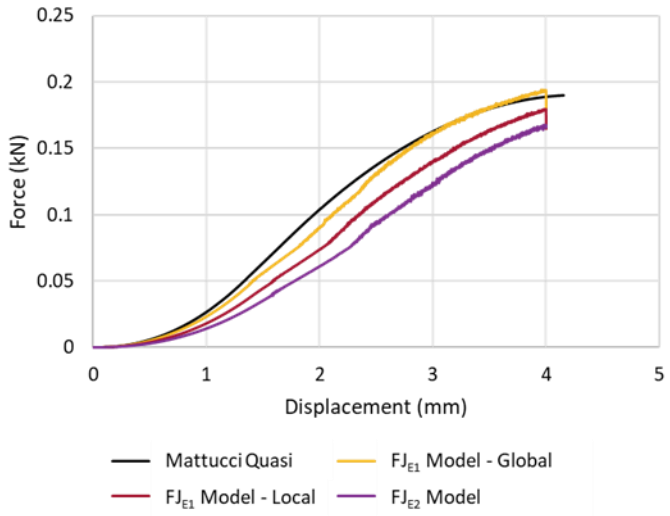

Figure D.4: FJ_{E2} model loaded in Mattucci quasi-static tension.

The force in tension was lower in the FJ_{E2} model than the FJ_{E1} model, but this can be attributed to the different orientations with respect to the tension axis between the FJ_{E1} model and FJ_{E2} model. Additionally, the FJ_{E2} model load was applied through the potting, rather than the rigid endplate (as in the tension model), and some deflection of the lamina was observed. It was difficult to observe small deflections in the video analysis of the experiment in Chapter 3 because of overlying soft tissue and some relative movement of the pot and specimen. However, what is possibly small deflections can be observed in several of the specimens. Additionally, a study by Quarrington et. al. [100] quantified facet deflection during anterior shear and flexion, suggesting the deflection observed in the model may be physiological. The response in AP shear of the FJ_{E1} and FJ_{E1} models were very similar once the FJ_{E1} model had been reoriented. Note that the orientations were not exactly the same, as the alignment was done manually.

A spike in the LT shear loading direction observed in model development was found to be the result of the geometry of the C5 articular cartilage causing 'sticking' between the opposing surfaces. The cartilage geometry was defined as a function of the relative location in the plane of the facet joint and the underlying geometry of the facet pillar [5]. A dip in the underlying C5 pillar caused a dip in the C5 articular cartilage which interacted with the C4 articular cartilage. Changing the contact to incorporate sliding reduced the magnitude of the spike in the LT loading direction but otherwise had very little effect on the force magnitude in the LT loading direction and very little effect on the AP shear and tension loading directions (Figure D.5).

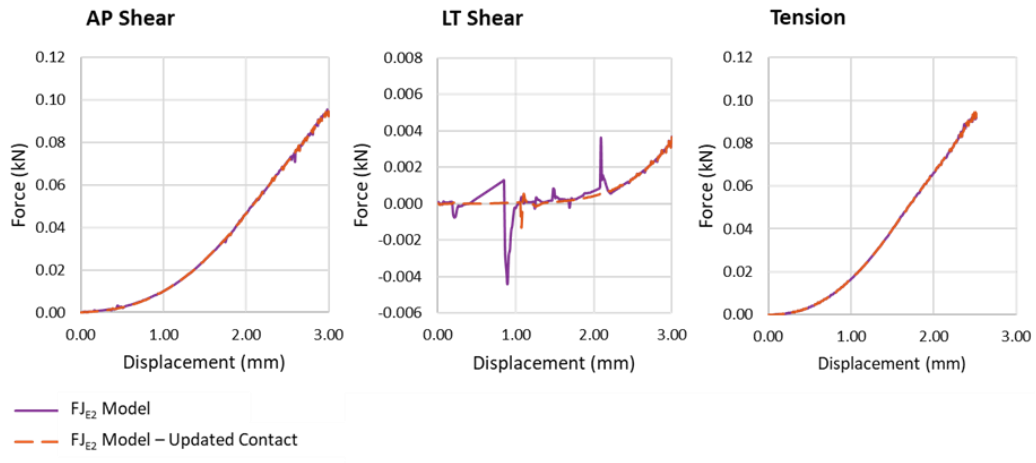

Figure D.5: Comparing the FJ_{E2} model with and without the updated contact between opposing articular pillars.

Appendix E: Developing the Diagonal Element Implementation

Methods

In the first study attempt at implementing diagonal elements, ligament shear (not joint shear) data was used to characterize diagonal 1D tension-only elements added to the FJ_{E1} model capsular ligament, with a pair of diagonal elements forming a cross between two original elements (Figure E.1). Note that the original 1D tension-only elements in the tension model capsular ligament will be referred to as the *original elements* and the added 1D tension-only elements as *diagonal elements*.

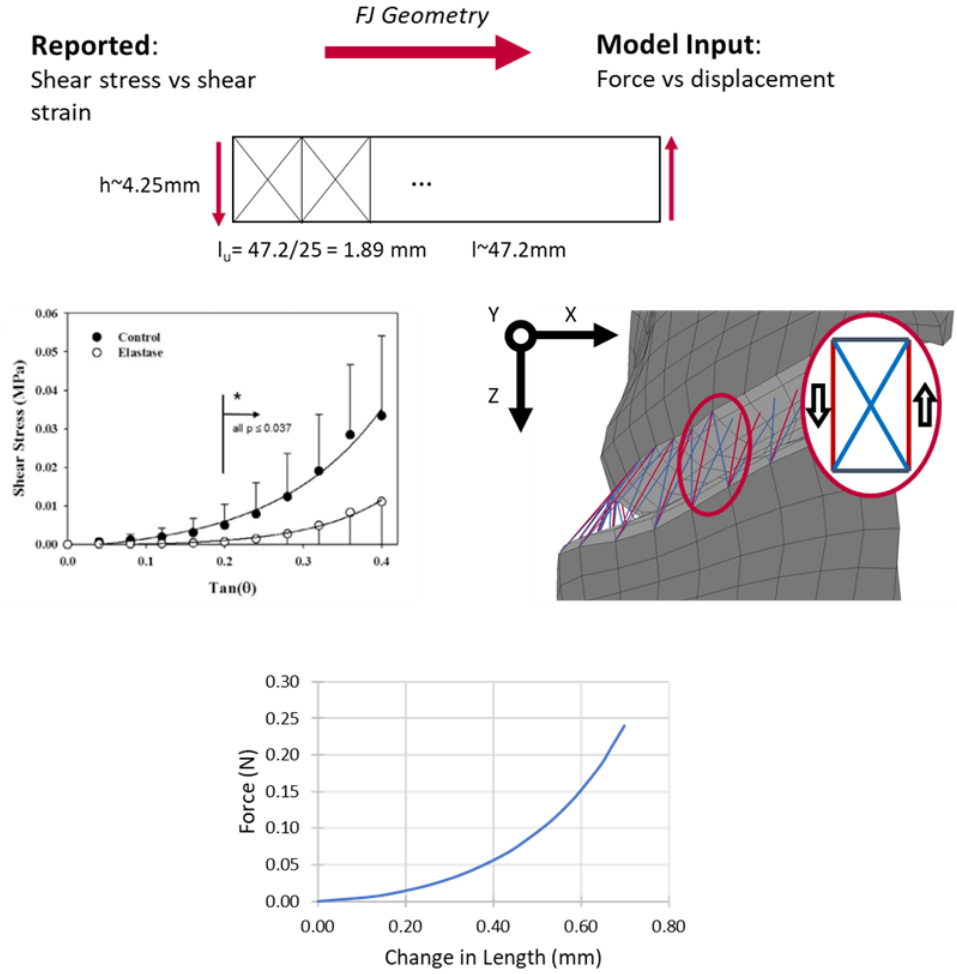

Figure E.1: Formulation of diagonal elements for ligament shear. (Top) Shows simplified geometry of the capsular ligament used to convert the literature data (Left) from shear stress vs tan(ϑ) to force vs change-in-length. (Right) Shows the implementation of diagonal elements in FJ_T model with a simplified single unit in the insert. (Bottom) Shows the material input (force vs change-in-length) for the diagonal elements.

There was limited experimental data in literature on cervical capsular ligament shear data, so shear stress vs angle (shear strain) data from porcine medial collateral ligament reported by Henninger et. al. [55] was used to characterize the diagonal elements. A simplified geometry of the capsular ligament was used to convert the shear stress vs angle to change in length vs force for the diagonal element material model input. To do this, the capsular ligament was laid flat, with the length equal to the circumference of the facet joint and the height equal to the average distance between facet pillars (taken as the average length of the original elements). The original elements were assumed to be equally spaced, creating 25 uniform 'units' of capsular ligament. The thickness of the capsular ligament was assumed to be 1.6 mm. The shear stress was converted to force by multiplying by the surface area (height vs thickness), then divided by the number of units. The change in length of the diagonal elements during ligament shear loading was estimated by using trigonometry based on the shear angle and the height of a unit. The change in length vs force curves were then used as input for the diagonal elements (Figure E.1). To ensure the elements were tension-only, the force corresponding to a negative change in length (i.e. a decrease in length) was set to 0.

A single unit of height 4.25 mm and length 1.89 mm with diagonal elements was first tested in shear by displacing the two right nodes in the positive z direction at 3.76E-05 mm/ms. The left nodes were constrained in all degrees of freedom and the right nodes constrained in all degrees of freedom except z-translation. The change in length of the diagonal elements and the boundary forces of the nodes were extracted. The diagonal elements were then added to the FJ_{E1} model (FJ_{E1_Di} model), which was loaded in tension as defined in Section 4.1.2. The change in length vs force input curve of the original elements was modified to maintain the facet joint force-displacement response. The difference between the FJ_{E1} model force and the sum of forces from the diagonal elements in the FJ_{E1_Di} model was multiplied by the fraction of change in length of a single original element to the sum of all original element changes in length, giving the updated change in length vs force input curve for the original elements. The FJ_{E1_Di} model was then run in Mattucci quasi-static tension and positive and negative shear as defined in Section 4.1.3 (Mattucci rates) using LS-DYNA R9.2 with double precision. Force and displacement of the C4 rigid endplate were extracted.

Results

The single unit case loaded in ligament shear showed the expected output (Figure E.2).

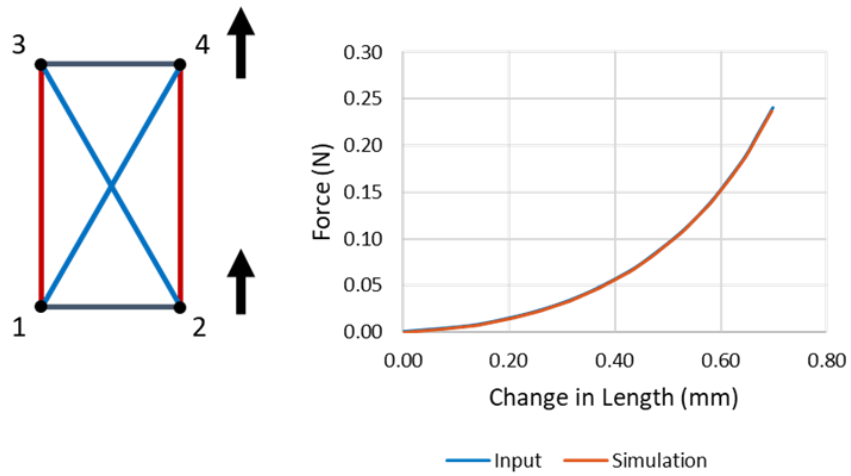

Figure E.2: Single unit test of diagonal elements loaded in ligament shear.

The FJ_{E1} model and the FJ_{E1_Di} model display very similar responses in tension and in positive shear. In negative shear, the peak magnitude at about 8 mm of both models is the same, but the toe region is shorter in FJ_{E1_Di} model (Figure E.3). 1D tension-only elements start to engage around 3 mm rather than about 4.5 mm. Note that the curves are cropped to show force-displacement curves until elements start to fail. Ligament failure was not adjusted with the addition of diagonal elements.

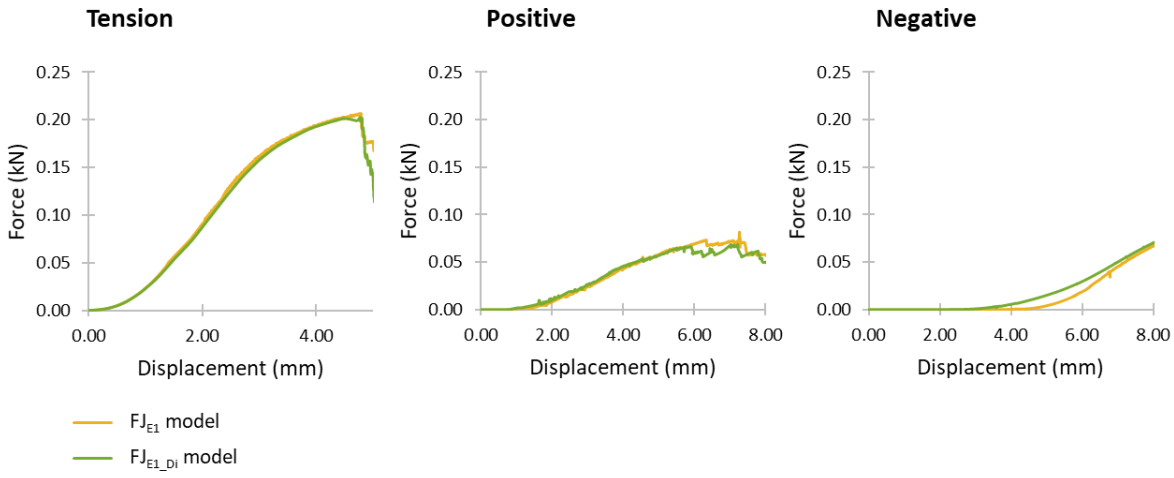

Figure E.3: FJ_{E1_Di} model with original elements adjusted for tension. Simulated at Mattucci Quasi-static rate.

Discussion

In the FJ_{E1} model, the diagonal elements were characterized using ligament shear data and demonstrated that it was possible to modify the facet joint response in joint shear using 1D tension-only elements. At this point, the response of the FJ_{E1_Di} was not compared to experimental data as the experimental data in Chapter 3 had yet to be completed.

However, several checks can be performed. First, the FJ_{E1_Di} model shows very little change during tension loading, which is expected given the original elements were modified to maintain the response in tension as the tension data performed well compared to experimental data. However, the FJ_{E1_Di} model in tension is only applicable up to the point where ligament elements begin to fail, as the failure response of the diagonal elements were not characterized, and the original elements not updated.

Second, while FJ_{E1_Di} model in negative shear shortens the toe region compared to the FJ_{E1} model, there is very little difference in positive shear. In both positive and negative shear, the diagonal elements engaged earlier than the original elements, although the difference is greater in the negative shear direction by about 1.5 times. This may partly account for the shorter toe region in negative shear, but not positive shear. Note that both the diagonal elements and original elements engage earlier in positive shear, likely due to the bias of element orientation towards positive shear.

Ultimately, the intention was to determine whether adding diagonal beams could modify the facet joint response in shear. In this, the study was successful and provided the basis for characterizing the diagonal elements using joint shear data from Chapter 3.

Appendix F: Facet Joint Kinematics During Vehicle Impact Simulation

To evaluate FJ kinematics during vehicle impact, the GHBMC v6-0f full head and neck model, an internal version of the GHBMC v6 model, was simulated in nine loading scenarios: frontal impact (2g, 8g, and 15g); oblique impact (4g, 7g, and 10g); lateral impact (4g and 7g); and rear impact (7g). The models were solved using a commercial finite element code (LS-DYNA R9.2, single precision). The T1 vertebra was considered a rigid material and loaded according to the impact scenario.

Relative AP shear, LT shear and tension of the right C4 - C5 FJ was evaluated as the displacement of a point on the C4 facet pillar relative to a local coordinate system defined on the C5 facet pillar (Figure F.1), similar to the approach outlined by Corrales et. al. [5]. The C4 point, approximately in the center of the facet pillar, was calculated by averaging the position of two nodes on the outer circumference of the facet pillar. The local coordinate system was defined with three points on the C5 facet pillar. The origin was defined as a point on the posterior aspect of the facet pillar. The second point was selected on the anterior aspect of the facet pillar, defining the positive AP direction (x'-axis). The third point was on the antero-medial aspect of the C5 facet pillar, defining a second vector in the plane of the C5 facet pillar. The local z'-axis was defined by finding the cross product between the two vectors and the local y'-axis by the cross product between the resulting z'-axis and the x'-axis. The local coordinate system was redefined at each timestep so the relative displacement between C4 and C5 facet pillars was tracked.

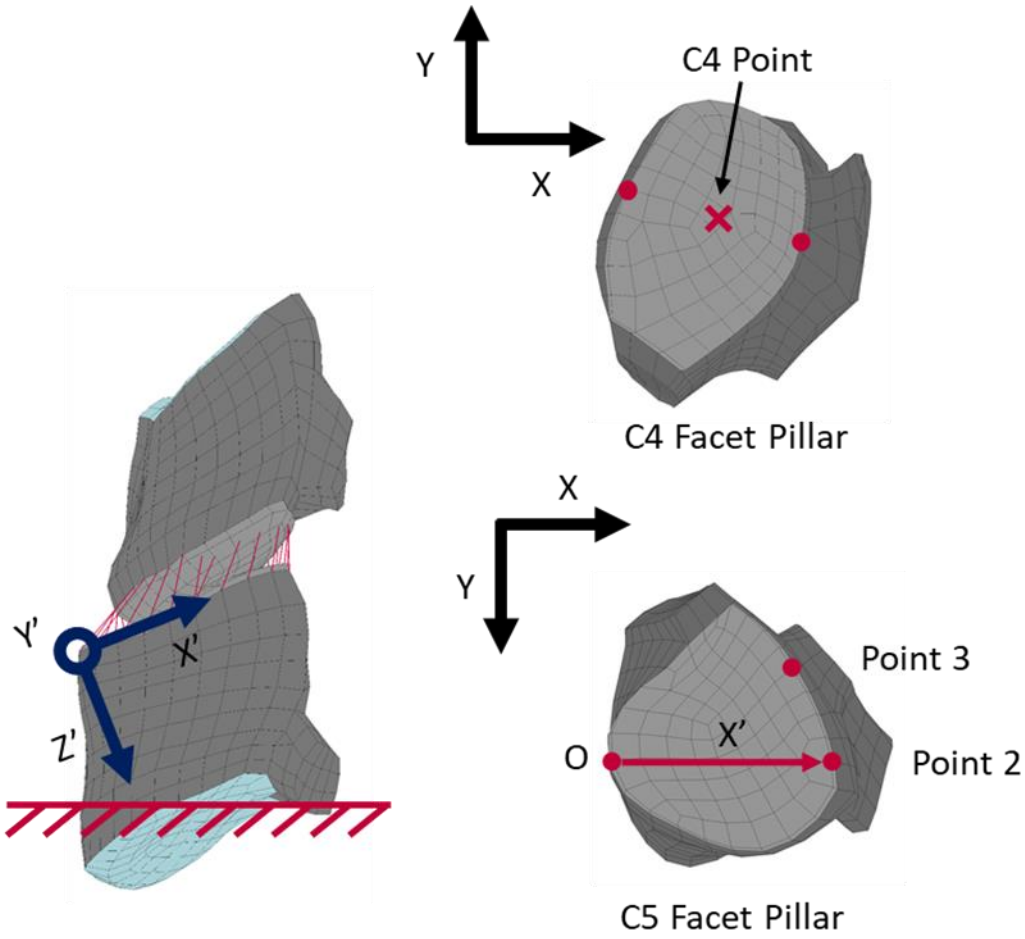

Figure F.1: Point on C4 and Local Coordinate System to Calculate C4-C5 FJ Kinematics during vehicle impact simulations. Positive AP shear was defined as the superior (C4) facet pillar moves anteriorly with respect to the inferior (C5) facet pillar. Positive relative LT shear, for the right FJ, was defined as the superior facet pillar moves laterally with respect to the inferior facet pillar. Positive relative compression, in the positive z'-direction, was defined when the superior facet pillar moves towards the inferior facet pillar.

Relative AP shear was defined as the relative displacement of the C4 point along the local x'-axis with respect to the local coordinate system origin. Relative LT shear was defined in the same manner along the local y'-axis and tension as the local z'-axis. A Matlab script was used to calculate the local coordinate system and the relative displacement at each timestep. The maximum (in positive direction) and minimum (in negative direction) was determined for each direction (Table F.1).

Table F.1: Relative kinematics of C4 - C5 FJ during vehicle impact simulations. Relative AP shear is in the x'-axis, relative LT shear in the y'-axis and tension in the z'-axis. Max shear is the highest relative shear in the positive direction while min is the highest relative shear in the negative direction. For the z'-axis, max is highest relative displacement in compression and min is highest relative displacement in tension.

		x'-axis		y'-axis		z'-axis		Ratio AP:LT
		Max	Min	Max	Min	Max	Min	
Frontal	2g	1.59	-0.08	0.01	-0.08	0.13	-0.07	20.37
	8g	3.55	-0.00	0.07	-0.02	0.00	-0.21	53.30
	15g	3.86	-0.00	0.32	-0.00	0.00	-1.03	12.12
Rear	7g	0.03	-2.06	0.22	-0.16	0.19	-0.77	9.44
Lateral	4g	1.65	-0.35	0.00	-0.51	0.08	-2.11	3.21
	7g	2.35	-0.28	0.11	-1.04	0.03	-3.52	2.61
Oblique	4g	2.49	-0.04	0.01	-0.30	0.00	-0.98	8.22
	7g	3.46	-0.05	0.00	-0.60	0.00	-1.75	5.73
	10g	4.15	-0.04	0.01	-0.77	0.00	-2.22	5.41

The maximum displacement occurred in AP shear in all modes of loading except lateral impact, where the maximum displacement occurred in tension. Relative LT shear was lower than AP shear in every scenario, with LT shear being closest in magnitude in lateral shear. The maximum absolute shear in the AP direction usually occurred in the positive direction, except for in rear impact where the maximum was in the negative direction.

This study revealed patterns in the relative kinematics of the C4 - C5 facet joint. However, there are several considerations to note. First, the lateral impact occurred on left side, on the opposite side to the right facet joint. The oblique impact occurred on the anterior-left angle, also on the opposite side to the right facet joint. The response of the left facet joint in these two scenarios would be different than the response of the right facet joint. Secondly, only the displacement of a single point on the superior facet pillar with respect to a point on the inferior facet pillar was considered. As such, rotations of the facet joint were not considered and would have contributed to relative displacements of the facet joint. If a different point was selected on the superior pillar or different nodes used to create the local coordinate system, the kinematics would likely be slightly different.